BULGARIAN CHEMICAL COMMUNICATIONS

2023 Volume 55 / Number 4

Journal of the Chemical Institutes of the Bulgarian Academy of Sciences and of the Union of Chemists in Bulgaria

IN MEMORIAM

To the memory of Professor Lachezar Angelov Petrov

Professor Lachezar Angelov Petrov, PhD, DSc, corresponding member of the Bulgarian Academy of Sciences (BAS), passed away unexpectedly on 18th July 2023 after a severe brain stroke. He was a reputed scientist in the field of catalysis and international catalysis community.

Lachezar Petrov was born on 2nd February 1939 in Sofia. He graduated from Institute of Chemical Technology, currently University of Chemical Technology and Metallurgy, in Sofia in 1962. In 1965, he joined the Institute of Organic Chemistry at BAS as a full-time graduate student. Since 1969, he has been a research assistant and in the same year received his PhD in Chemical Kinetics and Catalysis from the same institution. In 1977, he was elected. a senior research associate.

Since 1983, L. Petrov has worked at the Institute of Kinetics and Catalysis of the BAS, now Institute of Catalysis. In 1988, he obtained his DSc degree, and the following year was elected full professor at the same institute. He specialized in Catalysis Institute, Novosibirsk (Russia, 1969), Tokyo Institute of Technology (Japan, 1971), Catalytic Research Centre at Sumitomo Chemicals, Niihama (Japan, 1972), and University of Bremen (Germany, 1976). He made long-term scientific visits to the USA, Germany, Spain, Israel, France, China, Brazil, Saudi Arabia, and Zambia. In 2008, he was elected a corresponding member of the Bulgarian Academy of Sciences.

He successively held the positions of scientific secretary of the Unified Centre for Chemistry at BAS (1978–1988), department head (from 1983), deputy director (1983–1989; 1995–1997), and director of the Institute of Catalysis in Sofia (1989–1993; 1997–2007).

Prof. L. Petrov's scientific interests include kinetics and mechanisms of heterogeneous catalytic reactions over metal, metal oxide, and zeolite catalysts in stationary and non-stationary conditions; application of catalysis in petrochemicals and oil refining, catalyst deactivation; catalyst carriers, and synthesis and application of zeolites in catalysis. Second, efforts were being made to look into application of catalysis for environmental protection: hydrodesulfurization of oil fractions, complete oxidation of organic compounds and carbon monoxide, reduction of NO_x gases, desulfurization of gasolines, purification of sulfide-polluted wastewater. Further research comprised applied catalysis as kinetic models of industrial catalytic processes, development of industrial catalysts, methods of industrial-scale catalyst testing, automation of kinetic systems for research; methods for building kinetic models; oscillating reactions; ceramic fibres: refractories and additives for composite materials.

The main scientific contributions of Prof. Lachezar Petrov involve mathematical modelling of heterogeneous catalytic reaction kinetics under stationary and non-stationary conditions; studies of heterogeneous catalytic reaction mechanisms; studies of the influence of composition on the structure and properties of heterogeneous catalysts; photocatalysis; development and implementation of production technologies of industrial catalysts; and instrumentation and automation of kinetic studies.

Lachezar Petrov is one of the authors of the national program 'Kinetics and Catalysis' and one of the founders of the Bulgarian industry for the production of industrial catalysts. Under his leadership, a number of technologies for the production of industrial catalysts and carriers and catalytic processes for their use were developed and put into practice.

L. Petrov took active part in teaching and learning activities. He gave lectures in the Faculty of Chemistry and Pharmacy of St. K. Ohridski University of Sofia, Faculty of Chemistry of P. Hilendarski University of Plovdiv, V. Levski National Military University at Veliko Tarnovo, Bremen University (Germany), Israel Technion Institute of Technology, Haifa (Israel), University of Zambia, Lusaka (Zambia), European Institute of Chemistry, Polymers, Materials, Strasbourg (France), National Centre in Catalysis, Chinese Academy of Sciences, Dalian (China), Federal University of San Carlos, San Carlos (Brazil). He also held the Chair of Catalysis at King Abdulaziz University, Jeddah (Saudi Arabia). He was the supervisor of 11 doctoral students, 7 postdoctoral fellows, and 8 visiting specialists.

Prof. Lachezar Petrov is the author and co-author of about 300 scientific works, 8 books, 2 textbooks, and 20 patents and author's certificates. His scientific achievements find wide international resonance and recognition. They have been cited about 2000 times. With his participation, 27 technologies for producing catalysts, catalyst carriers, adsorbents, catalytic technologies, and scientific instruments were developed and implemented. In most cases, he was the head of the work teams.

Prof. L. Petrov was a member of the editorial boards of 6 international and 3 Bulgarian scientific journals. For 10 years, he was the editor-in-chief of the journal Chemistry and Industry (Khimiya & Industriya, Sofia). He was the editor of nine books with works presented at international scientific events, as well as invited editor in international journals.

Since 1992, L. Petrov has been a member of the Russian Academy of Natural Sciences. For three times he was a reviewer for the Nobel Committee in Chemistry, three times for the Third World Academy of Sciences, for international and national foundations, for the European Science Foundation, for many international journals, and for doctoral theses in France, Sweden, and Finland.

Prof. L. Petrov was a member and vice-chairman (1996–2007) of the Union of Chemists in Bulgaria. Since 1992, he was the president of the Bulgarian Catalysis Society, a member of the Council of the European Federation of Catalysis Societies (since 1993) and member of its Executive Council (2003–2005). He was also a member of the Council of the International Federation of Catalysis Societies since 1996. He was an expert of the International Centre for Science and High Technologies, ICS-UNIDO Trieste (1997–2005), vice president of the Balkan Association for Environmental Protection (B.EN.A) and co-chair of its Bulgarian branch, a member of the International Supervisory Committee of the State Key Laboratory of Catalysis, Chinese Academy of Sciences, Dalian, China (since 2006).

He was a member of the organizing committees of more than 70 international forums, including multiple European and international congresses on catalysis; he was the chair of the Organizing Committee of the Seventh European Congress on Catalysis held in 2005 in Sofia.

Prof. Lachezar Petrov is a knight of the orders Cyril and Methodius and 1300 Years of the Bulgarian State. He is the winner of a gold medal from Plovdiv International Fair in 1980, a silver medal from National Technical University of Ukraine, a bronze medal from Bulgarian Patent Institute, a Prof. Dr. Asen Zlatarov gold medal of the Federation of Scientific and Technical Unions, a Marin Drinov Honorary Medal with ribbon of BAS, and many international awards. He was elected an Honorary Member of the Union of Chemists in Bulgaria.

Prof. L. Petrov was a man with broad cultural interests, an excellent organizer, and a wonderful colleague and friend.

Chavdar Bonev

Bulgarian Chemical Communications, Volume 55, Issue 4 (pp. 385-389) 2023 DOI: 10.34049/bcc.55.4.11NCC01

Analysis of serum antioxidant activity in women with impaired bone density and effect on it of serum concentrations of copper and zinc

R. Tomova[1*], S. Asenova[1], L. Atanasova[2], B. Atanasova[2], R. Nestorova[3], M. Nikolova[4], M. Slavova[5]

[1]*Faculty of Pharmacy, Medical University of Pleven, 5800 Pleven, Bulgaria*
[2]*Faculty of Medicine, Medical University of Sofia, 1431 Sofia, Bulgaria*
[3]*Rheumathology Center "Saint Irina", 1750 Sofia*
[4]*Department of Mental Health, Social Work and Integrative Medicine, Middlesex University, London, United Kingdom*
[5]*Institute of Electrochemistry and Energy Sources, Bulgarian Academy of Sciences, 1404 Sofia, Bulgaria*

Received: November 15, 2022; Revised: November 21, 2023

This study aims to investigate the relationship between total antioxidant activity (AOA), serum copper and zinc levels, and their impact on bone mineral density (BMD) in menopausal and postmenopausal women. After measuring BMD through dual-energy X-ray absorptiometry (DEXA), participants were categorized into a control group, osteopenic patients, and osteoporotic patients. We determined the radical scavenging activity of serum samples (RSA%) and their trolox equivalent representing the total AOA, using a spectrophotometric ABTS-assay. The variance analysis of the results revealed a statistically significant difference among the groups based on the RSA% indicator, with mean values of 67.69±6.74 for osteopenia, 62.46±7.83 for osteoporosis, and 55.64±2.05 for the control group. Blood serum copper and zinc levels were measured *via* flame atomic absorption analysis. The results indicated a clear trend of increasing microelement concentrations as BMD decreased. The t-test demonstrated statistically significant results for copper concentration when comparing groups with reduced bone density and the control group. Additionally, a statistically significant difference was observed between the osteoporosis group and the control group concerning the Cu/Zn indicator, whose values consistently changed with the severity of the disease. The analysis of the results shows that patients with reduced bone density have higher RSA%, higher concentrations of copper and zinc, and higher Cu/Zn ratio values compared to the control group. The elevation of serum levels of Cu and Zn in patients with reduced bone density can be explained by the fact that copper and zinc are components of enzymes involved in bone metabolism, which degrade at increased levels of reactive oxygen species (ROS) in cells during osteoporosis. The increased concentration of copper ions in the serum initiates secondary radical processes and enhances its AOA. The results confirm the synergistic action of free radicals and redox-active metals such as copper on AOA and bone mineral density.

Keywords: serum antioxidant activity; copper; zinc; Cu/Zn; osteoporosis.

INTRODUCTION

Reactive oxygen species (ROS) are produced in the body as a result of cellular metabolism. Some of the ROS are free radicals that are generated primarily in the mitochondria. A main characteristic of ROS is their high reactivity, penetrating ability, and ability to participate in secondary chain-radical processes, leading to more aggressive radical and non-radical oxygen species. Small amounts of ROS are necessary for the human body as cell signaling substances. For example, they participate in the regulation of the processes of cell division and cell death, activate the expression of certain genes, initiate the renewal of tissues, the elimination of damaged cells as a protective mechanism of the body against DNA mutations, etc.

Endogenous ROS formation is a natural process. Concurrently, there are also biochemical mechanisms for scavenging free radicals through a combination of enzymatic and non-enzymatic antioxidants. When antioxidant defense mechanisms in cells are reduced and ROS production is increased, they react with lipids, proteins, DNA molecules and disrupt their structure. Mitochondrial DNA damage due to free radicals leads to the loss of organelle functions and, consequently, to a lack of cellular energy, which also leads to the loss of functions of the entire cell. As cells age, free radicals contribute significantly to both genome damage and mutations. The body can tolerate mild oxidative stress, but a greater one leads to numerous pathologies. The complex of occurring harmful and irreversible changes is observed at all levels of

* To whom all correspondence should be sent:
E-mail: rtomova@mail.bg

organization of the organism - molecules (DNA, proteins, lipids), cells and organs. These damages to biologically active molecules are the essence of oxidative stress. As the damage process progresses, the incidence of various diseases, such as osteoporosis, increases [1]. Oxidative stress affects a significant part of the population such as menopausal women, the elderly, obese people and those with long-term exposure to environmental pollutants.

Research has proven that uncontrolled production of ROS is associated with disruption of the structure of metalloprotein enzymes and disruption of homeostasis of redox-active metal ions. Upon incubation of Cu, Zn - superoxide dismutase with AAPH (2,2'-azobis(2-methylpropionamidine) dihydrochloride), an azo compound that is a source of model peroxide radicals, the enzyme is oxidatively damaged by the radicals, inactivated, the protein is fragmented, and the copper ions are released [1, 2].

The increased concentration of redox-active metal ions, such as copper, accelerates the formation of free radicals, as well as disturbances of calcium and sulfhydryl homeostasis. Copper participates in free-radical processes with lipid peroxides formed by the attack of radicals on polyunsaturated fatty acid residues of phospholipids [1, 3].

The intake of low-molecular weight antioxidants such as vitamin C, vitamin E, carotenoids, flavonoids, and other antioxidants, which are capable of chelating metal ions, reduces free metal ions and the formation of free radicals. Oxidative stress is reduced [4, 5].

Zinc has no antioxidant effect, but as a component of some antioxidant enzymes, it supports their activity. Zinc has the following indirect roles in limiting oxidative damage to the body: protection against vitamin E depletion; stabilization of the membrane structure; contribution to extracellular antioxidant enzyme structure; maintenance of tissue concentrations of metallothionein; free radical scavenger. Depletion of zinc in cells increases DNA damage by disrupting DNA repair mechanisms [1, 4].

There is a limited number of studies in the literature on the role of oxidative stress in the pathogenesis of osteoporosis. Antioxidant activity of mesenchymal stem cells from people with osteoporosis was found to differ from that of healthy controls. Mesenchymal stem cells in women with osteoporosis adapt their functioning to a higher level of oxidation [1, 6].

Other research has found that the use of antioxidants in food suppresses the activity of osteoclasts and slows the development of osteoporosis. Evidence has been found for a positive relationship between the amount of ascorbic acid in the diet and bone mineral density [7].

More research is needed to establish the cellular and molecular mechanisms linking oxidative stress, antioxidants, and bone metabolism. The basis for the search for such a relationship is the significant decrease in plasma antioxidants with age. Oxidative stress alters the bone remodeling process, causing an imbalance between osteoclasts and osteoblasts and leading to the pathogenesis of the skeletal system characterized by low bone mass [8].

One study confirmed the antioxidant role of adding vitamins D3, K1 and B6 to the diet of postmenopausal women. After one year of supplementation, a reduction in oxidative stress and a significant increase in bone mineral density was reported [9].

Published studies on serum copper and zinc concentrations in women with reduced bone density deliver conflicting results. A potential relationship between the level of these trace elements, the level of oxidative stress and bone density has not been investigated. The aim of our study is to measure serum concentrations of copper and zinc and total antioxidant activity and to investigate their effect on bone density. Measurement and monitoring of these parameters may contribute to finding new aspects in the etiology, pathogenesis and treatment of osteoporosis.

MATERIALS AND METHODS

Data collection

The study included 66 menopausal and postmenopausal women. The included women were not receiving treatment for osteoporosis or osteopenia. Other exclusion criteria are concomitant endocrine disorders, intake of estrogens and biogenic elements with an impact on bone density. The study included participants who were close in age and BMI. This eliminates from the analysis the influence of these factors on BMD, as noted by many researchers. Bone density was measured using DEXA in all patients and controls. A T-Score was also determined from the BMD results. The T-score measurement is the ratio of the measured bone density compared to standard bone density, determined by measuring a large group of healthy 30-year-olds. The participants were divided into three groups, according to their T-scores: with osteoporosis (T-Score below -2.5 SD); osteopenia (T-Score between -1.0 and -2.5 SD); and control group with normal density (T-Score above -1.0 SD). The number of patients with a borderline T-Score value of -2.5 SD is small.

Venous blood was collected using a standard procedure in accordance with quality assurance requirements in the pre-analytical phase. RSA% and their Trolox equivalent, which reflects the total AOA, were determined in serum from the samples by spectrophotometric ABTS-test. Blood serum copper and zinc levels were measured by flame atomic absorption analysis.

Investigation of the antioxidant status of selected patients and controls

Experimentally, the antioxidant status of serum from patients was determined by ABTS-test [10]. The essence of the methodology is based on spectrophotometric recording of the change in absorption of the chromophore used in the system as a result of free-radical processes. Based on the changes in the measured indicator, after interaction with potential antioxidants from the blood serum, conclusions are made about the intensity of the ongoing processes and their influence on the patients' condition. In this model system, the stable radical cation of 2,2'-azinobis(3-ethylbenzothiazoline-6-sulfonic acid) ($ABTS^{•+}$) is used.

The literature review demonstrated the applicability of the method to study the antioxidant properties of a wide variety of sample types, including multicomponent systems. This includes samples of animal origin. Therefore, it can be applied in the monitoring the antioxidant capacity of biological fluids taken from patients with various diseases [11]. The method is fast, simple, allows automated measurement of a large number of samples simultaneously. The radical cation has good solubility in both aqueous and organic solvents, indicating its applicability to both hydrophilic and hydrophobic antioxidants. The method exhibits no pH sensitivity over a wide range and little influence of ionic strength.

The experimental part of this study was divided into four main steps:

1) Preparation of radical stock solution. $ABTS^{•+}$ is derived by the reaction:

$$2\ ABTS + K_2S_2O_8 \rightarrow 2\ ABTS^{•+} + K_2SO_4 + H_2SO_4$$

Approximately 18 hours are required for the reaction to progress, as judged by the cessation of increase in absorbance of the solution – an indication that no more radical is generated.

The $ABTS^{•+}$ solution is blue-green in color. It has a characteristic absorption spectrum with absorption peaks in the visible region at 420 nm, 734 nm and 829 nm.

The interaction of $ABTS^{•+}$ with substances with radical scavenging activity in the samples leads to a decrease in its concentration, the color intensity of the solution and the measured absorbance. We performed the analysis of the serum samples at 734 nm to avoid the strong absorption at 420 nm of remaining traces of erythrocytes and haemoglobin in the serum. Extinction at this length allows testing and comparison of antioxidants.

2) Preparation of a working solution of the radical: The finished stock solution is diluted with water to obtain a working solution with an absorbance of 0.7 at 734 nm.

3) Evaluation of the interaction of the radical with potential antioxidants: The tested substance is added to 1 ml of working solution. The amount was determined so that no complete decolorization of the reaction mixture was observed after 1 hour of incubation. For the purposes of the study, the blood serum was diluted 20 times in PBS buffer and 50 microliters were added to the radical. 3 replicates were done for each sample. After one-hour incubation, the absorbance A(sample) and the absorbance A(control) of a sample containing only radical and 50 microliters of PBS buffer were measured. Mean value and SD were calculated for each sample. RSA% is calculated by the formula: RSA% = [1–A(sample)/A(control)].100 %. Complete decolorization corresponds to RSA% = 100 % and corresponds to maximum antioxidant capacity.

4) Construction of a calibration curve concentration of Trolox (the water-soluble analogue of vitamin E) – the radical scavenging effect, RSA%: The RSA% data of the Trolox referent standard solutions with different concentrations were used to construct a calibration curve with high correlation coefficient $R^2 = 0.9983$ and to estimate the total antioxidant capacity of the serum of the studied patients as µmol Trolox/µL serum - Trolox equivalent (TE). Based on the results obtained from the extinction of the samples, the effect of RSA% for the respective concentration was determined. Calculations of RSA% of the samples take into account that 1 mol Trolox captures 1.9 mol $ABTS^{•+}$ [12].

Examination of serum concentrations of Cu and Zn

Serum concentrations of bioelements were measured using a Perkin-Elmer AAnalyst 300 flame atomic absorption spectrophotometer. Prior to analysis, serum samples were diluted with bidistilled water 1:3 for copper and 1:5 for zinc, respectively, to avoid transport interference. Measurement of both elements is based on routine calibration with aqueous standard solutions of known concentration prepared by suitable dilution with bidistilled water of the stock standard [13]. The quality of the results was ensured through the implementation of internal quality control schemes, certified reference materials for the respective trace elements, and participation in external quality assessment programs.

Statistical analyses

Data obtained for each parameter are expressed as mean value ± SD. Assessment of statistical significance of differences in variables between groups was performed by analysis of variance with unpaired t-test. Significance was defined as $p < 0.05$.

RESULTS AND DISCUSSION

The first step of the experiments was to construct a calibration curve RSA% /Trolox, μmol/L to trace the radical-scavenging activity against $ABTS^{\bullet+}$ as a function of the concentration of the Trolox reference. This is an established practice for standardizing data obtained from studies in the ABTS system [14, 15]. Pooling the experimental results as Trolox equivalent concentration will allow them to be compared, if more data is obtained by other teams. We assessed the results using variance analysis and an unpaired t-test among the study groups, revealing statistical significance (Table 1).

Table 1. Average values of RSA %, $X_{average}$ ± SD

Parameter	Patients with osteopenia	Patients with osteoporosis	Control group
RSA %	67.69 ± 6.74 $p^* < 0.01$	62.46 ± 7.83 $p^* = 0.01$; $p^{**} < 0.05$	55.64 ± 2.05

p* against controls; p** against osteopenia

Table 2. Mean serum levels of Cu, Zn, Cu/Zn, μmol Trolox/μL serum, X mean ± SD

Parameter	Patients with osteopenia	Patients with osteoporosis	Control group
Number of patients	20	36	10
Age	61.15 ± 9.22 $p^* > 0.05$	63.67 ± 7.78 $p^* > 0.05$, $p^{**} > 0.05$	61.3 ± 9.96
BMI	24.42 ± 4.52 $p^* > 0.05$	23.61 ± 3.49 $p^* > 0.05$, $p^{**} > 0.05$	25.57 ± 3.42
BMD (g/cm^2)	0.77 ± 0.11 $p^* < 0.01$	0.70 ± 0.10 $p^* < 0.01$ $p^{**} < 0.05$	1.13 ± 0.12
Cu, μmol/L	23.13 ± 4.48 $p^* < 0.01$	22.89 ± 4.20 $p^* < 0.01$, $p^{**} < 0.05$	18.22 ± 2.53
Zn, μmol/L	14.61 ± 2.92 $p^* > 0.05$	13.14 ± 2.08 $p^* > 0.05$, $p^{**} < 0.05$	12.83 ± 2.24
Cu/Zn	1.63 ± 0.37 $p^* > 0.05$	1.82 ± 0.51 $p^* < 0.05$, $p^{**} > 0.05$	1.45 ± 0.17
μmol Trolox/μL	6.81 ± 0.46	6.28 ± 0.49	5.60 ± 0.11

p* against controls; p** against osteopenia

The statistical significance of the mean values of all variables, assessed through an unpaired t-test between different groups with $p < 0.05$ and $p < 0.01$, is presented in Table 2. The results obtained by the age parameter confirm the accurate selection of the age group, and the BMD data validate the appropriate grouping of individuals. Regarding BMI, the groups do not have statistically significant differences, despite the clear trend of decreased BMI in patients with osteoporosis. Statistically significant results for Cu concentration were obtained when assessing the osteopenia and osteoporosis groups ($p^{**} < 0.05$), as well as when contrasting them with the control group ($p^{*} < 0.01$).

We observed elevated serum Zn levels in the groups with decreased bone density in comparison to the control group. However, a statistically significant difference in the Zn index was identified solely between the osteoporosis and osteopenia groups ($p^{**} < 0.05$). We obtained a statistically significant difference ($p^{*} < 0.05$) only between the groups with osteoporosis and the controls for the Cu/Zn indicator, the values of which naturally change with the degree of the disease.

CONCLUSIONS

Patients with reduced bone density exhibit higher RSA% values, elevated copper and zinc concentrations, and increased Cu/Zn ratio values compared to the control group. The rise in serum levels of copper and zinc among patients with decreased bone density can be attributed to the degradation of copper and zinc, which are components of enzymes involved in bone metabolism. This degradation is triggered by an elevated level of reactive oxygen species (ROS) within cells in the context of osteoporosis. The heightened concentration of copper ions in the serum initiates secondary radical processes, subsequently boosting its antioxidant activity (AOA). In contrast, patients with normal bone metabolism maintain lower serum concentrations of Cu and Zn because their intracellular function remains intact. The reduced generation of extra radicals accounts for the lower serum AOA observed in the control group. These findings substantiate the collaborative impact of free radicals and redox-active metals, like copper, on both AOA and bone mineral density.

REFERENCES

1. 1. J. S. Kimball, J. P. Johnson, D. A. Carlson, *J. Bone Joint Surg. Am.,* **103(15)**, 1451 (2021).
2. M. Valko, K. Jomova, C. J. Rhodes, K. Kuča, K. Musílek, *Arch Toxicol.*, **90(1)**, 1 (2016).
3. D. L. de Romaña, M. Olivares, R. Uauy, M. Araya, *J. Trace Elem. Med. Biol.*, **25**, 3 (2011).
4. J. Wang, F. Xing, N. Sheng, Z. Xiang, *Osteoporos. Int.* (2023).
5. R. Sotler, B. Poljšak, R. Dahmane, T. Jukić, D. P. Jukić, C. Rotim, P. Trebše, A. Starc, *Acta Clin Croat.*, **58(4)**, 726 (2019).
6. F. Román, C. Urra, O. Porras, A. M. Pino, C. J. Rossen, J. P. Rodríguez, *J. Cell. Biochem.*, **118(3)**, 585 (2017).
7. M. Rondanelli, G. Peroni, F. Fossari, V. Vecchio, M. A. Faliva, M. Naso, S. Perna, E. Di Paolo, A. Riva, G. Petrangolini, M. Nichetti, A. Tartara, *Nutrients*, **13(3)**, 1012 (2021).
8. A. E. Bădilă, D. M. Rădulescu, A. Ilie, A. G., Niculescu, A. M. Grumezescu, A. R. Rădulescu, *Antioxidants (Basel)*, **11(2)**, 318 (2022).
9. P. P. da F. Grili, C. V. Vidigal, G. F. da Cruz, B. H. Albergaria, J. L. Marques-Rocha, T. S.S. Pereira, V. R. Guandalini, *Nutrients,* **15**, 1670 (2023).
10. R. Re, N. Pellegrini, A. Proteggente, A. Pannala, M. Yang, C. Rice-Evans, *Free Radic. Biol. Med.*, **26(9-10)**, 1231 (1999).
11. V. Georgieva, N. Hristova-Avakumova, D. Tzoneva, A. Todorov, V. Hadjimitova, *Comptes rendus de l'Académie Bulgare des Sciences*, **68 (8)**, 1007 (2015).
12. M. J. Arts, G. R. Haenen, H. P. Voss, A. Bast, *Food Chem Toxicol.*, **42(1)**, 45 (2004).
13. R. Tomova, S. Asenova, B. Atanasova, K. Tzoneva, M. Slavova, *Bulgarian Chemical Communications*, **52** (1), 76 (2020).
14. I. R. Ilyasov, V. L. Beloborodov, I. A. Selivanova, R. P. Terekhov, *Int. J. Mol. Sci*., **21**, 1131 (2020).
15. Y. Lang, N. Gao, Z. Zang, X. Meng, Y. Lin, S. Yang, Y. Yang, Z. Jin, B. Li, *Journal of Future Foods*, **3**, 193 (2024). https://doi.org/10.1016/j.jfutfo.2023.07.002

Formation of environmentally friendly protective Ce_2O_3-CeO_2 conversion coatings on Al, modified by phosphate layers: chemical and electrochemical characterization

R. Andreeva[1], A. Tsanev[2], D. Stoychev[1]*

[1]*Institute of Physical Chemistry "Acad. R. Kaischew" – BAS, Acad. G. Bonchev Str. Bl. 11, Sofia 1113, Bulgaria*
[2]*Institute of General and Inorganic Chemistry – BAS, Acad. G. Bonchev Str. Bl. 11, Sofia 1113, Bulgaria*

Received: May 10, 2022; Accepted: November 21, 2023

Conversion ceria coatings were deposited on substrates of Al-1050 in a solution containing $CeCl_3 \times 7H_2O$ and $CuCl_2 \times 2H_2O$. The post-treatment of as deposited coatings was realized in phosphate-containing solutions: 0.08 M Na_3PO_4 or 0.22 M $NH_4H_2PO_4$. The XPS characterization of the surface of samples was carried out on an AXIS Supra electron-spectrometer (KratosAnalytical Ltd.). The electrochemical investigations and determination of the basic corrosion parameters (E_{cor}, i_{cor}, E_{pit}, E_{OCP}, Rp, CR, etc.) for the studied systems were carried out on a Gamry Interface 1000 (EISSFR Analyzer EIS300). Based on the XPS investigations, it was ascertained that there is a substantial influence of the "pre-treatment" and "post-treatment" operations on the chemical composition and chemical state of the elements on the samples` surface. It is expressed by a strong decrease in the concentration of Al_2O_3 and Ce_2O_3+CeO_2 components in the ceria coatings at the expense of formation of $AlPO_4$ and AlOOH, $CePO_4$, as well as PO_3^-, P_2O_5 and P_4O_{10} compounds with Al and Ce.

The comparison of the results of Rp values and concentrations of Ce^{3+}/Ce^{4+}, Al and P shows that the changes in Rp and quantity of Ce^{4+} and P on the surface of the studied samples are directly related. The supposed and proved formation of low-soluble corrosion products on the surface of the studied systems and accomplished synergic effect of protective action by the formed cerium and aluminum oxides/phosphates layers determine the increase of the Rp and decrease of i_{cor} and CR, respectively. It was also concluded that the mixed conversion layers are a more effective barrier for the chloride ions diffusion to the metal surface and increase the corrosion resistance of Al 1050 to pitting and general corrosion.

Keywords: aluminium, corrosion, ceria/phosphate conversion coatings

INTRODUCTION

The attention in the application of ceria conversion coatings deposition on Al and its alloys is driven by the potential opportunity to replace highly toxic and carcinogenic Cr^{6+}-containing conversion coatings [1]. The latter, though providing excellent corrosion protection for Al surfaces [2], need to be replaced with ecological alternatives, according to EU directives [3, 4]. Conversion layers based on lanthanide metals are considered among the most promising for this purpose [1, 5-12].

We have previously reported our findings regarding the effects of pre-treatment operations of Al substrates, covered with conversion ceria coatings (CCOC) and additionally post-treated in different types of phosphate-containing solutions (leading to the formation of thin phosphate layers (PhL(s)) on the surface chemical composition of the so formed Al/CCOC/PhL(s) systems. Based on the XPS investigations, a strong decrease in the concentration of Al_2O_3 and Ce_2O_3+CeO_2 components in CCOC at the expense of the formation of $AlPO_4$ and AlOOH, $CePO_4$ as well as PO_3^-, P_2O_5 and P_4O_{10} compounds of Al and Ce [13] was established.

Having in mind these changes in the qualitative and quantitative composition on the surface of the studied systems, the aim of the present study was to obtain, include and comment additional corroborative in detail information about the influence of both "pre-treatment" and "post-treatment" operations connected to formation of CCOC and PhL(s) with improved corrosion-protective ability of Al 1050.

EXPERIMENTAL

Layers of cerium oxide(s) (obtained by chemical immersion treatment) were deposited on substrates of "technically pure" Al 1050 (containing 0.40% Fe, 0.25% Si, 0.05% Mn, 0.05% Cu, 0.07% Zn, 0.05% Mg) selected as a model object by us as it finds wide range of applications as a construction material.

The studied samples of dimensions 2.5×2.5×0.1 cm, were cut out of rolled Al 1050 sheets. Their pre-treatment, as described in [14], involved degreasing in organic solvent and etching in 1.5 M NaOH (the abbreviator of these samples in the further text is "$Al_{(NaOH)}$") or etching in 1.5 M NaOH and consecutive activation in 5 M HNO_3 (acidic deoxidation) at room temperature (abbreviator

* To whom all correspondence should be sent:
E-mail: stoychev@ipc.bas.bg

"$Al_{(NaOH\&HNO_3)}$"). After each one of these operations, the obligatory standard rinsing of the samples was made with distilled water.

The formation of CCOC was implemented in a solution containing 0.5 M $CeCl_3 \times 7H_2O$ (Alfa Aesar) + 1×10^{-5} M $CuCl_2 \times 2H_2O$ (Merck). *No H_2O_2, or other type of oxidizing agent, was added*. The chemical process was carried out at pH = 4.1, temperature of 25 ºC and time interval of deposition till 120 min as described in [15-18]. The abbreviators of these samples covered with CCOC, depending of pretreatment operations, are: "$Al_{(NaOH)}/CCOC_{(Ce+Cu)}$" or "$Al_{(NaOH\&HNO_3)}/CCOC_{(Ce+Cu)}$". The thickness of the deposited CCOCs was 110 nm for the $Al_{(NaOH)}/CCOC_{(Ce+Cu)}$ system and 212 nm for the $Al_{(NaOH\&HNO_3)}/CCOC_{(Ce+Cu)}$ system (measurements based on XPS in-depth profiles, which allow to track changes of the ratio between the elements Ce, Al and O in the depth of $CCOC_{(Ce+Cu)}$ [18]). After formation of CCOC, the specimens were rinsed fully in distilled water, dried at room temperature and kept in a desiccator (if it is necessary) for subsequent investigation or phosphate conversion treatment.

The post-treatment of as deposited on Al substrate thin ceria coatings, aiming at an additional formation of phosphate layers (PhL(s)) on them, was implemented in two types of phosphate-containing solutions: 0.08 M Na_3PO_4 or 0.22 M $NH_4H_2PO_4$ (Alfa Aesar), applied and studied in details as described in [19-22]. The working solutions were used at pH = ~4.4, temperature of deposition 85ºC and time of immersion 5 min. For these cases the abbreviators of the as prepared samples are: "$Al_{(NaOH)}/CCOC_{(Ce+Cu)}/PhL_{(Na_3PO_4)}$" or "$Al_{(NaOH)}/CCOC_{(Ce+Cu)}/PhL_{(NH_4H_2PO_4)}$" and "$Al_{(NaOH\&HNO_3)}/CCOC_{(Ce+Cu)}/PhL_{(Na_3PO_4)}$" or "$Al_{(NaOH\&HNO_3)}/CCOC_{(Ce+Cu)}/PhL_{(NH_4H_2PO_4)}$", respectively.

The X-ray photoelectron spectroscopy (XPS) aimed the investigation of the chemical composition and chemical state of the elements on the surface of the studied samples was studied on AXIS Supra electron-spectrometer (Kratos Analitycal Ltd.) using monochromatic AlKα radiation, with a photon energy of 1486.6 eV. The analysed area was 0.75 mm^2 as described in [13]. The chemical composition (in at. %) and state of elements of cerium-based CCOC on Al 1050, with different contents of $Ce^{3+}(Ce_2O_3)$ and $Ce^{4+}(CeO_2)$, was examined and determined for the as deposited samples before and after their phosphate post-treatment in solutions of Na_3PO_4 or $NH_4H_2PO_4$, as well as after long exposure (up to 168/336 h) in model corrosion media.

The corrosion behavior of the samples was studied in a standard three-electrode cell (equipped with a reference calomel electrode) in 0.1 M NaCl ("p.a." Merck) model (open to air) corrosion medium (CM) at 25ºC, frequently used for corrosion tests of Al protected by ceria conversion coatings. The anodic and cathodic polarization curves were obtained by means of a potentiostat/galvanostat Gamry Interface 1000, as described in [18]. Open circuit potential (OCP) transients and corrosion current (i_{corr} at E_{pit} for Al 1050 = –0.500 V) transients vs. time were plotted in the same CM. The investigations of the time-depending changes of polarization resistance (Rp, $\Omega m.cm^2$), as well as corrosion rate (CR, μm/year) of studied samples (as deposited and after definite time of exposure (up to 168/336 h) in CM) were carried out on Gamry Interface 1000 (Software and Frequency Response Analyzer EIS300). All potentials were referenced to Ag/AgCl reference electrode (SCE). The scan range was ± 15 mV relative to corrosion potential (E_{cor}) and the scanning was carried out in the anodic direction. The initial delay was 15 minutes, and the temperature was 25 C ± 0.5ºC. The specimen's area exposed to corrosion in CM was 1.54 cm^2. The reproducibility of all tests was an average of 3 samples per sample type.

RESULTS AND DISCUSSION

XPS investigations

The results from the XPS studies of the chemical composition and chemical state of the elements for the studied systems are represented in Figs. 1 - 3 and in Tables 1, 2. The comparison of the compositions of samples, whose substrates have been pretreated in NaOH, with those, whose substrates have been pretreated in both NaOH and HNO_3, shows that in case of pretreatment only with NaOH, the concentration of Al (Al oxide/hydroxide, respectively) on the surface is high (Table 1). In the case of as-deposited CCOC (Table 1, samples a and d, obtained in Ce^{3+} and Cu^{2+} containing conversion solution) it is 21.2 % and 6.3 %, respectively; for the couple of samples, covered with CCOC and post-treated in Na_3PO_4 (Table 1, samples b and e) it is 10.7 and 0.5 %, respectively while for the samples covered with CCOC and post-treated in $NH_4H_2PO_4$ (Table 1, samples c and f) it is 7.6 and 4.8 %, respectively. The Ce concentration (Ce_2O_3 and CeO_2, respectively) change for the same samples is inverted. This change is also inverted for the concentration of P on the COCC deposited phosphate layers (Table 1 (b and e), and (c and f).

These „inverted" relationships are connected to forming cathode areas of electroless-deposited copper on the Al surface. They are deposited preferentially on the aggregates of Al3Fe intermetallic phase of Al 1050 [14], which gain eminence after additional treatment in HNO_3 (Table 1 (e and f). It is important to note the considerable result presented in Table 1 about the concentration change of Ce^{4+} (CeO_2) depending on the pretreatment of the Al support. This unambiguously shows that copper deposited on the Al surfaces catalyses forming of CCOC (Table 1) [17, 18]. Below, these results and conclusions are exposed and commented in detail.

Table 1. Chemical composition and chemical state of the elements on the surface of the studied samples.

Sample	O	Al	Ce_{total}, (Ce^{3+}+Ce^{4+})	Cu	P	Ce^{4+}, % of Ce_{total}
a-$Al_{(NaOH)}$/$CCOC_{(Ce+Cu)}$	71.9	21.2	6.9	0	-	79
b-$Al_{(NaOH)}$/$CCOC_{(Ce+Cu)}$/PhL_{Na3PO4}	73.7	10.7	2.8	0	12.9	23
c-$Al_{(NaOH)}$/$CCOC_{(Ce+Cu)}$/$PhL_{NH4H2PO4}$	76.3	7.6	1.4	0.7	14.1	11
d-$Al_{(NaOH\&HNO3)}$/$CCOC_{(Ce+Cu)}$	75.7	5.9	17.2	1.2	-	85
e-$Al_{(NaOH\&HNO3)}$/$CCOC_{(Ce+Cu)}$/PhL_{Na3PO4}	70.1	0.5	10.0	2.6	16.8	0
f-$Al_{(NaOH\&HNO3)}$/$CCOC_{(Ce+Cu)}$/$PhL_{NH4H2PO4}$	75.3	4.8	4.5	0.8	14.7	35

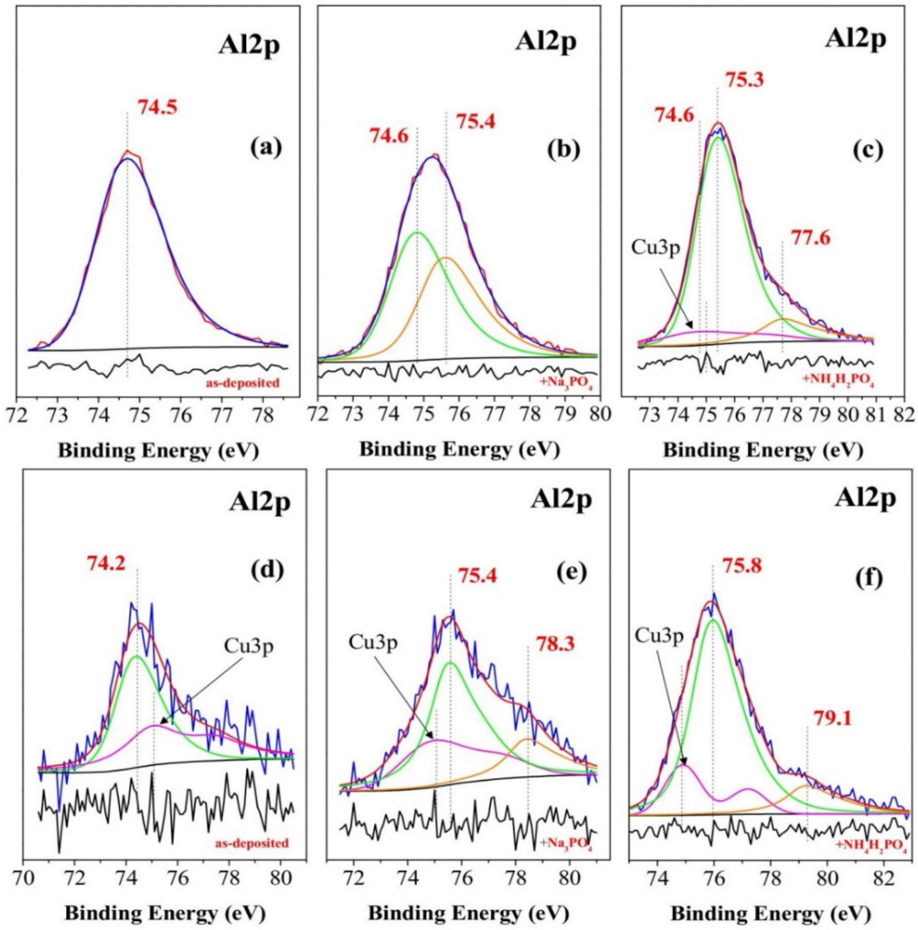

Fig. 1. XPS Al2p spectra obtained for as-deposited CCOC (a, d) and after its post-treatment in Na_3PO_4 (b, e) or $NH_4H_2PO_4$ (c, f). The peak contributions are colored in green and orange whereas their sum is marked in red. The difference between experimental and deconvoluted spectra is indicated in the inset below. Violet peak(s) on Figs. 1(c – f) show the presence of copper (Cu3p) which is a component of CCOC.

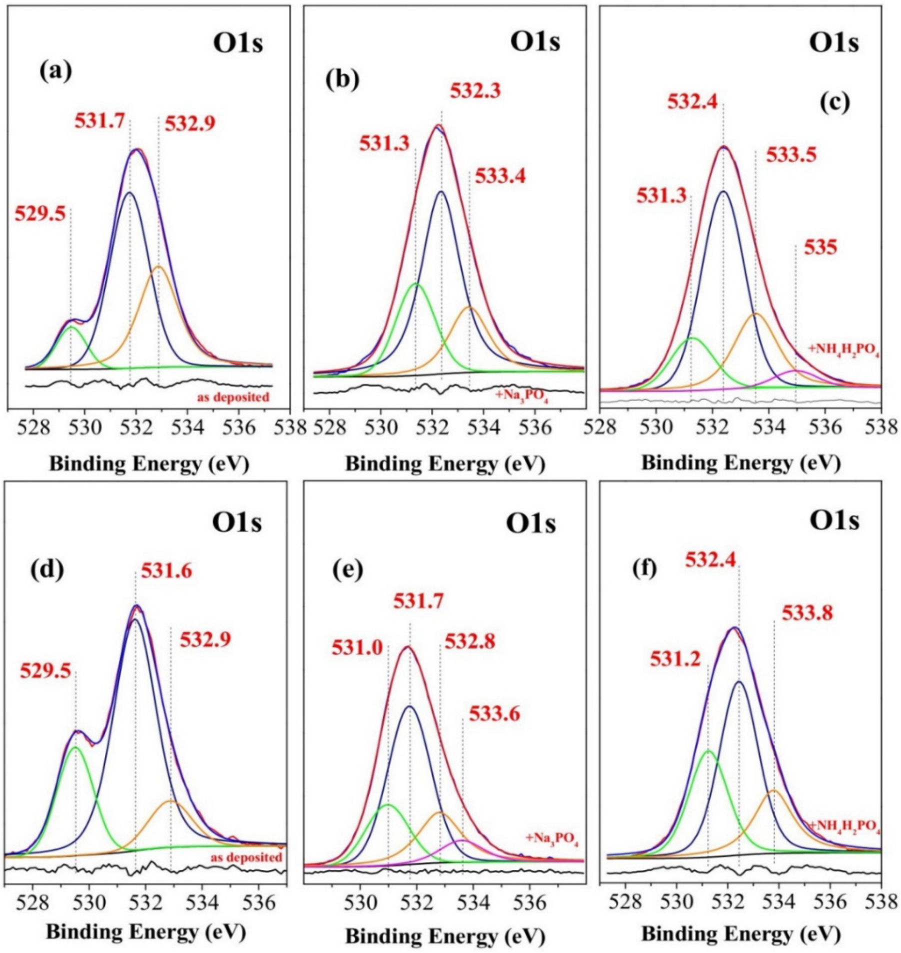

Fig. 2. XPS O1s spectra obtained for as-deposited CCOC (a, d) and after its post-treatment in Na_3PO_4 (b, e) or $NH_4H_2PO_4$ (c, f). The peak contributions are colored in green, orange and pink whereas their sum is marked in red. The difference between experimental and deconvoluted spectra is indicated in the inset below.

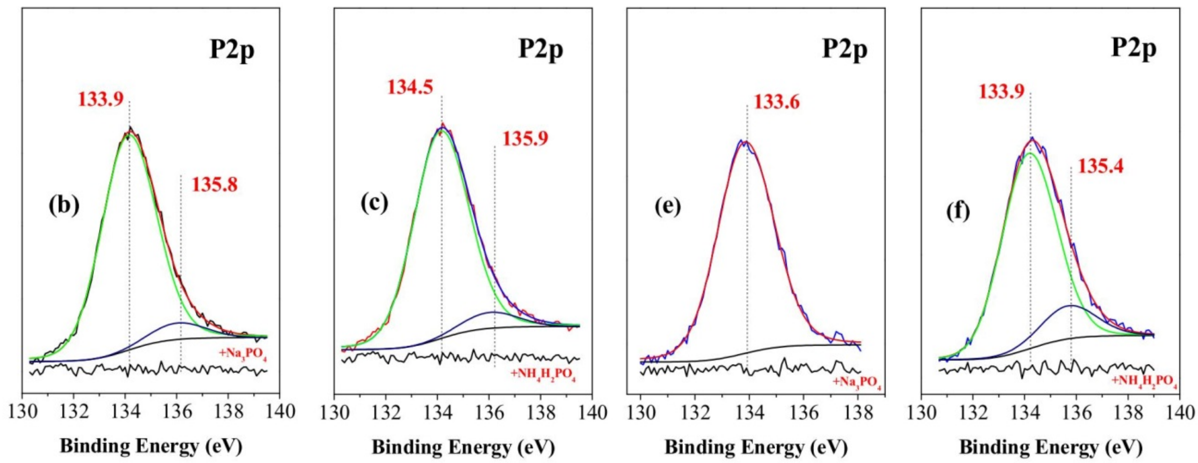

Fig. 3. XPS P2p spectra obtained for CCOC after its post-treatment in Na_3PO_4 (b, e) or $NH_4H_2PO_4$ (c, f). The peak contributions are colored in green and blue whereas their sum is marked in red. The difference between experimental and deconvoluted spectra is indicated in the inset below.

Fig. 1 presents the deconvoluted peaks of the characteristic Al2p-spectra for the studied samples. In the case of as-deposited $CCOC_{(Ce+Cu)}$ (Fig. 1a) a single peak was registered at 74.2 – 74.5 eV, revealing the presence of Al on the surface only in the form of Al_2O_3. The deconvolution of O1s – (Fig. 2d) confirms this fact. The spectra of O1s consist of three peaks. The one with the lowest energy at 529.5 eV corresponds to oxygen species bonded in the crystal lattice of the CeO_2 [24]. The peaks, positioned at 531.6-531.7 eV, correspond to oxygen bound in Al_2O_3 [24]. In the case of sample a-$Al_{(NaOH)}$/$CCOC_{(Ce+Cu)}$, the ratio between the areas of the Al2p–peak and the respective O1s–peak actually corresponds to the stoichiometric ratio 2:3. In the case of sample d-$Al_{(NaOH\&HNO3)}$/$CCOC_{(Ce+Cu)}$ a large excess of oxygen is registered, which could be due to the effect of screening by oxygen atoms (in the system only Al and Ce are present, while the area for just this O1s-peak is much larger than the stoichiometric quantity, calculated on the basis of the areas of Ce3d and Al2p peaks).

It is important to note that the registered Ce3d-spectra are characterized by a complex structure due to strong final photoelectron effects involving the influence of the oxygen ligands from chemical bonds with Ce [25]. According to [25] we can calculate the relative concentrations of Ce^{4+} and Ce^{3+} ions with respect to the total amount of Ce. These results are shown in Table 1. The highest relative concentrations of Ce^{4+} ions as 79% and 85% are observed in the samples a-$Al_{(NaOH)}$/$CCOC_{(Ce+Cu)}$ and d-$Al_{(NaOH+HNO3)}$/$CCOC_{(Ce+Cu)}$, respectively. This is a very useful and important information, in view of the established influence of Ce^{4+} and Ce^{3+} (having in mind the lower solubility of CeO_2 in comparison with the soluble Ce_2O_3) on the corrosion-protection ability of CCOC [18].

The spectra of Al2p of samples, treated with Na_3PO_4, are presented in Fig. 1 (b and e). In the case of sample b-$Al_{(NaOH)}$/$CCOC_{(Ce+Cu)}$/PhL_{Na3PO4} (pretreated in NaOH) - Fig. 1b - two peaks appear in the spectrum of Al2p at 74.6 and 75.4 eV. The peak, located at 74.6 eV, can be associated with a mixture of Al_2O_3 and non-stoichiometric Al-hydroxide. The other peak, positioned at 75.4 eV can be attributed to the presence of $AlPO_4$ [26]. The quantitative ratio between the two phases is approximately 1:1. In contrast to it, the spectrum of Al2p for the sample e-$Al_{(NaOH\&HNO3)}$/$CCOC_{(Ce+Cu)}$/ PhL_{Na3PO4}, treated in advance in NaOH & HNO_3 and post-treated in Na_3PO_4 has the lowest intensity and noise due to the thick coating of the sample, covered with phosphate layer (Fig. 1e [23]). A deconvolution allows to see a peak at 75.4 eV, an indication about the presence mainly of $AlPO_4$, whereupon presence of nonstoichiometric AlOOH [27] is a possibility.

The deconvolution of the O1s peaks for both samples (Fig. 2 (b and e) confirms the above-made conclusions. The spectrum of O1s for both samples is deconvoluted into two basic peaks – a first one at 531.0 – 531.3 eV, corresponding to oxygen in the lattice of Ce^{3+}. The second one, located at 531.7 and at 532.3 eV corresponds to oxygen in the crystal lattice of metal phosphate. The other peaks at 532.8, 533.4 and 533.6 eV could be attributed to the presence, respectively, of hydroxyl groups, crystallized water and H_3O^+-groups. Their quantities were estimated based on the integral areas of their peaks [23].

The deconvolution of the P2p peaks (Fig. 3) shows that in both types of phosphate treatment metal phosphate phases are formed [28]. In both samples the phosphorus peak is positioned at 133.6 and 133.9 eV. In the case of the sample, pretreated only in NaOH, these phosphates cover the surface in a thicker way. In this sample a second phosphorus peak of lower intensity at 135.8 eV is also present, which could correspond to the presence of phosphorus compounds from the type of P_2O_5 or P_4O_{10} [29].

The concentration of Ce^{4+} calculated from the spectrum of Ce3d (Table 1), shows that the phosphate treatment with Na_3PO_4 decreases the concentration of Ce^{4+} in the conversion layer [29]. Thereupon, in the sample, pretreated in NaOH, the content of Ce^{4+} is 23% of the total amount of cerium oxide, while in the case of the sample, pretreated in NaOH&HNO_3 Ce^{4+} is practically absent (Table 1).

For the samples, pretreated in NaOH or in NaOH & HNO_3, followed by post-treatment with $NH_4H_2PO_4$, the Al2p spectra are given in Fig. 1 (c and f). Here, in both samples one registers a single peak, located at 75.3 – 75.8 eV. This peak is characteristic for Al, bonded with phosphate groups (P-O-Me) [30]. The second peaks for both samples, respectively at 77.6 and at 79.1 eV, are due to the presence of particles with different sizes. Peaks, characteristic for oxides or hydroxides of aluminum are missing. At the same time the characteristic peaks of O1s for these two samples (Fig. 2 (c and f), are splitted into three basic peaks. The peak at 531.3 eV can be associated with the presence of oxygen, bonded in the lattice of Al_2O_3 and Ce_2O_3 [29]. The second peak at 533.4 eV can be attributed again to the presence of oxygen, involved in P-O-Me – bonding [24]. The third peak, at approximately 533.5, 533.8 eV, is due to the presence of adsorbed or crystallized water.

The P2p-peak of the sample, pretreated in NaOH and post-treated in Na_3PO_4, consists of two components (Fig. 3b). The one, having the highest intensity at 133.9 eV, is due to the presence of PO_3^- - groups. The second one at 135.8 eV again can be associated with the presence of phosphorus compounds of the type of P_2O_5 or P_4O_{10} [31]. The spectrum of the sample, pretreated in NaOH & HNO_3 and post-treated in Na_3PO_4, consists of one single P2p - peak at 133.6 eV (Fig. 3e), due to PO_4^{3-} – groups. Comparing the peak areas for P2p, Al2p and Ce3d shows that the quantity of elemental phosphorus is much higher than needed for the formation of stoichiometric phosphate compounds of aluminum and cerium [23].

The analysis of the XPS spectra of the systems under consideration allows to draw a conclusion about the composition of the most probable phases, formed on the aluminum surface. They are listed in Table 2.

Table 2. The most probable phases on the aluminum surface according to the analysis of the XPS spectra.

Sample	Al	Ce	P
a-$Al_{(NaOH)}$/$CCOC_{(Ce+Cu)}$	Al_2O_3	Ce_2O_3+ CeO_2	-
b-$Al_{(NaOH)}$/$CCOC_{(Ce+Cu)}$/PhL_{Na3PO4}	$AlPO_4$, AlOOH	Ce_2O_3+ CeO_2 $CePO_4$	PO_4^{3-} P_2O_5 (P_4O_{10})
c-$Al_{(NaOH)}$/$CCOC_{(Ce+Cu)}$/$PhL_{NH4H2PO4}$	$AlPO_4$	$CePO_4$	PO_3^- P_2O_5 (P_4O_{10})
d-Al(NaOH&HNO_3)/$CCOC_{(Ce+Cu)}$	Al_2O_3	Ce_2O_3+ CeO_2	-
e-Al(NaOH&HNO_3)/ $CCOC_{(Ce+Cu)}$/PhL_{Na3PO4}	AlOOH $AlPO_4$	Ce_2O_3+ CeO_2 $CePO_4$	PO_4^{3-}
f-Al(NaOH&HNO_3)/ $CCOC_{(Ce+Cu)}$/$PhL_{NH4H2PO4}$	$AlPO_4$	$CePO_4$	PO_4^{3-} P_2O_5 (P_4O_{10})

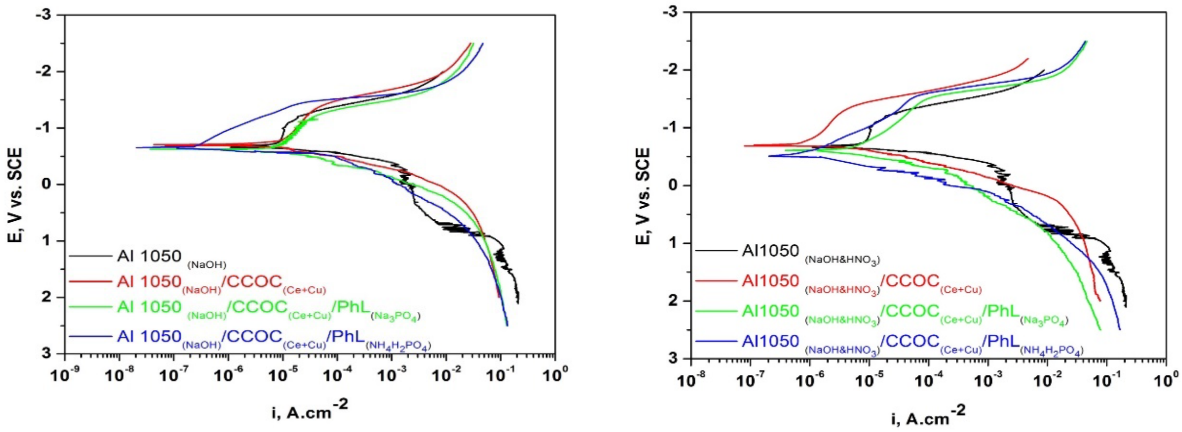

(a) (b)

Fig. 4. Tafel polarization curves of the studied systems, Al substrate(s) of which are pretreated in 1.5 M NaOH (a) or in 1.5 M NaOH and 5 M HNO_3 (b).

Table 3. Electrochemical parameters of the studied systems determined from potentiodynamic polarization E-lg i curves: i_{cor} – corrosion current; E_{cor} – corrosion potential; Z – degree of protection.

Sample	i_{cor}, A.cm^{-2}	E_{cor}, V	Z, %
$Al_{(NaOH)}$	8.0×10^{-6}	-0.660	
a-$Al_{(NaOH)}$/$CCOC_{(Ce+Cu)}$	1.0×10^{-6}	-0.695	87.5
b-$Al_{(NaOH)}$/$CCOC_{(Ce+Cu)}$/$PhL_{(Na3PO4)}$	6.3×10^{-6}	-0.612	21.3
c-$Al_{(NaOH)}$/$CCOC_{(Ce+Cu)}$/$PhL_{(NH4H2PO4)}$	2.4×10^{-7}	-0.649	97.0
d-$Al_{(NaOH\&HNO3)}$/$CCOC_{(Ce+Cu)}$	4.0×10^{-7}	-0.700	95.0
e-$Al_{(NaOH\&HNO3)}$/$CCOC_{(Ce+Cu)}$/$PhL_{(Na3PO4)}$	3.5×10^{-6}	-0.586	56.3
f-$Al_{(NaOH\&HNO3)}$/$CCOC_{(Ce+Cu)}$/$PhL_{(NH4H2PO4)}$	8.9×10^{-7}	-0.531	88.9

The results shown above give us the reason to draw the conclusion, that this way of pre-treatment for Al substrate and the application of additional post-treatment of the CCOC deposited on it in Na_3PO_4 or $NH_4H_2PO_4$ lead to the formation of PhL(s) on the surface of the CCOC. This conclusion has been reached also by some other authors. For instance, according to [27], in case of similar treatment, the surface of Al 2024-T3 was completely phosphated. It is logical to suppose that the additional PhL(s) being formed will exert synergistic effect, from corrosion-protection point of view, together with CCOC in regard to the Al substrate.

Electrochemical and corrosion investigations of the studied systems

Polarization investigations. Fig. 4 presents the polarization curves in coordinates E-lg i, obtained in 0.1 M NaCl for samples having formed CCOC after preliminary activation of the Al substrate in a solution of NaOH (Fig. 4a) and two-stage preliminary treatment in solutions of NaOH and HNO_3 (Fig. 4b), sealed in solutions of Na_3PO_4 or $NH_4H_2PO_4$, respectively.

One can see in Fig. 4a that after the pre-treatment of the aluminum substrate in a solution of NaOH, the sealing of the samples in a solution of $NH_4H_2PO_4$ (the system $Al_{(NaOH)}/CCOC_{(Ce+Cu)})/\ PhL_{(NH4H2PO4)})$ determines the strong influence on the kinetics of the cathode reaction of reduction of oxygen in the CM, which is reflected on the enhancement of the corrosion protection degree Z reaching 97 % (Table 3). When the preliminary activation of the aluminum substrate is carried out in a solution of NaOH and HNO_3 (Fig. 4b), the post-treatment in both types of phosphate solutions leads to a substantial shift of the anodic potentiodynamic curves towards more positive potentials and lower values of the corrosion currents under the conditions of anodic polarization (Table 3). In this case, the treatment in a solution of $NH_4H_2PO_4$ exerts a more strongly expressed barrier effect in regard to the processes of anodic dissolution of the aluminum substrate. A characteristic feature of the anodic potentiodynamic curves is the absence of a zone of passive state, which justifies the consideration that the corrosion potential of the studied systems coincides with the potential of pitting formation. This coincidence is a prerequisite for the local character of the corrosion process under the conditions of stationary corrosion. This means that the definite protection degree Z (Table 3) obtained by treatment of the samples in a solution of $NH_4H_2PO_4$ characterizes both the protection from total corrosion and from local corrosion. The results obtained show that the combination of phosphate and ceria conversion layers are not only static barrier coatings, but they also change the kinetics of the conjugated electrochemical reactions characterizing the corrosion process in Cl^- containing media, i.e. they determine the electrochemical protection of the Al substrate.

These results, obtained under conditions of external polarization (potentiodynamic polarization - PDP), inform on the kinetics of the related corrosion process reactions, but do not fully characterize them since the real corrosion processes occur at the open circuit potential (OCP/E_{OCP}). At the same time, it is shown that the change in OCP as a function of immersion time can be used to monitor the chemical stability and corrosion process of the Al alloys [32]. Although OCP does not provide any direct information on the corrosion kinetics, it suggests the corrosion susceptibility [33]. To gain the needed additional insights, we conducted investigations of self-occurring corrosion processes in the systems of interest at OCP and at the potential of pitting corrosion (E_{pit}), by following:

- the change in OCP values monitored through E_{OCP} *vs*. time plot**;**
- the changes in anodic current (i_a) transients at E_{pit};
- the changes in Rp as a function of samples exposure time in CM (in OCP conditions) and the related change in CR.

Open circuit potential measurements. The bare $Al_{(NaOH)}$ and the coupons of the systems $Al_{(NaOH)}/PhL_{(Na3PO4)}$; $Al_{(NaOH)}/PhL_{(NH4H2PO4)}$; $Al_{(NaOH)}/CCOC_{(Ce+Cu)}$; $Al_{(NaOH)}/CCOC_{(Ce+Cu)}/PhL_{(Na3PO4)}$ and $Al_{(NaOH)}/CCOC_{(Ce+Cu)}/PhL_{(NH4H2PO4)}$ were immersed in CM for 1 hour. During this time of immersion, the changes in E_{OCP} *vs.* time for these samples were recorded and are given in Fig. 5a.

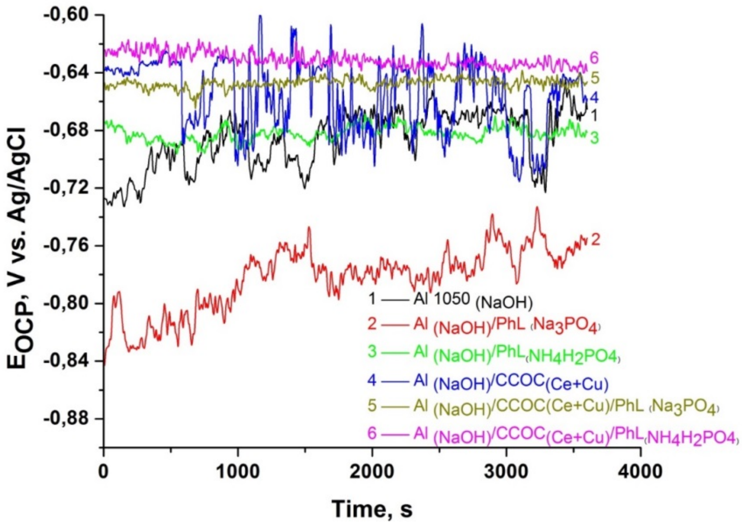

(a)

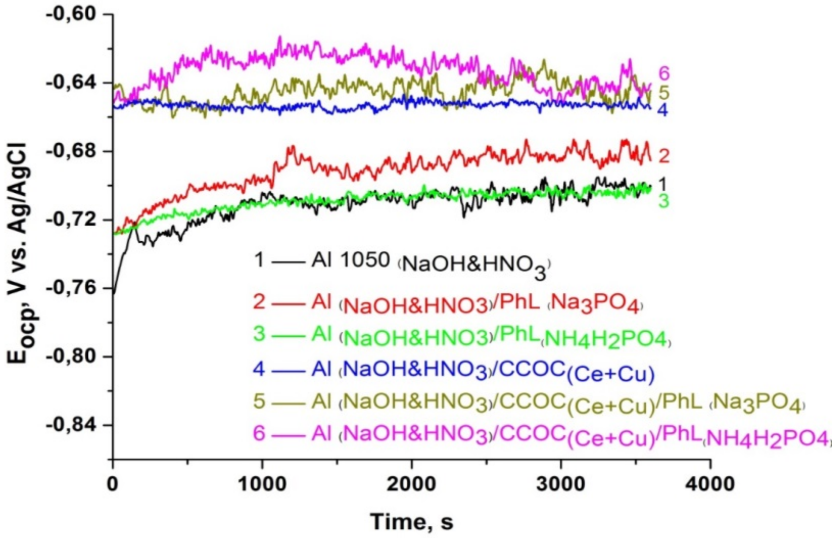

(b)

Fig. 5. OCP *vs*. time plots during immersion in 0.1M NaCl of the studied systems, Al substrate(s) are pretreated in 1.5 M NaOH (a) or in 1.5 M NaOH and 5 M HNO_3 (b).

For the bare $Al_{(NaOH)}$, the registered average value for E_{OCP} is ~ -686 mV with big fluctuations (black curve 1) indicating the dissimilarities in potential of different intermetallic inclusions, metastable pit formation and re-passivation in the CM. For the system $Al_{(NaOH)}/PhL_{(Na3PO4)}$ (red curve 2), there was a large decrease in E_{OCP} (initially to ~ -820 mV, and it started to stabilize after 1500-rd s to ~ -780 mV) which could be due to the progress of heterogeneous reactions. These effects could be due to the saturation of the $AlPO_4$ surface with Cl^-/H_2O. The fluctuation in E_{OCP} also could be due to the partial incorporation of the aqua ion and formation of Al oxides/hydroxides. When it was exposed to the aggressive environment, the corrosive Cl^- ions penetrated through the active region and lead to more negative E_{OCP}. $Al_{(NaOH)}/PhL_{(NH4H2PO4)}$ coupon (the green curve 3) showed position and fluctuations in the E_{OCP} similar to that for the bare $Al_{(NaOH)}$. E_{OCP} fluctuations are most notable for the $Al_{(NaOH)}/CCOC_{(Ce+Cu)}$ system (blue curve 4), with an average E_{OCP} value of ~ -665 mV. However, when $Al_{(NaOH)}/CCOC_{(Ce+Cu)}$ is sealed in a solution of Na_3PO_4 (the $Al_{(NaOH)}/CCOC_{(Ce+Cu)}/PhL_{(Na3PO4)}$ system – dark yellow curve 5) - E_{OCP} shifts further in a positive direction (to ~ -647 mV). Post-treatment of $Al_{(NaOH)}/CCOC_{(Ce+Cu)}$ in $NH_4H_2PO_4$ (the $Al_{(NaOH)}/CCOC_{(Ce+Cu)}/PhL_{(NH4H2PO4)}$ system - magenta curve 6) brings an even greater shift in E_{OCP} (to ~ -630 mV), which is of ~ 55 mV more positive than that of bare $Al_{(NaOH)}$. This shift in E_{OCP} distinguishes the $Al_{(NaOH)}$/$CCOC_{(Ce+Cu)}$/$PhL_{(NH4H2PO4)}$ system as the most stable one from a corrosion-protection perspective. These conclusions are in good agreement with the noted effective increase in the protective effect of CCOC following the additional deposition of PhLs, including mixed $AlPO_4$ and AlOOH, $CePO_4$ as well as PO_3^-, P_2O_5 and P_4O_{10} compounds with Al and Ce marked and discussed above.

It is seen on Fig. 5b that during the immersion, the course and changes in OCP for the bare $Al_{(NaOH\&HNO3)}$ sample (black transient 1) and the coupon of the system $Al_{(NaOH\&HNO3)}$/$PhL_{(NH4H2PO4)}$ (green transient 3) practically coincide at about -0.705 V. A small displacement in positive direction (to ~ -0.685 V) is observed for the system $Al_{(NaOH\&HNO3)}$/$PhL_{(Na3PO4)}$ (red transient 2). The consecutive increase for the values of E_{OCP} have been observed for: the covered with CCOC Al substrate (the system $Al_{(NaOH\&HNO3)}$/$CCOC_{(Ce+Cu)}$ (blue transient 4)) – to ~ - 0.655 V and post-treated in Na_3PO_4 or $NH_4H_2PO_4$ $Al_{(NaOH\&HNO3)}$/$CCOC_{(Ce+Cu)}$ system - the mixed systems $Al_{(NaOH\&HNO3)}$/ $CCOC_{(Ce+Cu)}$/$PhL_{(NH4H2PO4)}$ (dark yellow transient 5) – to ~ -0.645 V and $Al_{(NaOH\&HNO3)}$/$CCOC_{(Ce+Cu)}$/ $PhL_{(NH4H2PO4}$ (magenta transient 6) – to ~ -0.640 V, respectively. The fluctuations registered practically for all studied systems indicate,–(similar to that on Fig. 5a) dissimilarities in potential of different intermetallic inclusions, metastable pit formation and re-passivation in the CM. Also, the fluctuation in OCP could be due as well to the partial incorporation of the aqua ion and formation of Al oxides/hydroxides. When the samples have been exposed to the aggressive environment, the corrosive ions penetrated through the active regions and lead to more negative OCP.

Totally, the average change of E_{OCP} in positive direction under the action of phosphate post-treatment of the CCOC is ~ 0.055 V. This positive shift (in the area of E_{OCP} from ~ -0.705 to ~ -0.640 V vs. Ag/AgCl) compared to the bare $Al_{(NaOH\&HNO3)}$ indicated the effective incorporation and stabilization of the phosphate modified systems.

Chronoamperometric investigations. In these investigations, polarizing the samples anodically at E_{pit} (–0.500 V *vs*. SCE), we aimed to approach to a maximal extent the actual corrosion process, respectively to characterize corrosion in view of pitting corrosion, which is a basic characteristic of aluminum and its alloys in Cl^--containing CM -[19, 34]. Based on the course of the registered curves we could judge the character of the corrosion attack and the appearance of pitting damages. Fig. 6 presents the results of the studied samples. On Fig. 6a we observe that for the Al substrate ($Al_{(NaOH)}$) the corrosion current density is sharply increased (until reaching the ~180-th second of exposure), whereupon the surface film on the Al is disrupted (Fig. 6a, curve 1), which is a prerequisite for the appearance and development of pitting corrosion during the interaction with the CM. After breaking through the passive film, there starts a process of local corrosion characterized by values of the anodic current (i_a) and current oscillations specific for it, owing to unstable pittings which are repassivated/activated. Similar behavior is also observed for the current transients of the $Al_{(NaOH)}$/$PhL_{(Na3PO4)}$ and $Al_{(NaOH)}$/$PhL_{(NH4H2PO4)}$ systems (Fig. 6a, curves 2, 3).

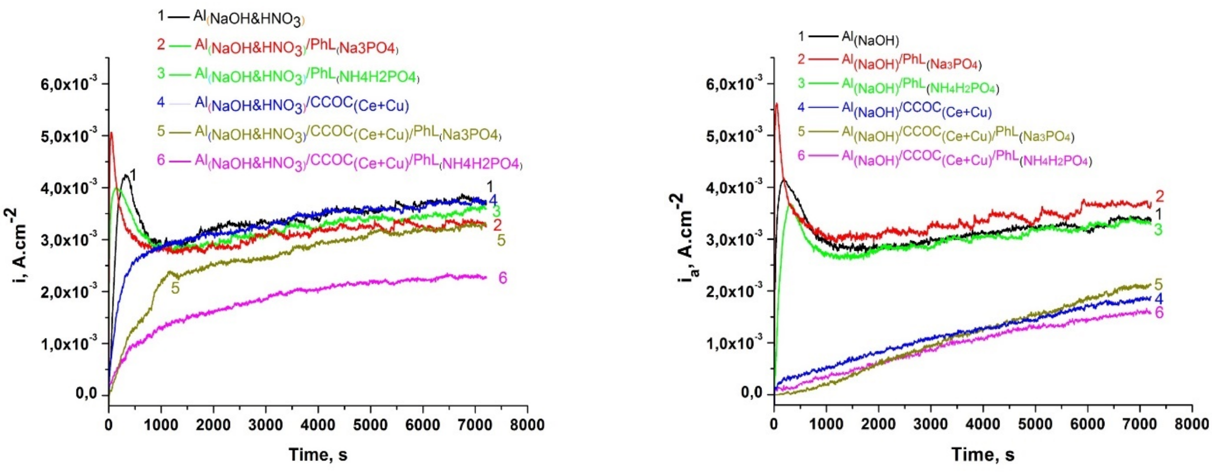

(a) **(b)**

Fig. 6. Chronoamperometric transients of the studied systems, Al substrate(s) of which are pretreated in 1.5 M NaOH (a) or in 1.5 M NaOH and 5 M HNO_3 (b) in 0.1M NaCl at the E_{pit} of Al 1050.

The course of the current transients is conceptually different for samples protected with CCOC and post-treated in phosphate solutions (Fig. 6a, curves 4-6). At the same time there are no current fluctuations characteristic for localized breakdown of the passive film, which leads to the initiation and growth of corrosion pits in CM. The transients have a course characteristic of processes of general corrosion. i_a of the $Al_{(NaOH)}$/$CCOC_{(Ce+Cu)}$ system increases gradually, remaining about three times lower (1.2×10^{-3} A.cm^{-2} *vs.* 3.2×10^{-3}) than i_a of $Al_{(NaOH)}$. This difference in i_a drop is enhanced by ~ 10%, resp. 20%, for the $Al_{(NaOH)}$/$CCOC_{(Ce+Cu)}$/ $PhL_{(Na3PO4)}$ and $Al_{(NaOH)}$/$CCOC_{(Ce+Cu)}$/$PhL_{(NH4H2PO4}$ systems (Fig. 6a, curves 5 and 6).

Fig. 6b presents the results of the chronoamperometric investigations using the samples, obtained after preliminary treatment of the Al substrate consecutively in NaOH&HNO_3. We observed that for $Al_{(NaOH\&HNO3)}$, after its immersion in the CM at E_{pit}, the corrosion current density is sharply increased (until reaching the ~380-th second of exposure) up to values of ~ 4.22×10^{-3} A.cm^{-2}, whereupon the surface film on the aluminum is disrupted (Fig. 6b, black curve 1), which is a prerequisite for the appearance and development of pitting corrosion during the interaction with the CM. After breaking through the passive film, there starts a process of local corrosion characterized by values of the anodic current (i_a) of ~ 3.40×10^{-3} A.cm^{-2} (at 3600-ed s) and current oscillations specific for it, owing to unstable pittings which are repassivated/activated. Similar behavior is also observed for the current transients of the $Al_{(NaOH\&HNO3)}$/$PhL_{(Na3PO4)}$ and $Al_{(NaOH\&HNO3)}$/ $PhL_{(NH4H2PO4)}$ systems (Fig. 8b, red 2 and green 3 curves, respectively).

The course of the current transients is again quite different for samples protected with CCOC and post-treated in phosphate solutions (Fig. 6b, blue 4, dark yellow 5 and magenta 6 curves, respectively). There are no current fluctuations characteristic for localized breakdown of the passive film, which leads to the initiation and growth of corrosion pits in CM. The transients have a course characteristic of processes of general corrosion. i_a of the $Al_{(NaOH\&HNO3)}$/$CCOC_{(Ce+Cu)}$ system increases gradually, coinciding with the transient for Al substrate ($Al_{(NaOH\ \&HNO3)}$ after about 1000-nd second. The chronoamperometric current transients characterizing the systems $Al_{(NaOH\&HNO3)}$/ $CCOC_{(Ce+Cu)}$/$PhL_{(Na3PO4)}$ and $Al_{(NaOH\&HNO3)}$/ $CCOC_{(Ce+Cu)}$/$PhL_{(NH4H2PO4}$ (Fig. 6b, dark yellow 5 and magenta 6 curves, respectively) remain lower. This difference in i_a drop is enhanced to 2.6×10^{-3} A.cm^{-2} and 1.7×10^{-3} A.cm^{-2}, respectively *vs.* 3.4×10^{-3} A.cm^{-2} – i_a for the Al substrate.

Investigations of Rp at E_{OCP}. Comparison with the XPS data for the studied systems. Fig. 7 shows histograms reflecting the changes in Rp of the studies systems as a function of exposure time (0.25 – 168/336 hours) in CM. Histograms 1–3 characterize the change in Rp for: $Al_{(NaOH)}$ before (1) and after immersion treatment in Na_3PO_4 (2) or $NH_4H_2PO_4$ (3); respectively for $Al_{(NaOH\&HNO3)}$ before (7) and after immersion treatment in Na_3PO_4 (8) or $NH_4H_2PO_4$ (9). They indicate that the direct phosphate treatment of the Al substrate leads to a considerable increase in Rp (especially for the substrates $Al_{(NaOH)}$), but that diminishes substantially upon reaching 168 h of exposure in CM. Histograms 4 – 6 in Fig. 7 characterize the change in Rp for the system $Al_{(NaOH)}$/$CCOC_{(Ce+Cu)}$ before (4) and after immersion treatment in Na_3PO_4 (5) or $NH_4H_2PO_4$ (6); respectively for $Al_{(NaOH\&HNO3)}$/$CCOC_{(Ce+Cu)}$ before (10) and after immersion treatment in Na_3PO_4 (11) or $NH_4H_2PO_4$ (12). They show that the system $Al_{(NaOH)}$/$CCOC_{(Ce+Cu)}$ and especially $Al_{(NaOH\&HNO3)}$/ $CCOC_{(Ce+Cu)}$ are characterized by low Rp values. Its additional phosphate treatment in Na_3PO_4 (5) and respectively (11) does not considerably increase Rp.

After post-treatment in $NH_4H_2PO_4$, however, the change in Rp for the system $Al_{(NaOH)}$/ $CCOC_{(Ce+Cu)}$/$PhL_{(NH4H2PO4)}$ over exposure time in CM increases systematically (up to ~ 1000 kΩ.cm^2), oscillating during the interval of 144 – 288 h of exposure in CM. It begins to decline after 312 hours, reaching the even greater Rp value of ~ 160 kΩ.cm^2 at 336 hours. In the same time the value of Rp for the system $Al_{(NaOH\&HNO3)}$/$CCOC_{(Ce+Cu)}$/$PhL_{(NH4H2PO4)}$ after the 168-th hour is lower than 30 kΩ.cm^2.

The information obtained from the Rp method differs from that gathered *via* the "destructive" potentiodynamic polarization (PDP) curve method showed in Figs. 4 (a, b) and Table 3. Specifically, during measurements of Rp, the studied samples are under the influence of an E_{OCP}, except for a short period of time (~ 3 min), during which they are polarized and their Rp is measured. The Rp method lends the opportunity to assess the change in corrosion protective behavior of the studied systems during an actual corrosion process under conditions of self-dissolution (at E_{OCP}), over a sufficiently long period of time. This assessment is usually associated with (change in) physical-chemical properties and composition of the conversion layers, as well as the influence of the formed corrosion products during extended exposure in the model corrosion medium. (The results obtained with this method are highly relevant to experiments/tests conducted in natural corrosion conditions). In this aspect we have a reason to compare the Rp results obtained with the data detected by XPS analysis for the studied samples (Tables 4 and 5). The comparison and analysis of the obtained results give us a ground to conclude that:

- The type of pre-treatment of the Al substrate (in NaOH or in NaOH&HNO_3) influences the content of $Al(OH)_3$, non-stoichiometric AlOOH and Al_2O_3 on its surface before and after deposition of CCOC and PhLs;
- The type of pre-treatment of the Al substrate strongly influences the content of ceria in as-deposited CCOC, their thickness respectively. Especially, the inclusion of an additional de-oxidation pre-treatment in HNO_3 increases the number of active s ections (zones of island like Al3Fe phase as a rull coated by Cu) on the Al-1050 surface. In the same time these active sections (leading to the formation of galvanic pairs) can play negative role, provoking corrosion processes, increasing of i_{corr};
- The type of pre-treatment of the Al substrate influences strongly the time of exposure in CM at which the values of Rp are hold back enough high;
- The type of the phosphate post-treatment of the Al/CCOC/PhLs systems strongly influences the content of ceria in as-deposited CCOC, their thickness and composition, respectively. It is expressed in a strong decrease in the concentration of Al_2O_3 and Ce_2O_3+CeO_2 components in CCOC at the expense of the formation of $AlPO_4$ and AlOOH, $CePO_4$ as well as PO_3^-, P_2O_5 and P_4O_{10} compounds with Al and Ce;
- Depending on the type of phosphate operation/solution (Na_3PO_4 or $NH_4H_2PO_4$), the CCOC can change the relation of Ce^{3+} and Ce^{4+} in the deep of mixed conversion layers, increasing the concentration of soluble Ce_2O_3 and decreasing the low-soluble CeO_2, respectively;
- The type of phosphate operation/solution strongly influences on the change/decrease of the Rp of the mixed CCOC and PhLs on the Al surface *vs*. time of exposure in the model corrosion medium.

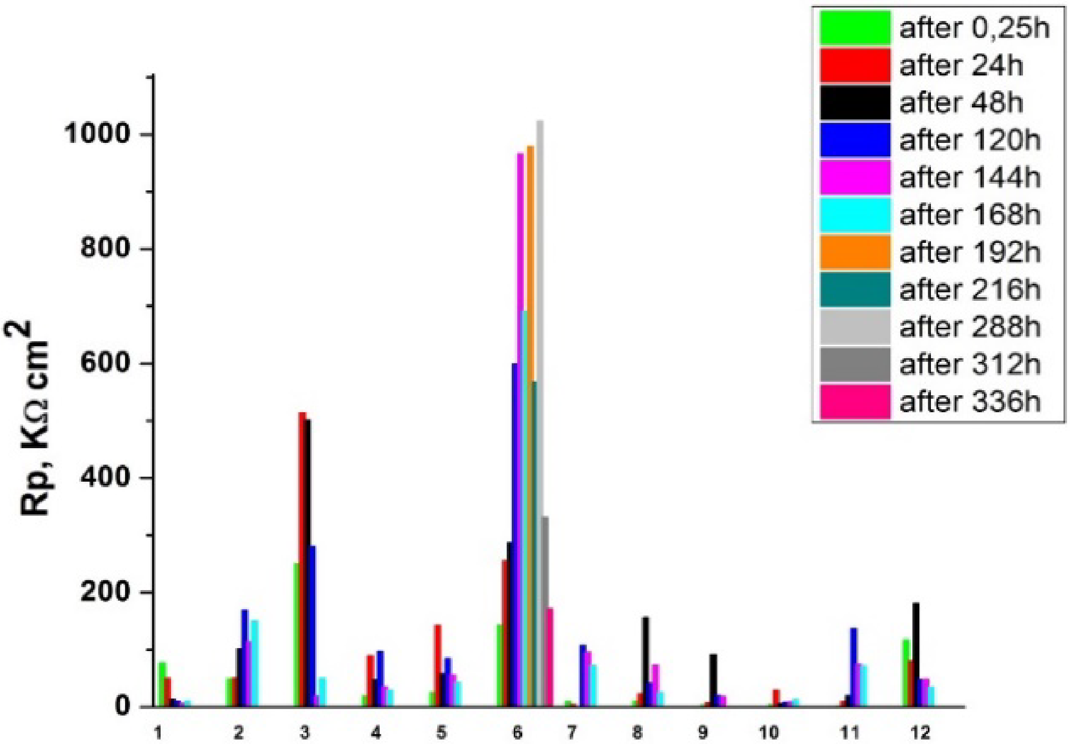

-

Fig. 7. Change in *Rp* (during exposure in 0.1 M NaCl.) of samples of Al 1050: pre-treated in 1.5 M NaOH (1); pre-treated in 1.5 M NaOH and post-treated by immersion in Na_3PO_4 (2) or $NH_4H_2PO_4$ (3); pre-treated in 1.5 M NaOH and coated with CCOC (4); pre-treated in 1.5 M NaOH, coated with CCOC and post-treated in Na_3PO_4 (5) or $NH_4H_2PO_4$ (6); or consecutively pre-treated in NaOH & HNO_3 (7); pre-treated in NaOH & HNO_3 and post-treated by immersion in Na_3PO_4 (8); or $NH_4H_2PO_4$ (9); pre-treated in NaOH & HNO_3 and coated with CCOC (10); pre-treated in NaOH & HNO_3, coated with CCOC and post-treated in Na_3PO_4 (11) or $NH_4H_2PO_4$ (12).

Table 4. The quantitative electrochemical (Rp in kΩ cm^2 and CR in µm/year) and XPS (in at. %) results of: Al 1050 samples, pre-treated in NaOH (1) and post-treated in: Na_3PO_4 (2); $NH_4H_2PO_4$ (3); coated with CCOC (4); coated with CCOC and post-treated in Na_3PO_4 (5); coated with CCOC and post-treated in $NH_4H_2PO_4$ (6) - as deposited and after exposure in CM for 168 (and 336 for No 6) hours.

Sample	Rp, kΩ cm^2	CR, µm/y	Chemical composition on the surface of the studied samples according to XPS investigations, at. %								
			O	Al	Ce (total) (Ce^{3+}+Ce^{4+})	Cu	P	Fe	Cl	No	Ce^{4+}, % of Ce (total)
Al$_{(NaOH)}$ as pretreated	76.7	3.7	61.0	39.0	-	-	-			-	-
after 168 h in 0.1M NaCl	10.2	27.8	75.2	24.6	-	-	-		0.2	-	-
Al$_{(NaOH)}$/PhL$_{(Na_3PO_4)}$ as deposited	49.0	5.7	58.4	28.2	-	-	12.1	1.3	0	-	-
after 168 h in 0.1M NaCl	150.4	1.9	76.3	22.0	-	-	1.4		0.3	-	-
Al$_{(NaOH)}$/PhL$_{(NH_4H_2PO_4)}$ as deposited	250	1.0	62.2	12.8	-	-	18.4	1.6	0	5	-
after 168 h in 0.1M NaCl	49.6	5.6	72.9	16.7	-	-	5.8	1.9	0.3	2.4	-
Al$_{(NaOH)}$/CCOC$_{(Ce+Cu)}$ as deposited	18.9	11.8	71.9	21.2	6.9		-		0	-	79
after 168 h in 0.1M NaCl	29.7	9.6	74.8	22.1	1.5	1.1	-		0.5	-	37
Al$_{(NaOH)}$/CCOC$_{(Ce+Cu)}$/PhL$_{(Na_3PO_4)}$ as deposited	25.5	11.3	73.7	10.7	2.8	0	12.9			-	23
after 168 h in 0.1M NaCl	43.1	6.6	74.4	23.7	1.2	0.7				-	78
Al$_{(NaOH)}$/CCOC$_{(Ce+Cu)}$/ PhL$_{(NH_4H_2PO_4)}$ as deposited	143.2	2.0	76.3	7.6	1.4	0.6	14.1				11
after 168 h in 0.1M NaCl	691.8	0.4	72.4	19.1	0.8	0	7.7	0	0	0	0
after 336 h in 0.1M NaCl	171.7	2.0	74.3	7.8	5.4	0	5.2	0	0	7.3	17

Table 5. The quantitative electrochemical (Rp in kΩ cm^2 and CR in μm/year) and XPS (in at. %) results of: Al 1050 samples, pre-treated in NaOH&HNO_3 (1) and post-treated in: Na_3PO_4 (2); $NH_4H_2PO_4$ (3); coated with CCOC (4); coated with CCOC and post-treated in Na_3PO_4 (5); coated with CCOC and post-treated in $NH_4H_2PO_4$ (6) - as deposited and after exposure in CM for 168 hours.

Sample	Rp, KΩcm^2	CR, μm/y	Chemical composition on the surface of the studied samples according to XPS investigations, at. %									
			O	Al	Ce (total) (Ce^{3+}+Ce^{4+})	Cu	P	Fe	Cl	N	Na	Ce^{4+}, % of Ce (total)
$Al_{(NaOH\&HNO_3)}$ as pretreated	9.5	30.0	59.1	40.9								
after 168h in 0.1M NaCl	71.8	4.0	81.1	18.0				0.4	0.5			
$Al_{(NaOH\&HNO_3)}$/$PhL_{(Na_3PO_4)}$ as deposited	10.4	27.2	68.9	23.0			2.9	5.2				
after 168h in 0.1M NaCl	25.3	11.2	79.8	17.4			0.1	0.7			2.0	
$Al_{(NaOH\&HNO_3)}$/$PhL_{(NH_4H_2PO_4)}$ as deposited	3.1	93.2	63.7	24.0			10.6	0.6		1.1		
after 168h in 0.1M NaCl	14.8	19.1	70.9	22.1					2.7		4.3	
$Al_{(NaOH\&HNO_3)}$/$CCOC_{(Ce+Cu)}$ as deposited	4.1	69.0	76.5		13.8	4.5		5.2				100
after 168h in 0.1M NaCl	12.2	23.3	73	23.5		2.5		0.2	0.8			
$Al_{(NaOH\&HNO_3)}$/$CCOC_{(Ce+Cu)}$/ $PhL_{(Na_3PO_4)}$ as deposited	1.5	187.5	70.1	23.8			3.5	2.6				
after 168h in 0.1M NaCl	71.0	4.0	83.8	15.6		0.3			0.3			
$Al_{(NaOH\&HNO_3)}$/$CCOC_{(Ce+Cu)}$/ $PhL_{(NH_4H_2PO_4)}$ as deposited	117.0	2.4	67.9	14.4	0.8		13.2	0.6		2.2	0.9	8
after 168h in 0.1M NaCl	34.6	8.2	75.2	18.0	0.2		3.0	0.5		2.4	0.7	0

Consideration of Rp at E_{OCP} and CR of the studied systems. On Fig. 8 are shown the results obtained for the systems of Al substrates which are pre-treated in NaOH (Fig. 8a) or consecutively in NaOH and HNO_3 (Fig. 8b). Fig. 8a, in which exposure time in CM is plotted on the X-axis, simultaneously illustrates the course of change in Rp (left ordinate) and CR (right ordinate) for the investigated systems. Our results indicate that the most effective, from a corrosion perspective, is the protection of Al 1050, based on the consecutive pre-treatment in NaOH and formation of conversion layers of CCOC and PhL, deposited in $NH_4H_2PO_4$. In this case, the values of CR are of the order of 0.8 μm/y, while with post-treatment with Na_3PO_4 the range is 5.5 μm/y (the value for the unprotected Al substrate - 25 μm/y).

The analysis of these results and their comparison to the data for the changes in the concentrations of Ce^{3+}/Ce^{4+} and P (resp. Ce_2O_3, CeO_2, $AlPO_4$ and AlOOH, $CePO_4$ as well as PO_3^-, P_2O_5 and P_4O_{10} compounds with Al and Ce) on the surface of the formed conversion layers (during the time of exposure in CM - Tables 4, 5 and 2) indicates a direct correlation between these two aspects. Also, the formation of $AlPO_4$ and $CePO_4$ leads to considerable increase in Rp of the mixed CCOC/PhL conversion coating. At the same time increased duration of exposure in CM leads to a decrease in the concentrations of Al_2O_3 and Ce_2O_3+CeO_2 (as components in CCOC) at the expense of the formation of $AlPO_4$ and AlOOH, $CePO_4$, as well as PO_3^-, P_2O_5 and P_4O_{10} compounds of Al and Ce in the mixed conversion layers. As a result of this higher Rp values which determine lower values of CR (Fig. 8a) are achieved and maintained. In this aspect the maximum effect is reached for the system $Al_{(NaOH)}$/$CCOC_{(Ce+Cu)}$/$PhL_{(NH4H2PO4)}$.

On Fig. 8b are shown the results reflecting the changes in Rp and CR of the studied systems, the Al substrates of which are pre-treated in NaOH and HNO_3. The analysis of the results obtained showed that at the direct immersion treatment of the Al substrate ($Al_{(NaOH\&HNO3)}$) by PhLs better results from a corrosion point of view determine the post-treatment by Na_3PO_4. However, highly impressive is the effect of this phosphate post-treatment for the Rp and CR at the time of exposure only till 48-th h.

CCOC, deposited on $Al_{(NaOH\&HNO3)}$ (the $Al_{(NaOH\&HNO3)}$/$CCOC_{(Ce+Cu)}$ system), is characterized by lowest indices in comparison to these for the systems $Al_{(NaOH\&HNO3)}$/PhLs, more probably because of the higher concentration of Cu and Fe (Al3Fe) sections in them (Table 5) [17]. The phosphate(s) processing of the $Al_{(NaOH\&HNO3)}$/$CCOC_{(Ce+Cu)}$ system however improves substantialy the protective indicators of the mixed $Al_{(NaOH\&HNO3)}$/$CCOC_{(Ce+Cu)}$/ PhLs systems. This improvement is connected with a noteworthy decrease of the deviations of Rp and i_a (Fig. 8b) starting from the beginning of exposure in CM. At this reached maximum protective effect is for the system $Al_{(NaOH\&HNO3)}$/$CCOC_{(Ce+Cu)}$/ $PhL_{(NH4H2PO4)}$. The deviations and oscillations in Rp and CR (corresponding E_{cor} and i_a), respectively, for this system are decreased and stabilized in maximum degree.

CONCLUSION

Ceria-based conversion coatings, formed on technically pure Al-1050, were post-treated in phosphate containing solutions. We paid extra attention to the influence of the type of "pre-" and "post-treatment" operations.

The chemical composition on the surface of the obtained conversion systems was characterized by means of X-ray photoelectron spectroscopy. Based on the obtained results it was ascertained that there is substantial influence of the "pre-treatment" and "post-treatment" operations on the chemical composition and chemical state of the elements on their surface. It is expressed by a strong decrease in the concentration of Al_2O_3 and Ce_2O_3+CeO_2 components in the as-deposited CCOCs at the expense of formation of $AlPO_4$ and AlOOH, $CePO_4$ as well as PO_3^-, P_2O_5 and P_4O_{10} compounds with Al and Ce, after their post-treatment in phosphate solutions.

Electrochemical and corrosion investigations and the determination of the basic corrosion parameters as E_{cor}, i_{cor}, Z, E_{OCP}, i_a, E_{pit}, Rp and CR of the studied systems (as-deposited and after definite time of exposure in a model 0.1M NaCl corrosion medium) were carried out. The comparison of these results with the changes in the concentrations of Ce^{3+}/Ce^{4+}, Al and P (their respective oxides and phosphates) before and after exposure of the samples in CM shows that the concentrations of Ce^{4+} and P on the surface of the studied samples are directly related. Polarization investigations simultaneously showed that the combined phosphate and ceria conversion layers are not only static barrier coatings, but they also change the kinetics of the conjugated electrochemical reactions characterizing the corrosion process in Cl^- containing media, i.e. they determine the electrochemical protection of Al substrate.

The established protective effect of the mixed conversion coatings on Al at long exposure in CM can be related to the beneficial transformation of the chemical composition of CCOC, formed on Al substrates after phosphate processing. This effect, as well as the formation of different types of corrosion products on the surface of Al/CCOC/PhLs systems, provide an effective barrier to the diffusion of Cl^- to the Al surface, which leads to corresponding positive and beneficial changes of the Rp and CR for the studied systems.

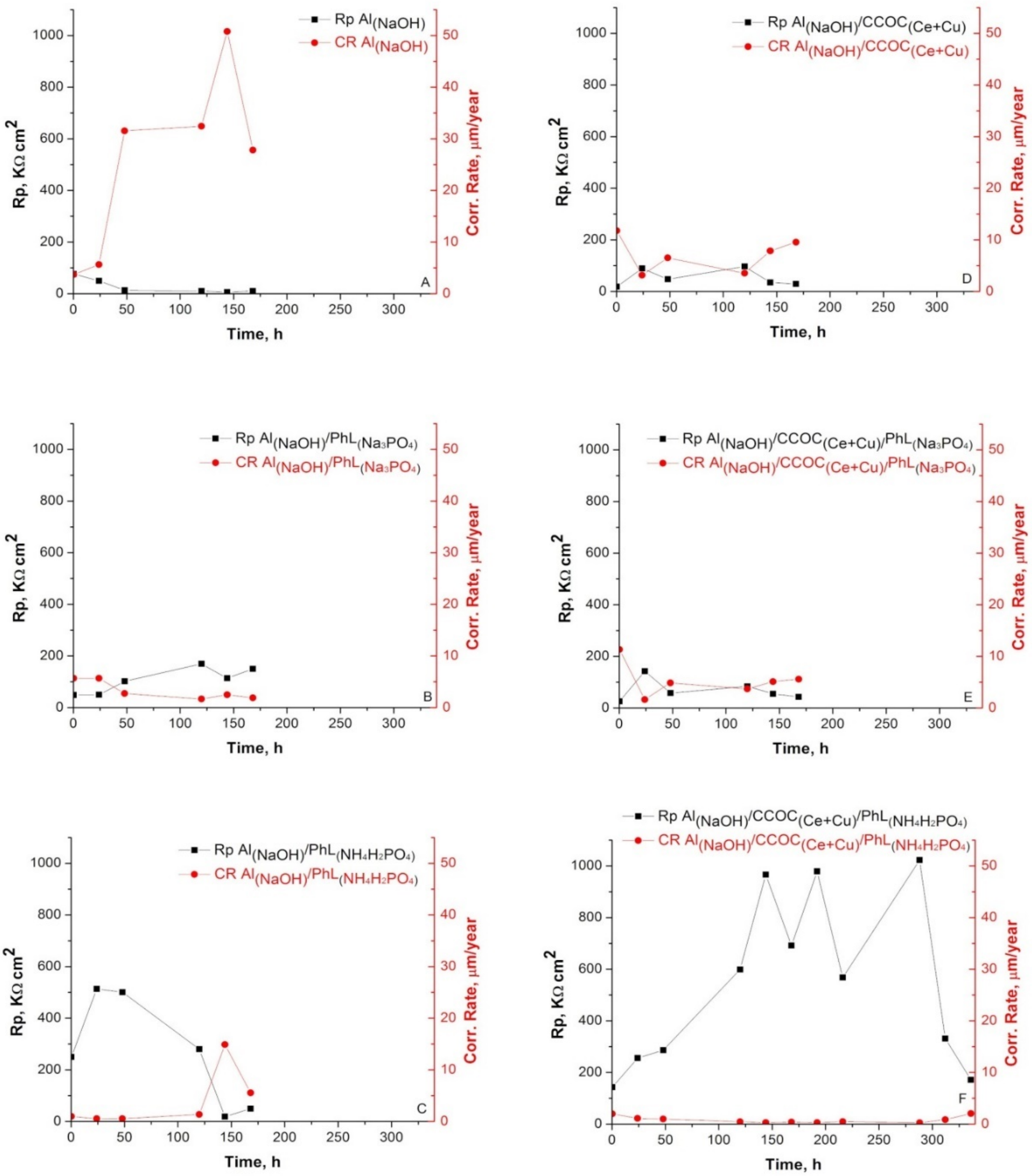
Rp Al(NaOH)
CR Al(NaOH)
A
Rp Al(NaOH)/CCOC(Ce+Cu)
CR Al(NaOH)/CCOC(Ce+Cu)
D
Rp Al(NaOH)/PhL(Na3PO4)
CR Al(NaOH)/PhL(Na3PO4)
B
Rp Al(NaOH)/CCOC(Ce+Cu)/PhL(Na3PO4)
CR Al(NaOH)/CCOC(Ce+Cu)/PhL(Na3PO4)
E
Rp Al(NaOH)/PhL(NH4H2PO4)
CR Al(NaOH)/PhL(NH4H2PO4)
C
Rp Al(NaOH)/CCOC(Ce+Cu)/PhL(NH4H2PO4)
CR Al(NaOH)/CCOC(Ce+Cu)/PhL(NH4H2PO4)
F
Rp, KΩ cm2
Corr. Rate, μm/year
Time, h

(a)

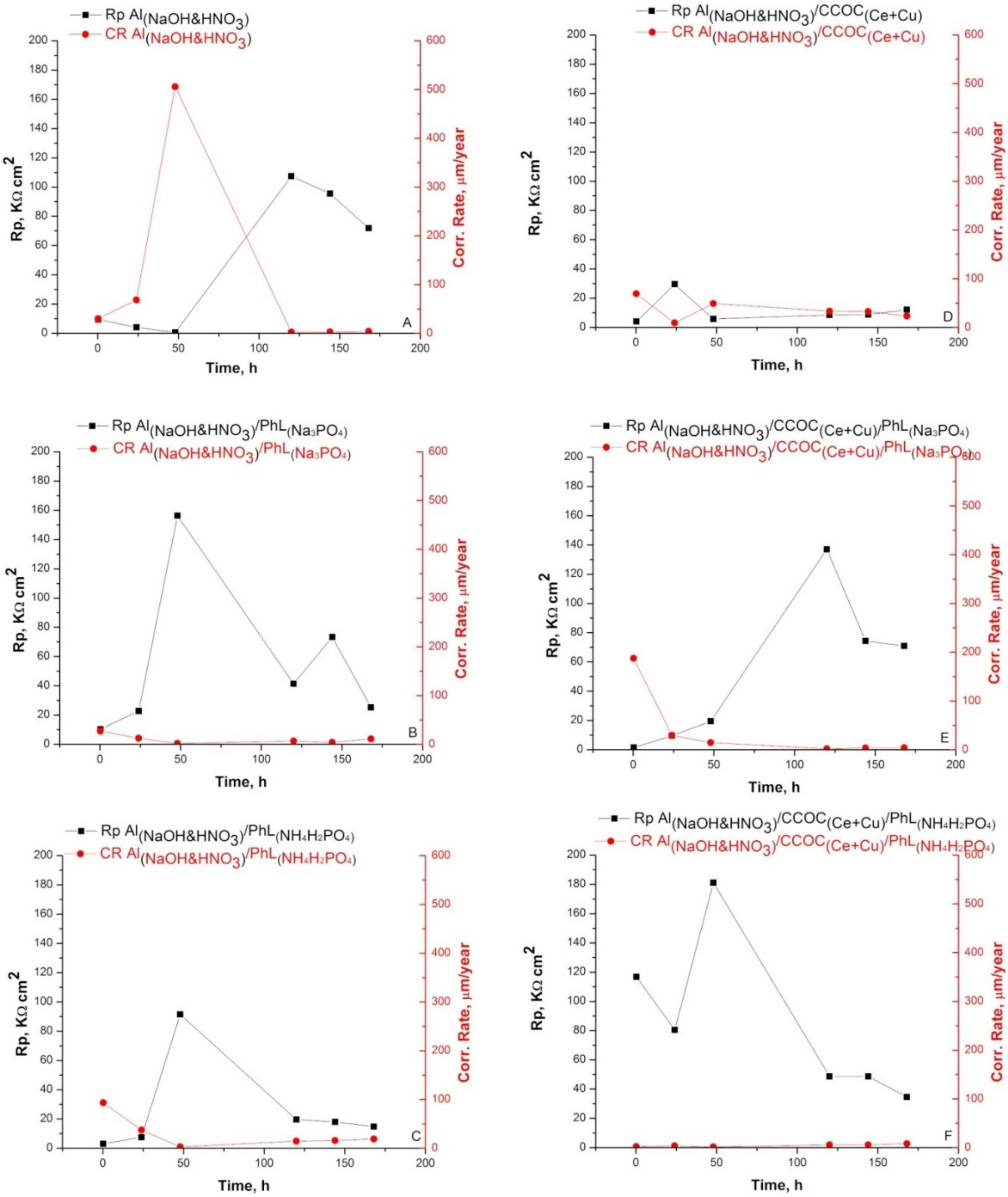

(b)

Fig. 8. Change in Rp and CR of the studied systems: Al substrate(s) of which are pretreated in 1.5 M NaOH (a) or in 1.5 M NaOH& 5M HNO_3 (b) during exposure in 0.1M NaCl.

Acknowledgement: *The authors are grateful to acknowledge: „Equipment supported/obtained under the project INFRAMAT (National Roadmap for Research Infrastructure) financed by Bulgarian Ministry of Education and Science was used in this investigation“; support from the CoC „Clean technologies for sustainable environment – water, waste, energy for circular economy“, (Project BG05M2OP001-1.002-0019), supported by the ERDF within the Bulgarian OP “SESG 2014–2020“ and the support from the CoE “National center for/of mechatronics and clean technologies” (Project BG05M2OP001–1.001–0008) supported by the ERDF within the Bulgarian OP “SESG 2014–2020.“*

REFERENCES

1. B. Hinton, *Corrosion*, **66**, 1 (2010).
2. S. Wernick, R. Pinner, P. Sheasby, ‘The Surface Treatments of Aluminium and Its Alloys’, 5th edn., ASM International and Finishing Publications Ltd.,

M Metals Park, Ohio, 1987.
3. Official Journal of the European Union, 'COMMISSION DIRECTIVE (EU) 2017/ 2096 - of 15 November 2017 - Amending Annex II to Directive 2000/ 53/ EC of the European Parliament and of the Council on End-of Life Vehicles'(2017).
4. Official Journal of the European Union, 'COMMISSION IMPLEMENTING DECISION (EU) 2019/2193 of 17 December 2019 Laying down Rules for the Calculation, Verification and Reporting of Data and Establishing Data Formats for the Purposes of Directive 2012/19/EU of the European Parliament and of the Council on Waste Electrical and Electronic Equipment (WEEE)' (2019).
5. T. G. Harvey, *Corros. Eng. Sci. Technol.*, **48**, 248 (2013).
6. C. Girginov, S. Kozhukharov, in: Extended Abstracts of 7th Regional RSE-SEE Symposium on Electrochemistry and 8th Kurt Schwabe Symposium, V. Horvat-Radošević, K. Kvastek, Z. Mandić (eds.), International Association of Physical Chemists, Split, Croatia, 132 (2019).
7. C. E. Castano, W. G. Fahrenholtz, M. J. O'Keefe, in: Metal oxides, Elsevier`s Book series "Ceria-Based Coatings and Pigments - Synthesis, Properties and Applications", 2020, p. 211.
8. S. Kozhukharov, C. Girginov, in: NATO Science for Peace and Security Series B: Physics and Biophysics, P. Petkov, M. Achour, C. Popov (eds.), Springer, Dordrecht, 2020, p. 437.
9. Q. Zhu, B. Zhang, X. Zhao, B. Wang, *Coatings*, **10**, 128 (2020).
10. J. So, E. Choi, J. T. Kim, J. S. Shin, J. B. Song, M. Kim, C. W. Chung, J. Y. Yun, *Coatings*, **10**, 103 (2020).
11. F. Czerwinski, *Journal of Materials Science*, **55**, 24 (2020) .
12. D. K. Heller, W. G. Fahrenholtz, M. J. O'Keefe, *Corros. Sci*., **52**, 360 (2010).
13. R. Andreeva, E. Stoyanova, A. Tsanev, D. Stoychev, *Comptes Rendus de l'Académie Bulg. des Sci.*, **72**, 1336 (2019).
14. R. Andreeva, E. Stoyanova, A. Tsanev, D. Stoychev, *J. Phys. Conf. Ser.*, **700**(1), 012049 (2016).
15. R. Andreeva, E. Stoyanova, A. Tsanev, P. Stefanov, D. Stoychev, *Trans. IMF*, **92**, 203 (2014).
16. R. Andreeva, E. Stoyanova, D. Stoychev, *J. Int. Sci. Publ. Mater. Methods Technol.*, **8**, 751 (2014).
17. E. Stoyanova, D. Stoychev, *J. Appl. Electrochem.*, **27**, 685 (1997).
18. R. Andreeva, E. Stoyanova, A. Tsanev, M. Datcheva, D. Stoychev, *Int. J. Electrochem. Sci.*, **13,** 5333 (2018).
19. H. Zhang, Y. Zuo, *Appl. Surf. Sci.*, **254**, 4930 (2008).
20. H. Hasannejad, M. Aliofkhazraei, A. Shanaghi, T. Shahrabi, A. R. Sabour, *Thin Solid Films*, **517**, 4792 (2009).
21. W. Pinc, P. Yu, M. O'Keefe, W. Fahrenholtz, *Surf. Coatings Technol.*, **203**, 3533 (2009).
22. D. K. Heller, W. G. Fahrenholtz, M. J. O'Keefe, *J. Electrochem. Soc.*, **156**, 400 (2009).
23. R. Andreeva, E. Stoyanova, A. Tsanev, D. Stoychev, *J. Phys. Conf. Ser.* **1492**(1), 012019 (2020,).
24. S. Damyanova, C. A. Perez, M. Schmal, J.M.C. Bueno, *Appl. Catal. A Gen.*, **234**, 271 (2002).
25. E. Bêche, P. Charvin, D. Perarnau, S. Abanades, G. Flamant, *Surf. Interface Anal.*, **40**, 264 (2008).
26. X. Yu, G. Li, *J. Alloys Compd.*, **364,** 193 (2004).
27. C. Girginov, I. Avramova, S. Kozhukharov, *J. Chem. Technol. Metall.*, **51**, 705 (2016).
28. R. Kumar, J. Rashid, M. A. Barakat, *RSC Adv.*, **4**, 38334 (2014).
29. M. Shimizu, Y. Tsushima, S. Arai, *ACS Omega*, **2**, 4306 (2017).
30. S. Bernal, G. A. Cifredo, J. M. Rodríguez-Izquierdo, *Artic. J. Phys. Chem. C*, **99**, 11794 (1995).
31. S. Fan, C. Yang, L. He, J. Deng, L. Zhang, L. Cheng, *Tribol. Int.*, **114**, 337 (2017).
32. I. Danilidis, J. Hunter, G. M. Scamans, J. M. Sykes, *Corros. Sci.*, **49**, 1559 (2007).
33. H. Zhang, G. Yao, S. Wang, Y. Liu, H. Luo, *Surf. Coatings Technol.*, **202** 1825 (2008).
34. Z. Szklarska-Smialowska, *Corros. Sci.*, **41**, 1743 (1999).

Bulgarian Chemical Communications, Volume 55, Issue 4 (pp. 407-413) 2023 DOI: 10.34049/bcc.55.4.5527

Thermodynamics and mechanism of liquid–liquid extraction of cerium (IV) from sulfuric acid solutions with di-(2-ethylhexyl) phosphoric acid (D2EHPA)

M. Ashtianifar[1], S.A. Milani[2], F. Zahakifar[2*]

[1]*Faculty of Mining Engineering, School of Engineering, Yazd University, P.O.Box 98195-741, Yazd, Iran*
[2]*Nuclear Fuel Cycle Research School, Nuclear Science and Technology Research Institute, AEOI, P.O.Box 14155-1339, Tehran, Iran*

Received: September 08, 2022; Revised: September 09, 2023

This paper reports studies on Ce (IV) extraction from sulfuric acid solutions using di-(2-ethylhexyl) phosphoric acid (D2EHPA) in kerosene as extractant with a view to elucidate the Ce (IV) extraction mechanism. The effects of pH, extractant concentration, metal-ion concentration in aqueous solution, temperature, and contact time between the two phases were observed in detail. The experimental results indicated that Ce (IV) could be effectively extracted from sulfuric acid medium; Ce (IV) was extracted into the organic phase in the form of $Ce(SO_4)_{0.5}A_2$. A cation exchange mechanism was proposed for the extraction of Ce (IV) in the H_2SO_4/ D2EHPA system and thermodynamic functions such as ΔG, ΔH, and ΔS were determined. The results of this research showed that the D2EHPA organic phase in kerosene can successfully be used to separate Ce (IV) from other RE (III) in binary initial solutions.

Keywords: Ce (IV); Liquid–liquid extraction; D2EHPA; Extraction mechanism; Thermodynamic functions.

INTRODUCTION

Cerium (IV) has received much attention in various fields, including the production of aluminum, aluminum alloys, certain steels, permanent magnets, catalysts, polishing powder, glass, in cinema and ceramic technology [1, 2]. Cerium is utilized in low-energy light bulbs, flat-screen TVs, and floodlights [3]. The pharmacological properties of the cerium compounds have also been shown [4, 5].

Metals are recovered from aqueous solutions by different techniques such as solvent extraction [6-12], liquid membrane [13-20], ion exchange (IX) [21-23], polymer inclusion membrane [24-26], electrodialysis [27-30], sorption [31-35], precipitation [36-38], and ultrafiltration [39-41]. In the industry, solvent extraction is one of the most effective techniques for purification of cerium [42]. Much research has been done on the extraction of Ce (IV) using various extractants including high-molecular weight amines [43, 44], organophosphorus acids [45, 46], and organophosphorus esters [47, 48].

The use of organophosphorus esters as extractants has attracted much attention [49]. Extraction of Ce (IV) from nitric acid (HNO_3) solutions by TBP has been reported in the first study by Warf [50]. Afterward, Korpusov *et al*. [51] and Healy and McKay [52] attributed Ce (IV) extraction from nitric acid solutions to the formation of $Ce(NO_3)_4(TBP)_2$ and $H_2Ce(NO_3)_6(TBP)_2$, respectively. As a neutral extractant, Cyanex 923 is considered to effectively extract Ce (IV). Lu *et al*. [53] reported the formation of $Ce(SO_4)_2$.2Cyanex923 species in the extraction of Ce (IV) from sulfate solutions. Cerium extraction with Cyanex 302 [46] and Cyanex 301 [45] extractants has been reported. However, the cost of Cyanex extractants is high [54].

Moreover, these well-established organophosphorus esters, essentially di (1-methylheptyl) methyl phosphonate (P350), TBP, TOPO, Cyanex 925 and Cyanex 923 have their own disadvantages for the extraction of cerium (IV). In between them, P350 cannot be used for the extraction of Ce (IV) because of the problem of removing possible reducing impurities. For Cyanex 925, Ce (IV) reduction is observed in the sulfate system [49]. Higher acidities are needed when using TBP as the extractant for Ce (IV), in addition, the extractability is lower compared with others. TOPO is a good extractant for Ce (IV), but its solubility in aliphatic diluents limits the maximum loading. In the case of Cyanex 923, the commercial outlook is not attractive due to the high cost compared with di- (2-ethylhexyl) phosphoric acid (D2EHPA). Therefore, the development of new extraction systems for the extraction of Ce (IV), especially in sulfuric acid solutions, is an issue of great importance.

D2EHPA is a well-known extractant of the

* To whom all correspondence should be sent:
E-mail: fazelzahakifar@gmail.com

organophosphorus acids group and therefore extracts metal ions by the cation exchange mechanism [55, 56]. D2EHPA, owing to its lower cost, good physicochemical properties, complete miscibility with all common hydrocarbon diluents even at low ambient temperatures, low aqueous solubility, good resistance to hydrolysis, and high purity (99%) has potential advantages. D2EHPA is a very strong acid extractant, commonly used in sulfuric acid solutions for the extraction of many metal ions such as uranium, vanadium, zinc, copper, iron, rare earths and other precious metals.

The present study aimed at the investigation of Ce (IV) extraction by D2EHPA, thermodynamics and mechanism of extraction from sulfuric acid solutions. The extracted species were determined from slope analysis and by graphic method, and thermodynamic functions ΔH, ΔG and ΔS of the investigated systems were calculated.

EXPERIMENTAL

Materials

Di-(2-ethylhexyl) phosphoric acid (D2EHPA), kerosene, n-hexane, and benzene were purchased from Fluka. Sulfuric acid and cerium oxide were products of Merck. The stock solution of Ce (IV) was obtained by dissolving a suitable amount of cerium oxide in deionized water. All of the used chemicals were of analytical grade and used without purification.

General procedure

All experiments, except experiments for temperature effect, were performed at 25±1 °C. Equal volumes (5 mL) of organic and aqueous phases were placed in laboratory tubes and mechanically stirred for 10 min. Then the two phases were separated and the ion concentration in the aqueous phase was measured with an inductively coupled plasma-atomic emission spectrometer (ICP-AES, Varian, Liberty150ax Turbo, Australia).

Concentrations of the metal ion in the organic phase were calculated by mass balance. Then, the distribution coefficient was calculated. The distribution coefficient is the most desirable index for determining the response of the solvent extraction process and is defined as the ratio of the equilibrium concentration of metal ion in the organic phase to its equilibrium concentration in the aqueous phase:

$$D = \frac{C_0 - C}{C} \quad (1)$$

where C_0 and C are the initial and the equilibrium concentration of the metal ion in the aqueous phase, respectively. The extraction percentage of extracted metal ion, E %, was calculated from the relation,

$$E(\%) = \frac{100D}{D + \frac{V_{aq}}{V_{org}}} \quad (2)$$

where D is the distribution ratio, V_{aq} and V_{org} are the volumes of the aqueous and organic phases, respectively.

RESULTS AND DISCUSSION

Effect of pH

For cationic extractants, the pH (acidity) of the solution has a great influence on the extraction process because the H^+ ions participate in the extraction (Eq. 3). D2EHPA is an acidic extractant, offering both hydrogen bond donor and acceptor. Extraction of metal ions by D2EHPA can be described by the equation [54]:

$$M^{+4}_{aq} + n(HA)_{2,org} \leftrightarrows (MA_{2n}H_{2n-4})_{org} + 4H^+_{aq} \quad (3)$$

where A represents the anion of D2EHPA.

The variation of aqueous phase pH within the range of 0.5-6 showed that the increase in pH of the aqueous solution from 0.5 to 2 noticeably increases the extraction percentage of Ce (IV), which reaches its maximum value at pH 2.1 and remains practically constant in the range 2.1-6, Fig. 1. From Equation (3) it can be seen that by increasing the pH (i.e., by decreasing acidity), the equilibrium will shift (according to Le Chatelier's principle) to the right to extract more Ce (IV). This indicates the importance of low acidity of the medium in Ce (IV) extraction.

Fig. 1. Effect of pH of the aqueous solution on the

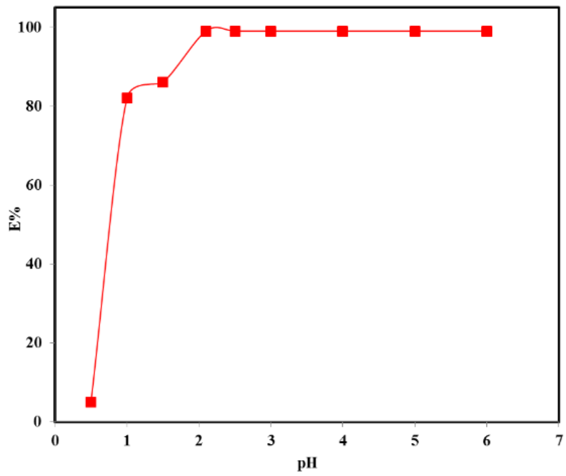

extraction percentage of Ce (IV) by 0.4 M extractant/kerosene solutions.

Effect of extractant concentration

The effect of extractant concentration on the extraction of 0.006 mol L^{-1} Ce (IV) was studied by varying the concentration of the considered extractants/kerosene solutions in the range 0.06-1.0 mol L^{-1}.

The results represented in Fig. 2 show that D2EHPA is an appropriate extractant for Ce (IV) extraction and the extraction percentage of Ce (IV) with D2EHPA increases with the increase in its concentration and reaches its maximum (>98 %) at extractant concentration of 0.7 mol L^{-1} or higher. The use of high extractant concentrations may be economically unjustified despite the higher extraction percentage. Extraction percentage of about 90% is usually considered to be the best option because it permits to extract the desired element in approximately one or two stages in a counter-current method.

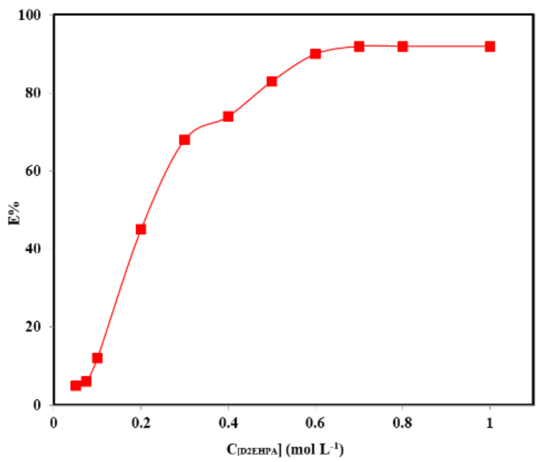

Fig. 2. Effect of extractant concentration on the extraction percentage (E%) of Ce (IV) from 0.01M sulfuric acid solution.

From the slope analysis of the log-log plot of the distribution coefficient *versus* extractant concentration (Fig. 3) it was concluded that two molecules of D2EHPA dimers are associated with an extractable complex.

Thermodynamic analysis and effect of temperature

The effect of temperature on the extraction of 0.006 M Ce (IV) by 0.4M D2EHPA in kerosene from 0.01M sulfuric acid was studied in the temperature range of 20-50 °C. The results represented graphically in Fig. 4 indicate the decrease in the percentage of extracted metal ion with the increase in temperature. Therefore, the Ce (IV) extraction process follows an exothermic reaction.

Thermodynamic parameters Gibbs free energy, enthalpy and entropy were calculated using the following equations [57-60]:

$$\log D = \frac{\Delta S}{2.303R} - \frac{\Delta H}{2.303RT} \quad (4)$$

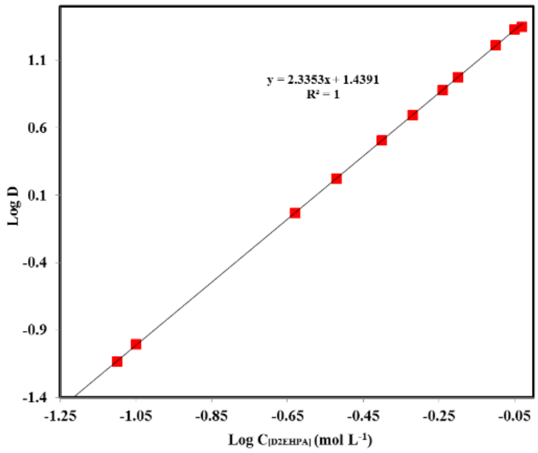

Fig. 3. Logarithm of the distribution coefficient (D) *versus* logarithm of the extractant concentration.

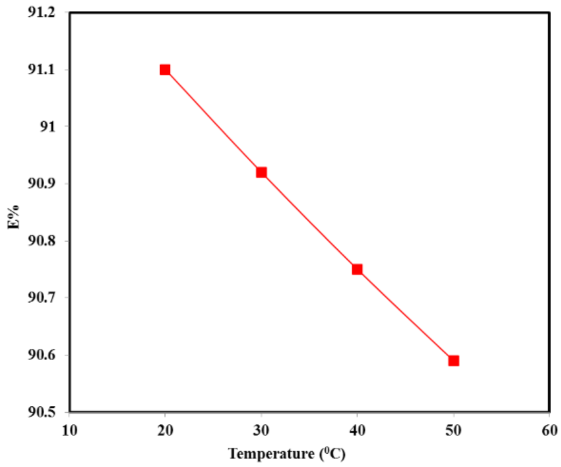

Fig. 4. Effect of temperature on the extraction percentage of 0.006M Ce(IV) with 0.4M D2EHPA from 0.01M sulfuric acid solution.

where R (8.31 J mol^{-1} K^{-1}) and T are the universal gas constant and absolute temperature, respectively. According to the Van 't Hoff equation (Eq. 4), the values of ΔH and ΔS can be determined by plotting the logarithm of the distribution coefficient (D) *versus* inverse temperature (Fig. 5).

The change in Gibbs free energy is obtained from the following equation:

$$\Delta G = \Delta H - T\Delta S \quad (5)$$

The values of the calculated thermodynamic parameters are shown in Table 1. Negative ΔH values indicate the exothermic reaction of Ce (IV) extraction by D2EHPA. Therefore, increasing the temperature will reduce Ce (IV) extraction from the aqueous phase. The negative ΔG value also indicates that the extraction reaction is spontaneous.

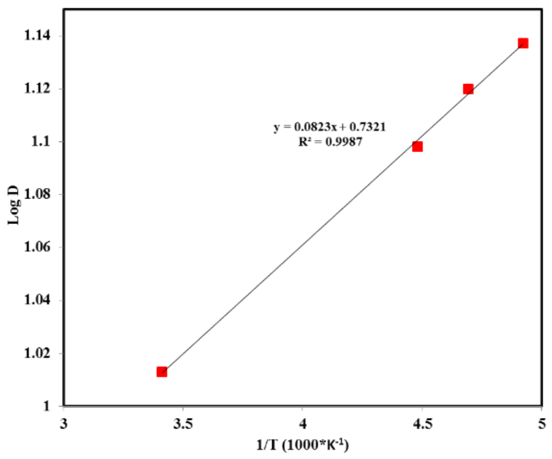

Fig. 5. Logarithm of the distribution coefficient (D) *vs.* inverse temperature.

Table 1. Standard molar thermodynamic quantities for the Ce (IV) extraction process at a temperature of 298.15± 1 K

ΔG ($kJ\ mol^{-1}$)	ΔS ($J\ mol^{-1}\ K^{-1}$)	ΔH ($kJ\ mol^{-1}$)
-2.47	-1.51	-2.02

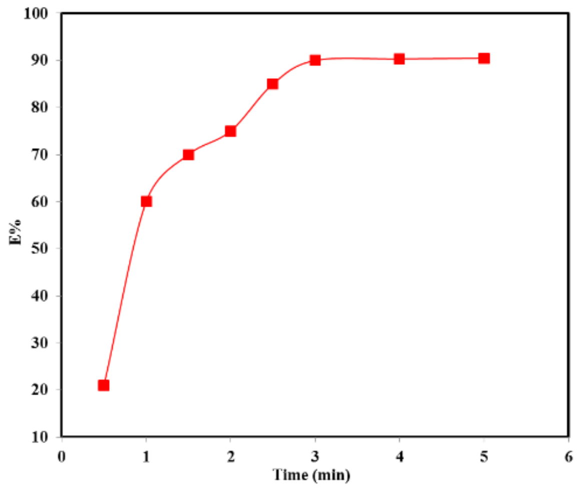

Fig. 6. Effect of contact time between aqueous and organic phases on cerium extraction at $C_{Ce(IV)} = 0.006$ mol L^{-1}.

Effect of phase contact time

The time needed to reach equilibrium between the amount of metal ions in aqueous and organic phases was investigated within the range of 3-10 min for the following constant parameters: pH 2.1; $C_{[Ce(IV)]} = 0.006$ mol L^{-1}; $C_{[D2EHPA]} = 0.4$ mol L^{-1} in kerosene; $V_{aq}:V_{org} = 1:1$; and temperature, 25±1 °C. The obtained results (Fig. 6) showed that the time required to reach equilibrium is ~3 min. Obviously, a 5-minute contact time is more than sufficient for the effective extraction of Ce (IV). Increasing the contact time beyond 3 minutes causes only slight changes in Ce (IV) extraction.

Effect of initial metal ion concentration

The increase in Ce (IV) concentration in the range 0.2×10^{-3}-0.011M decreased the extraction percentage of Ce (IV). The results shown in Fig. 7 depict a sharp decrease in Ce (IV) extraction percentage with the increase in its concentration. This could be attributed to the formation of other metal ion species which are not extracted by the used extraction system or to the capacity insufficiency of the extractant to extract metal ions of high initial concentrations.

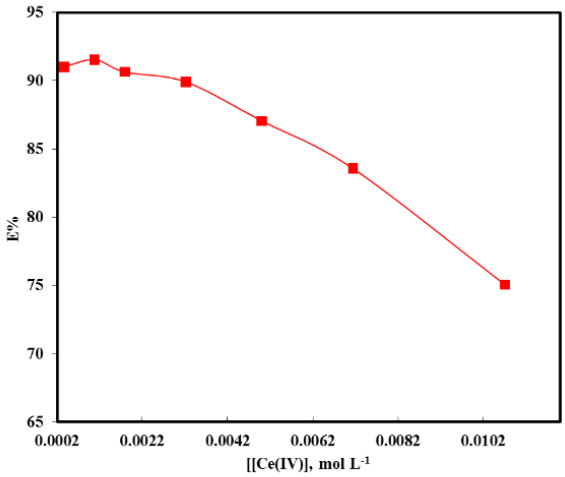

Fig. 7. Effect of Ce (IV) concentration on its extraction from 0.01M sulfuric acid by 0.4M D2EHPA /kerosene extraction system.

Effect of the nature of diluent

Three diluents, namely n-hexane, kerosene and benzene were selected to examine the influence of the diluent type on Ce (IV) extraction. As depicted in Table 2, the extraction percentage vigorously depends on the diluent nature. Diluents with low dielectric constant had better extraction performance for Ce (IV), so Ce (IV) extraction can be improved if kerosene is used as the diluent.

Table 2. Effect of diluent type on Ce (IV) extraction percentage. Aqueous solution pH 2, Contact time = 10 min, Temperature: 25±1 °C, $V_{aq}:V_{org} = 1:1$, $C_{[D2EHPA]} = 0.4$ mol L^{-1}, and $C_{[Ce(IV)]} = 0.006$ mol L^{-1}

Diluent	Dielectric constant at 20 °C	E%
Hexane	1.9	91.1
Kerosene	1.8	93
Benzene	2.3	81

Number of steps required to perform Ce (IV) extraction

Based on the obtained experimental results, McCabe-Thiele diagram was applied to determine the number of steps of the Ce (IV) solvent extraction.

The number of steps has been concluded graphically from the McCabe-Thiele diagram that consists of the equilibrium curve and the operating line. The equilibrium curve comprises a series of experimental points which represent the cerium content in the aqueous phase and the Ce content in the organic extract for different volumetric ratios and residence times. After contact, both phases are in equilibrium. The operating line sets the operating conditions and its slope is the A/O ratio. The McCabe-Thiele diagrams of Ce (IV) extraction process in the H_2SO_4/ D2EHPA system for A/O ratio of 1 and 2 are shown in Figures 8 and 9, respectively.

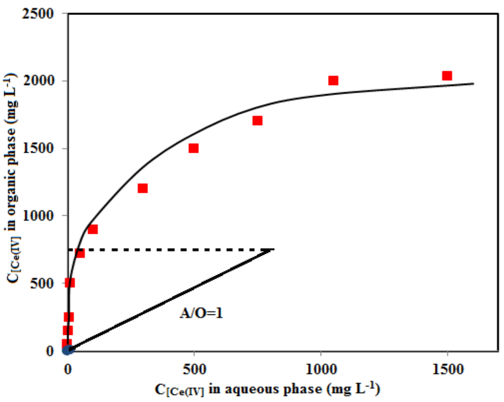

Fig. 8. McCabe-Thiele diagram of Ce (IV) extraction system with A/O =1

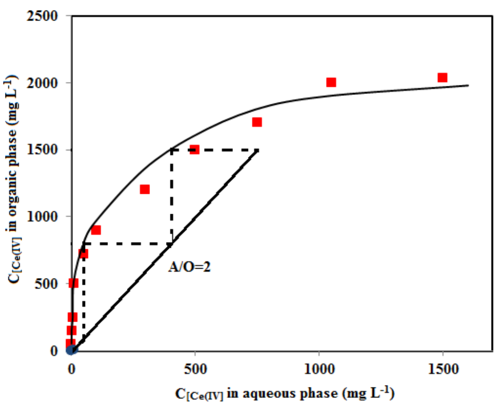

Fig. 9. McCabe-Thiele diagram of Ce (IV) extraction system with A/O =2.

As shown in Fig. 8, with one theoretical step, the extraction percentage is more than 90%. From Figure 9 is seen that three theoretical steps are required, and the extraction percentage achieved is 98%. According to Cox and Musikas [61], the number of real steps should be the theoretical number multiplied by 1.5–2. So, the real number of extraction steps should be two and five, respectively.

Extraction mechanism

It is well-established that organophosphorous-based acidic extractants exit as dimmers in nonpolar organic diluents [62]. Fig. 1 shows that by decreasing the solution acidity, the extraction of cerium in its tetravalent state by organophosphorus-based acidic extractants like D2EHPA from aqueous sulfuric media is enhanced. This phenomenon indicates that the mechanism of cerium (IV) extraction, especially at low acidities, is generally cation exchange [57]. Therefore, the mechanism of Ce (IV) extraction in sulfuric solutions can be expressed by the following cation exchange reaction [63]:

$$C^{4+} + nSO_4^{2-} + \frac{m}{2}(HA)_{2,org} \leftrightarrow Ce(SO_4)nA_{4-2n}(m-4+2n)HA + (4-2n)H^+ \quad (6)$$

Accordingly, the distribution coefficient (D) and the equilibrium constant (K) of the reaction are obtained from the following equations:

$$D = \frac{[Ce(SO_4)nA_{4-2n}(m-4+2n)HA]_o}{C^{4+}} \quad (7)$$

$$K = \frac{[Ce(SO_4)nA_{4-2n}(m-4+2n)HA][H^+]^{(4-2n)}}{[C^{4+}][SO_4^{2-}]^n[(HA)_2]^{\frac{m}{2}}} \quad (8)$$

The logarithmic form of Equation (8) is:

$$Log\ D = Log\ K + (4-2n)pH + n\ Log\ [SO_4^{2-}] + \left(\frac{m}{2}\right) Log\ [(HA)_2] \quad (9)$$

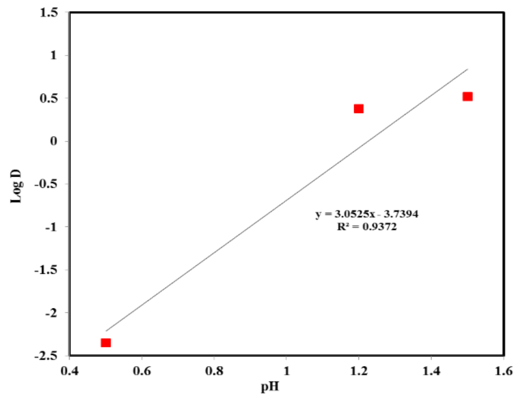

Fig. 10. Plot of log D *vs.* equilibrium pH for the extraction of cerium (IV) with D2EHPA.

The linear relationship between the log D values and pH (Fig. 10) shows that the distribution coefficient, D, of Ce (IV) increased with the increase in equilibrium pH value with a slope of about 3.0, indicating the release of 3 mol of H^+ ions in the aqueous medium with 1 mol of cerium (IV). Therefore, the value of *n* in Equation (6) is 0.5, which results in 0.5 mol of sulfate in the extracted complex.

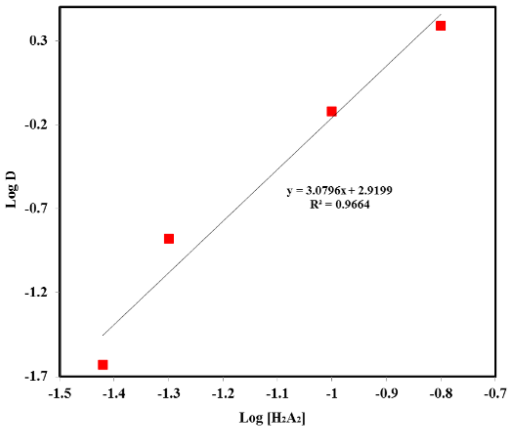

Fig. 11. Plot of log D *vs*. log[H_2A_2] for extraction of cerium (IV) with D2EHPA.

The plot of log D *vs*. log[H_2A_2] (Fig. 11) provides the metal-ion/extractant ratio of the extracted species. It can be seen from Fig. 11 that the plot of log D *vs*. log[H_2A_2] is linear with the slope of ~3.0 in the extraction system, indicating that the m value in Equation (6) is 6. This suggests the association of 3 mol of the monomer organophosphorus-based acidic extractant with the extracted species. Therefore, the overall cation exchange extraction reaction may be represented by the following reaction:

$$C^{4+} + 0.5SO_4^{2-} + 3(HA)_{2(o)} \rightarrow Ce\,(SO_4)_{0.5}A_3.3HA + 3H^+ \qquad (10)$$

As Equation (10) indicates, even in this cationic range, part of the solvent in the form of HA solvates the extracted complex, and this is because the reactive oxygen of D2EHPA is much more basic than the reactive oxygen of H_2O. As a result, D2EHPA easily replaces part of the coordination water molecules in the extracted complex.

Separation of Ce (IV) from RE (III)

The parameters that affect the Ce (IV) extraction process were experimentally investigated. The optimum conditions for Ce (IV) extraction can be summarized as follows: D2EHPA concentration in kerosene, 0.5 mol L^{-1}; aqueous feed solution pH, 2.1; volume ratio of organic phase to aqueous phase, 1; temperature: 25±1 °C; extraction time, 5 min. The obtained extraction efficiency of Ce (IV) under the experimentally determined optimal conditions, was over 98%.

RE (III) elements such as La (III), Pr (III), Nd (III) and Sm (III) generally accompany Ce (IV) in solution. Under the derived optimum conditions, the separation of Ce (IV) from other RE (III) elements was investigated.

The separation factor for Ce/RE was calculated as follows:

$$SF_{Ce/RE} = \frac{(C_{Ce}/C_{RE})_{org}}{(C_{Ce}/C_{RE})_{feed}} \qquad (11)$$

where C_{Ce} and C_{RE} are the concentrations of Ce (IV) and RE (III) in the organic and initial aqueous feed solution, respectively, in mol L^{-1}. The obtained results of the extraction of Ce (IV) and RE (III) are given in Table 3. Undoubtedly, the system is highly selective for Ce (IV), and the separation factors are relatively high.

Table 3. Standard molar thermodynamic quantities for the Ce (IV) extraction process at a temperature of 298.15±1 K

Initial concentration in the feed solution (mol L^{-1})	Percent extraction (%E)		$SF_{Ce/RE}$
	Ce(IV)	RE(III)	
Ce 0.002 + La 0.002	98.15	0.55	175.27
Ce 0.002 + Pr 0.002	97.68	0.88	109.75
Ce 0.002 + Nd 0.002	98.44	0.74	131.25
Ce 0.002 + Sm 0.002	98.70	0.44	219.33

CONCLUSIONS

The cerium (IV) extraction equilibria in the H_2SO_4-D2EHPA system were thoroughly studied using the organic ligand D2EHPA in kerosene as an extractant. The extracted species is $Ce(SO_4)_{0.5}.A_3.3HA$. Thermodynamic functions of the extraction reaction were calculated and considered. Cerium (IV) extraction is essentially an exothermic and spontaneous process. The obtained experimental results illustrate that D2EHPA has good extractability for Ce (IV) in H_2SO_4 media. Thus, based on experiments, one can conclude that D2EHPA is a potential extractant for separating Ce (IV) from other RE (III) in binary initial solutions.

REFERENCES

1. Y. Shan, Y. Liu, Y. Li, W. Yang, *Sep. Pur. Tech.*, **250**, 117 (2020).
2. K. R. Singh, V. Nayak, T. Sarkar, R. P. Singh, *RSC Adv.*, **10**, 27194 (2020).
3. M. Natali, A. Zanella, A. Rankovic, D. Banas, C. Cantaluppi, L. Abbadie, J.-C. Lata, *Env. Sci. Poll. Res.*, **23**, 23496 (2016).
4. S. Kalakotla, N. Jayarambabu, G. K. Mohan, R. B. S. Mydin, V. R. Gupta, *Coll. Sur. Bio.*, **174**, 199 (2019).
5. I. Celardo, J. Z. Pedersen, E. Traversa, L. Ghibelli, *Nano.*, **3**, 1411 (2011).
6. F. Khanramaki, F. Zahakifar, *Prog. Nuc. Ene.*, **160**, 104664 (2023).
7. S. Alamdar Milani, M. Hafizi, H. Abolghasemi, F. Zahakifar, *J. Wat. Wast.*, **32**, 68 (2021).
8. F. Zahakifar, R. Davarkhah, A. Charkhi, M. Torab-Mostaedi, *Nucl. Sci. Tech.*, **88**, 117 (2017).
9. S. Alamdar Milani, N. Omidvari, F. Zahakifar, *J. Min. Eng.*, **17**, 1 (2022).

10. F. Khanramaki, J. Safdari, A. S. Shirani, R. Torkaman, *Rad. Acta*, **106**, 631(2018).
11. F. Khanramaki, J. Safdari, A. S. Shirani, R. Torkaman, *Proc. Nucl. Energy*, **109**, 159 (2018).
12. F. Khanramaki, A. S. Shirani, J. Safdari, R. Torkaman, *Chem. Eng. Res. Des.*, **125**, 181 (2017).
13. S. Alamdar Milani, F. Zahakifar, A. Charkhi, *J. Iran. Chem. Soc.*, **16**, 455 (2019).
14. F. Zahakifar, A. Charkhi, M. Torab-Mostaedi, R. Davarkhah, *Rad. Acta*, **106**, 181 (2018).
15. F. Zahakifar, A. Charkhi, M. Torab-Mostaedi, R. Davarkhah, *J. Rad. Nucl. Chem.*, **316**, 247 (2018).
16. F. Zahakifar, A. Charkhi, M. Torab-Mostaedi, R. Davarkhah, A. Yadollahi, *J. Rad. Nucl. Chem.*, **318**, 973 (2018).
17. S. Milani, F. Zahakifar, M. Faryadi, *Rad. Acta*, **110**, 841 (2022).
18. A. Yadollahi, M. Torab-Mostaedi, K. Saberyan, A. Charkhi, F. Zahakifar, *Chin. J. Chem. Eng.*, **27**, 1817 (2019).
19. F. Zahakifar, A. Charkhi, M. TorabMostaedi, R. Davarkhah, *J. Nuc. Sci. Tech.*, **95**, (2021).
20. P. Zaheri, F. Zahakifar, M. G. Maragheh, *Bulg. Chem. Commun.*, **55**, 75 (2023).
21. A. B. Botelho Junior, E. F. Pinheiro, D. C. R. Espinosa, J. A. S. Tenorio, M. d. P. G. Baltazar, *Sep. Sci. Tech.*, **57**, 60 (2022).
22. T. Jumadilov, L. Yskak, A. Imangazy, O. Suberlyak, *Mat.*, **14**, 3491 (2021).
23. T. Jumadilov, A. Utesheva, J. Grazulevicius, A. Imangazy, *Poll.*, **15**, 816 (2023).
24. P. Zaheri, R. Davarkhah, F. Zahakifar, *J. Nucl. Sci. Tech.*, **42**, 28 (2021).
25. M. R. A. Shadbad, P. Zaheri, H. Abolghasemi, F. Zahakifar, *Chem. Eng. Proc. Int.*, **184**, 109268 (2023).
26. H. Arabi, S. Milani, H. Abolghasemi, F. Zahakifar, *J. Rad. Nucl. Chem.,* **327**, 653 (2021).
27. F. Zahakifar, A. Keshtkar, E. Nazemi and A. Zaheri, *Rad. Acta*, **105**, 583 (2017).
28. F. Zahakifar, A. Keshtkar, E. Z. Souderjani, M. Moosavian, *Proc. Nucl. Energy*, **124**, 103335 (2020).
29. F. Zahakifar, A. Keshtkar, A. Shirani, A. Zaheri, *J. Nuc. Sci. Tech.*, **8**, 12 (2014).
30. M. Ghasemi Torkabad, A. Keshtkar, F. Zahakifar, A. Yadollahi, A. Zaheri, *J. Nucl. Sci. Tech.*, **42**, 95 (2021).
31. G. Limousin, J.-P. Gaudet, L. Charlet, S. Szenknect, V. Barthes, M. Krimissa, *Appl. Geol.*, **22**, 249 (2007).
32. R. Rostamian, M. Firouzzare, F. Zahakifar, *J. Pol. Res.*, **28**, 193 (2021).
33. V. Alamdarlo, G. Solookinejad, F. Zahakifar, M. R. Jalal, M. Jabbari, *J. Water Wast.*, **32**, 108 (2021).
34. 3A. Doram, M. Outokesh, S. J. Ahmadi, F. Zahakifar, *Rad. Acta*, **110**, 37 (2022).
35. M. Taheri, M. Khajenoori, Z. Shiri-Yekta, F. Zahakifar, *Rad. Acta*, (2023).
36. A. E. Lewis, *Hyd.*, **104**, 222 (2010).
37. X. Zhang, L. Zeng, Y. Wang, J. Tian, J. Wang, W. Sun, H. Han, Y. Yang, *J. Env. Man.*, **344**, 118462 (2023).
38. R. K. Scopes, R. K. Scopes, *Pro. Pur. Prin. Pra.*, **1**, 39 (1982).
39. H.-J. Hong, H. Kim, Y.-J. Lee, J.-W. Yang, *J. Haz. Mat.*, **170**, 1242 (2009).
40. P. Ilaiyaraja, A. K. S. Deb, D. Ponraju, *J. Rad. Nuclear Chem.*, **303**, 441 (2015).
41. 4J. D. Roach, J. H. Zapien, *Water. Res.*, **43**, 4751 (2009).
42. G. Xu, C. Y. Yuan, *Sci. Pub., **12**, 190,* (1987).
43. D. Li, Z. Wang, G. Zeng, *Nucl. Chem. Radio. Chem.*, **6**, 153 (1984).
44. P. Nekovar, D. Schroetterova, M. Mrnka, *J. Rad. Nucl. Chem.*, **223**, 17 (1997).
45. S. Milani and F. Zahakifar, *Bras. J. Chem. Eng.*, **39**, 553 (2022).
46. S. Milani, F. Zahakifar, M. Faryadi, *Bulg. Chem. Commun.*, **54**, 295 (2022).
47. R. G. Bautista, *Hyd. Pro. Fun.*, **10**, 1, (2013).
48. W. Liao, G. Yu, D. Li, *Solv. Extr. Ion Exch.*, **19**, 243 (2001).
49. K. Soldenhoff, *Proc. Int. Solv. Extr. Con., **1***, 1 (1996).
50. J. C. Warf, *J. Amer. Chem. Soc.*, **71**, 3257 (1949).
51. G. Korpusov, V. Levin, N. Brezhneva, N. Prokhorova, I. Eskevich, P. Seredenko, *Russ. J. Inorg. Chem.*, **7**, 1167 (1962).
52. 5T. Healy, and H. McKay, *Rec. Trav. Chim. Pay.*, **75**, 730 (1956).
53. L. Jun, W. Zhenggui, L. Deqian, M. Gengxiqi, L. Dedong, C. Dali, Z. Guocheng, *Met. Ind.,* **2**, 178 (2005).
54. K. Soldenhoff, D. Wilkins, R. Ring, *Mt. Sci. For.*, **315**, 290 (1999).
55. S. Gueu, B. Yao, K. Adouby, G. Ado, *Int. J. Env. Sci. Tech.*, **4**, 11 (2007).
56. F. Zahakifar, A. R. Keshtkar, M. Talebi, *Proc. Nucl. Energy*, **134**, 103642 (2021).
57. F. V. Alamdarlo, G. Solookinejad, F. Zahakifar, M. R. Jalal, M. Jabbari, *J. Rad. Nucl. Chem.*, **329**, 1033 (2021).
58. F. Zahakifar, A. R. Keshtkar, M. Talebi, *J. Rad. Nucl. Chem.*, **327**, 65 (2021).
59. M. Cox, C. Musikas, G. Choppin, J. Rydberg, M. Cox, C. Musikas, G.R. Choppin (eds.), Marcel Dekker, Inc., New York, 2004, p. 455.
60. L. Xinghua, X. Huang, Z. Zhaowu, L. Zhiqi, L. Ying, *J. Rare Earths*, **27**, 119 (2009).
61. J. Brunette, F. Rastegar, M. Leroy, *J. Inorg. Nucl. Chem.*, **41**, 735 (1979).

Bulgarian Chemical Communications, Volume 55, Issue 4 (pp. 414-417) 2023 DOI: 10.34049/bcc.55.4.5549

Application of fiber-optical module for broadband scattering measurements with rod lenses and CCD photodiode in mobile analyses of peach juice

V. Slavova*

Department of Plant Breeding, Maritsa Vegetable Crops Research Institute, Agricultural Academy, Bulgaria

Received: January 07, 2023; Revised: June 15, 2023

It is well known that the use of peach juices in Europe is significant. Therefore, it is important to study scattering as the interaction of light with turbid biological media such as peach juices. This phenomenon is mainly related to the chemical composition of the material of the latter.

The objectives of the present study are to establish the mobile application of a broadband fiber optic system in the analysis of peach juice. The system should be compact enough to perform field analyses. The system must perform precise analysis of peach juices in the factory where they are produced or in the food chain where they are offered. It was established that a fiber-optical module for broadband scattering measurements with rod lenses is significantly sensitive even to a small number of particles in the composition of the peach juice. This fact means that precise analysis of peach juices can be carried out with the system, at the factory where they are produced or at the point of sale where they are available.

Keywords: peach juice, rod lenses, scattering, mobile analyses

INTRODUCTION

The use of natural juices in Europe has almost doubled in recent decades. For many, they are part of a healthier lifestyle. The problem with the quality of natural juices in the food industry is of great importance, since these are widely distributed products [1, 2].

80% of natural juices sold in the EU come from Brazil and the USA. The EU is the largest importer of peach juice in the world. However, this means high CO_2 emissions coming from transport. A Spanish MEP (Member of the European Parliament) presented a report to the EP Environment Committee proposing to encourage the use of locally produced juices that meet European quality standards [3-5].

The interactions of light with turbid biological media such as orange juice are complex phenomena, especially absorption and scattering. Photons often undergo multiple scatterings before being absorbed or passing through the medium in strongly scattering materials. The phenomena considered in the field of quantum electronics are mainly related to the chemical composition of the material.

As an effective replacement for optical fibers in endoscopes, in the late 1960s, Harold Hopkins first introduced rod lenses into optical production. Due to their increased efficiency for light transmission, they are quickly replacing the previously common lenses, almost completely filling the air gaps between the individual lenses. To increase the quality of the transmitted light signal, rod lenses are usually constructed as achromats.

Achromats greatly reduce the effects of chromatic and spherical aberration. They are made in such a way that they bring two or more spectra of a light source into focus [6, 7].

The most common achromat is the achromatic doublet. It is composed of two fused lenses with different dispersion coefficients. Usually, one lens is convex from flint glass, e.g., F2 with a higher dispersion coefficient, and the other is concave from crown glass, e.g., BK7 with a low dispersion coefficient. The radii of the two lenses are selected so that the chromatic aberration of one lens compensates for that of the other [8].

A CCD contains an array of square photosensitive cells that convert incoming photons of light into electrons and accumulate a resultant charge. The cells are connected in series, forming rows and columns, with each cell representing one element of the matrix, called a pixel. Quantum efficiency (QE) refers to the sensor's ability to match the incoming photon signal and convert it to a measurable electronic signal. It is wavelength-dependent or a function of photon energy, and the sensor is usually selected when considering the best QE region of interest for the best wavelength spectral range. Various means have been used to improve the quantum efficiency of CCD sensors [9].

By dint of the constructed fiber-optical module for broadband scattering measurements with rod lenses, a comprehensive analysis of the angular scattering of peach juices of 3 different companies and of freshly squeezed peach juices on site in the food chain that offers them was made [10].

* To whom all correspondence should be sent:
E-mail: vania_plachkova@abv.bg

MATERIALS AND METHODS

Samples

Samples of peach juices from three different companies producing peach juice and one sample of multivitamin juice containing peach juice were used. The samples should represent 20 g of liquid biological material.

Spectral measurements using a fiber-optical module for broadband scattering measurements with rod lenses and CCD photodiode

The installation is applicable in the spectral range of 450 – 710 nm and serves to register non-regulated constituents or bacteria by using the phenomenon of light scattering. The installation is compact enough to perform field analysis (it can be adjusted over an area 40 cm long and 50 cm wide) locally at the research site. The developed installation was applied to practical on-site research in the store that offers the products.

The aim of the mobile application of the system for the analysis of peach juice is to offer their rapid tests. The designed mobile installation is a perfect solution for optimization of experiments when repeated measurements are required for the analysis. A key point in the construction is the unique combination between speed, accuracy of the study and analysis of several scattering angles at the same time. This is a substantial advantage for rapid analysis of peach juices. The scattering effect was investigated by different producers of peach juice. It was precisely shown that the module successfully satisfied their needs.

The fiber-optical module for broadband scattering measurements with rod lenses performs rapid sample tests, and through the scattering effect it registers impurities in natural liquid samples. The detector surface is a 128-pixel InGaAs CCD (G9204-512D Hamamatsu Photonics) linear matrix with a built-in low-noise amplifier characterized by high sensitivity, low current in the dark and high stability in the 410-900 nm spectral range. Two capacitive high-speed analog-to-digital converters (ADCs) transform the analog signals received by the CCD sensor. The spectrum from each lens is visualized on a computer using specially developed software adapted to the specific CCD matrix model. During image generation, the control lines of the CCD cause their charge to be transferred to the adjacent cell in the row or column. Accumulated charge is transferred from cell to cell. Reading the image from the digital camera contains multiple repeated transfers by rows or columns. After all, the CCD output gives one pixel for each clock.

The rod lenses included in the composition of the fiber-optic system are arranged in a special way according to the dimensions of the cuvette, in order to cover the entire outer perimeter. The size of the quartz cuvette was matched to the size of the staff lenses. The latter are arranged in such a way around it that they cover its entire diameter. This precise alignment is done in order to be able to correctly detect the scattering angles of the particles that make up a particular liquid sample that is poured into the cuvette. One lens is convex from flint glass, e.g., F2 with higher dispersion coefficient and the other is concave from crown glass, e.g., BK7 with low dispersion coefficient. The radii of the two lenses are selected so that the chromatic aberration of one lens compensates that of the other, as shown in Figure 1.

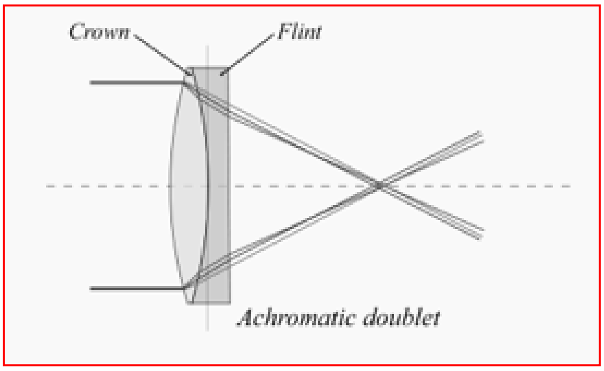

Fig. 1. Drawing of the achromatic doublet

As can be seen, there is more than one lens in the construction of the mobile fiber-optical module for broadband scattering measurements with rod lenses. Bearing in mind that scattered light falls on each lens at a different angle, it can be noted that the module is designed to simultaneously detect 7 scattering angles.

This advantage provides fast and high-quality measurements in biosensors for the analysis of peach juice. Various independent scattering angles can be probed with a single broadband source. Thus, a constructed fiber-optical module for broadband scattering measurements with rod lenses, can be used to determine the angular scattering spectra of peach juice. A quartz cuvette is included in the construction of the module where the desired sample is poured, after which it is irradiated with white light. Each one of the rod lenses receives the light from the different scattering angles of the particles included in the composition of the tested sample.

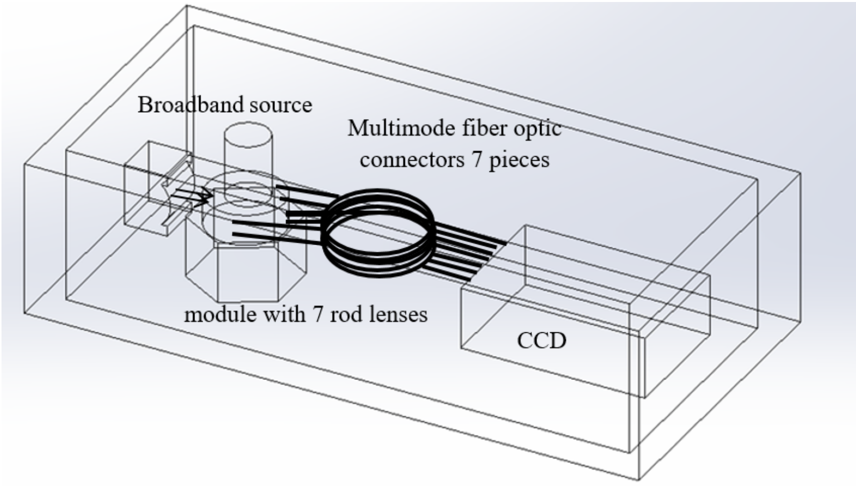

Fig. 2. Fiber-optical module for broadband scattering measurements with rod lenses and CCD photodiode

The multi-functionality of the fiber-optic module allows to detect several particles included in the composition of the liquid sample and thus to optimize the time for liquid analysis.

RESULTS AND DISCUSSION

By means of the constructed fiber-optical module for broadband scattering measurements with rod lenses and CCD photodiode, a comprehensive analysis of peach juices of 3 different companies and of freshly squeezed peach juices was made.

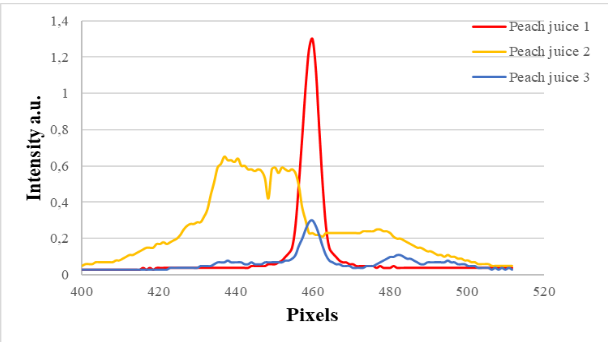

Fig. 3. Angular scattering comparison between the peach juices of three different producers

Figure 3 clearly shows the difference between the angular scattering of peach juice by three different manufacturers. The juice of the 1st producer company is the purest. There are no deviations from the angular scattering typical for peach juice. The peach juice of the first producer is naturally squeezed fresh at the time of the study. For this reason, we are sure that the distribution is pure peach fresh.

In Figures 4, 5 and 6, there is no significant deviation in the angular scattering comparison of natural peach juices and multivitamins, which means that peach is contained in multivitamin juice.

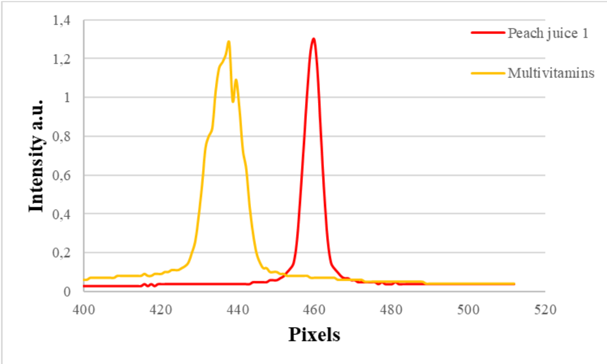

Fig. 4. Angular scattering comparison between the peach juice of producer 1 and multivitamins

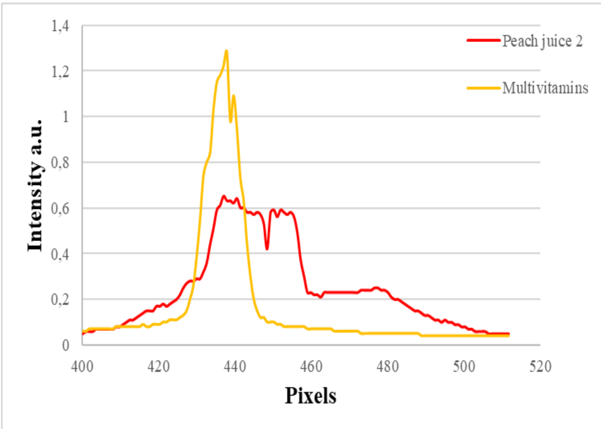

Fig. 5. Angular scattering comparison between producer 2's peach juice and multivitamins

From the analysis of the samples of peach juice it can be concluded that most of the companies producing peach juices work with preservatives and colorings, and not with natural products. Given the sensitivity of the module to very small particles, we can say that there are almost no peach organic substances in the composition of factory juices, with the exception of sample 1, which is the purest.

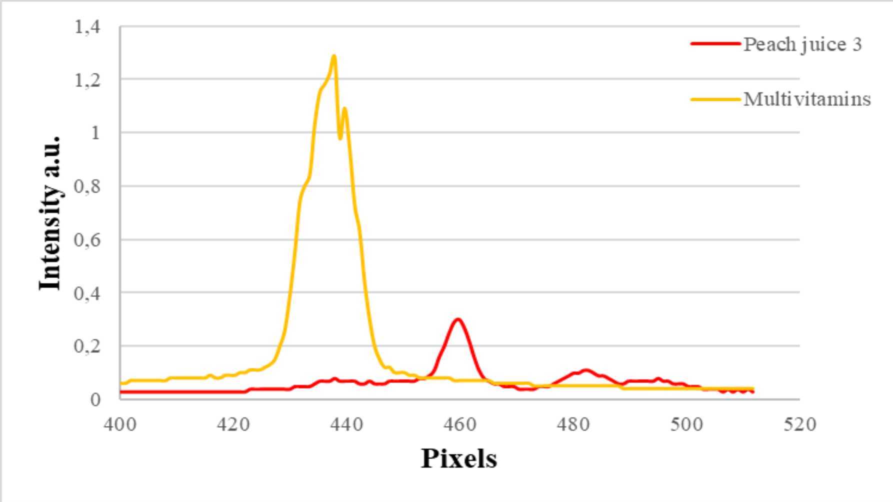

Fig. 6. Angular scattering comparison between the peach juice of producer 3 and multivitamins

A literature survey was conducted on similar research. It turned out that until now the described experimental approach for mobile analysis of peach juice has not been applied nationally or internationally. This gives us reason to claim that, for the first time, a module for broadband scattering measurements was applied for the analysis of peach juice at the distributor site.

CONCLUSIONS

It can be concluded that:

✓ A mobile wide-spectrum fiber-optic system with a staff lens is compact enough to perform field analysis (it is aligned on an area 40 cm long and 50 cm wide).

✓ The developed installation is applied for practical research in analysing peach juice.

✓ The wide-spectrum fiber-optic system with staff lenses is significantly sensitive even to a small number of particles in the composition of the peach juice.

✓ The system can perform precise analysis of peach juices, in the factory where they are produced or in the food chain where they are offered.

REFERENCES

1. G. Krapfenbauer, M. Kinner, M. Gössinger, R. Schönlechner, E. Berghofer, *J. Agric. Food Chem.*, **54**, 5453 (2006).
2. A. Shalini, N. Nachiappan, R. Waghmare, M. Bhat, *Food Production*, *Processing and Nutrition,* **5**, 458 (2023).
3. F. Ammari, L. Redjdal, D. N. Rutledge, *Analysis Food Chemistry*, **168**, 211 (2015).
4. J. E. Lozano, Fruit Manufacturing, Scientific Basis: Engineering Properties, and Deteriorative Reactions of Technological Importance, 2006, p. 103.
5. A. Kumar, M. Castro, J. Feller, *Sensors*, **23**(8), 4017 (2023)
6. M. T. Gale, *OSA Technical Digest*, **75**, 18 (2002).
7. G. Bal, M. Malinauskas, M. Farsari, S. Juodkazis, *Adv. Funct. Mater*., 5230 (2023).
8. J. C. Palais, *Applied Optics*, **19**, 2011 (1980).
9. G. Ghione, Semiconductor Devices for High-Speed Optoelectronics, Cambridge University Press, 2009, p. 255.
10. Handbook of Optoelectronics, J. P. Dakin, R. G, W Brown (eds.), Taylor and Francis, Boca Raton, 2006, p. 74.

Thermal stability of vegetable oil emulsions and influence on the texture parameters of cooked sausages

M. Momchilova[1*], G. Zsivanovits[1], M. Marudova[2]

[1]*Department of Food Technologies, Institute of Food Preservation and Quality, Agricultural Academy, 154 Vasil Aprilov Blvd., 4000 Plovdiv, Bulgaria*

[2]*Department of Physics, Faculty of Physics and Technology, Paisii Hilendarski University of Plovdiv, 24 Tsar Asen Street, 4000 Plovdiv, Bulgaria*

Received: February 15, 2023; Revised: August 07, 2023

This study is focused on the possibility of using two vegetable oil emulsions as substitutes for pork back fat in the traditional formulation of cooked sausages. The effect of these emulsions on the texture parameters of cooked sausages was investigated. The statistically significant difference ($P<0.05$) found in the texture parameters of the sausage samples was closely related to the solid fat index (SFI) which is a measure of the percentage of fat in crystalline (solid) phase to total fat (the remainder being in liquid phase) across a temperature gradient. The addition of vegetable oil emulsions reduced the solid fat index at temperatures above 0°C, which was the result of the animal fat substitution and lower melting temperature of the final product. The reduced crystalline phase content in the fats led to lower hardness, chewiness and gumminess values of the final products.

Keywords: Meat sausages, fat replacer, vegetable oil emulsions, DSC, texture

INTRODUCTION

Cooked sausages are widely distributed in a lot of countries and play a major role in the meat industry from an economic point of view. They can be made from different meat types, such as beef, pork, poultry, etc., with the addition of various flavours, fillers and binding agents. This type of sausages, however, is characterised by a high fat content, and the attempts at fat reduction aim to assist consumers in their efforts to limit the intake of large amounts of fats, including saturated fatty acids and cholesterol [1]. The excessive consumption of the latter is involved in the development of hypertension, obesity, cardiovascular and chronic diseases [2-4]. Fats, however, are an important factor that affects the emulsion stability and the water retention and emulsifying capacity of the meat batter [5], and these factors are directly responsible for the physical properties of meat products and their sensory perception by consumers [6-8]. The fat that is most commonly used in the manufacture of meat products, including cooked sausages, is pork back fat. The development of low-fat meat products without any changes in their technological and quality characteristics poses a challenge to the meat industry. Therefore, in recent years there has been growing interest in vegetable oils and the possibility of using them in meat product manufacture. In this regard chia and grape seed oils can be used in the production of cooked sausages because they contain ω-3 and ω-6 fatty acids [9], phytosterols, tocopherols, flavonoids, phenolic acids [10]. In this way they influence plasma cholesterol values with their cardioprotective and antidiabetic effects [11,12]. Compared to animal fats, vegetable oils contain larger amounts of unsaturated fatty acids and meet a number of dietary requirements [13]. This is one of the main reasons for the rising trend towards using vegetable oils in various food products, meat products in particular. Regardless of the positive effects of vegetable oils, each oil has different technological properties and depends largely on the characteristics of the raw material it is obtained from. The differences in melting and crystallisation points, the fatty acid composition, color, taste, liquid state, and the high unsaturated fatty acid content could have an adverse effect on a number of technological characteristics, e.g. the texture parameters of the meat products in which they are used [14-18]. In this aspect, pre-emulsification with a non-meat protein such as sodium caseinate is a promising approach to the manufacture of meat products by stabilising the meat batter so that the fat would not separate from the meat matrix [19] since this would affect the technological properties of meat products [20].

The aim of this study was to investigate the thermal characteristics of two types of emulsified oils as pork back fat substitutes and their effect on the texture parameters of reformulated cooked sausages.

* To whom all correspondence should be sent:
E-mail: masha821982@abv.bg

MATERIALS AND METHODS

For the purposes of the experiment, we made seven test formulations with different amounts of pork back fat and the type and amount of vegetable oil emulsions are specified in Table 1. In order to preserve the texture of sausages as much as possible, an alternative approach has been proposed, including the replacement of animal fat with pre-emulsified vegetable oils [21] and the inclusion of a non-meat protein source to stabilize the meat emulsion system [22, 23]. The meat raw materials were purchased from stores, the potato starch "Stärkina" and sodium caseinate from the company Picco - Bulgaria, and the vegetable oils from specialized health food stores. The ingredients for the formulation of the emulsions were vegetable oils, sodium caseinate and water in a 5:1:5 ratio. The vegetable oil emulsions, sodium caseinate and hot water (60°C) (in a 5:1:5 ratio) were prepared on a cutter (model CL/5, FIMAR, Italy) in advance, one day before they were used. The sodium caseinate and the hot water were stirred for 2 min, then the oils were added and the mixture was chopped for another 3 min. The emulsion was cooled to 6-8°C. The experimental sausages were made by grinding the pork meat and back fat in a meat grinder through a 4 mm grinder plate; then, the meat was placed in the cutter working at a slow speed and sodium chloride, nitrite, polyphosphate and half of the ice were added. The emulsion was chopped at a high speed and after the water was absorbed, the sodium caseinate, spices and the rest of the ice were added. The chopping continued until a temperature of 6-8 °C was reached; then, the fat and/or emulsions were added. The chopping continued until 12 °C and finally, the starch was added. The chopping went on until 14 °C. The finished filling mass was transferred to a stuffer and stuffed into 50-mm polyamide casings, the individual pieces weighing 0.250 kg each. Heat processing was performed at 65 °C until 45 °C were reached at the centre of the sausage; then, the cooking continued at 78 °C until 72 °C were reached at the centre of the sausage, and held for 5 min. After cooling, the sausages were kept in a cold store at 4 ± 2 °C until the time of the analyses. The technological steps in the manufacture of the experimental samples are presented in Fig. 1. For the analysis of the texture profile of the finished sausages from sample P1 to sample P7 [19], a TA-XT Plus (Stable Micro Systems, Surrey, GB) texture analyser was used. The cylinder was 25 mm in diameter. Discs 60 mm in diameter and 19±2 mm in height were made from the sausage samples for the test. The samples were compressed at a rate of 2 mm s^{-1} to 5 mm deformation. The relaxation time between two compressions was set at 5 s. The hardness, springiness, homogeneity, chewiness, resilience, gumminess and adhesiveness were calculated for further analysis [24-26]. The melting profiles of the fats extracted from the investigated sausage samples from P1 to P7, as well as from GVO sample P8, GSO sample P9 and sample P10 PBF, were examined using a DSC 204F1 Phoenix differential scanning calorimeter (Netzsch Gerätebau GmbH, Germany). The instrument was calibrated with indium standard (Tm = 156.6 °C, ΔHm = 28.5 J.g^{-1}). The sample was hermetically sealed in an aluminium pan. An empty, hermetically sealed aluminium pan identical to the sample pan was used as a reference. The experimental conditions were identical for all the products. The samples were heated at a heating rate of 5 °C/min to 80 °C and held for 30 min to ensure that the fat was fully melted and all the nuclei were destroyed [27]. After melting, the samples were cooled to -60 °C at a cooling rate of 5 °C.min^{-1}. The samples were stored at -60 °C for 30 min and finally, the melting curves were recorded by scanning the samples to 80 °C at a heating rate of 5.0 °C.min^{-1}. The solid fat index (SFI) was calculated as the percentage of fat in crystalline (solid) phase to total fat (the remainder being in liquid phase) across a temperature gradient.

All the data obtained were statistically analysed by one-way analysis of variance (ANOVA) using the Statgraphics 16 software product. Significant ($P < 0.05$) differences between the treatments were determined using Duncan's post hoc test. The experiments were made with fivefold repetitions, and the data in the graphs are the arithmetic means of the indicators measured. Statistically significant differences between the mean values were found at a probability less than 0.05. The interrelationships between the solid fat index (SFI) and the texture parameters were investigated by correlation analysis.

RESULTS AND DISCUSSION

The differences in the texture parameters of the reformulated sausages are presented in Table 2. The table shows that the use of emulsions of different oil types as animal fat substitutes had a considerable effect on all textural properties except for the resilience parameter, and there was a minor difference in the homogeneity parameter. As had been expected, the emulsions of the two vegetable oil types used as pork back fat substitutes and their quantity affected the hardness ($P<0.05$). The use of the emulsions resulted in a softer texture compared to the control sample, with the exception of sample P4 ($P<0.05$).

Table 1. Sample formulations of cooked meat sausages with vegetable oil emulsions

Ingredients, g.kg^{-1}	Samples						
	Sample P1 (control)	Sample P2	Sample P3	Sample P4	Sample P5	Sample P6	Sample P7
Pork meat	790	790	790	790	790	790	790
Pork back fat	210	-	-	105	105	-	70
Emulsion (chia oil + water + sodium caseinate)	-	210	-	105	-	105	70
Emulsion (grape seed oil + water + sodium caseinate)	-	-	210	-	105	105	70
Salt	20	20	20	20	20	20	20
Sodium nitrite	0.05	0.05	0.05	0.05	0.05	0.05	0.05
Black pepper	4	4	4	4	4	4	4
Nutmeg	1	1	1	1	1	1	1
Sugar	2	2	2	2	2	2	2
Phosphates	2	2	2	2	2	2	2
Potato starch	30	30	30	30	30	30	30
Sodium caseinate	10	10	10	10	10	10	10
Water/ice	290	290	290	290	290	290	290

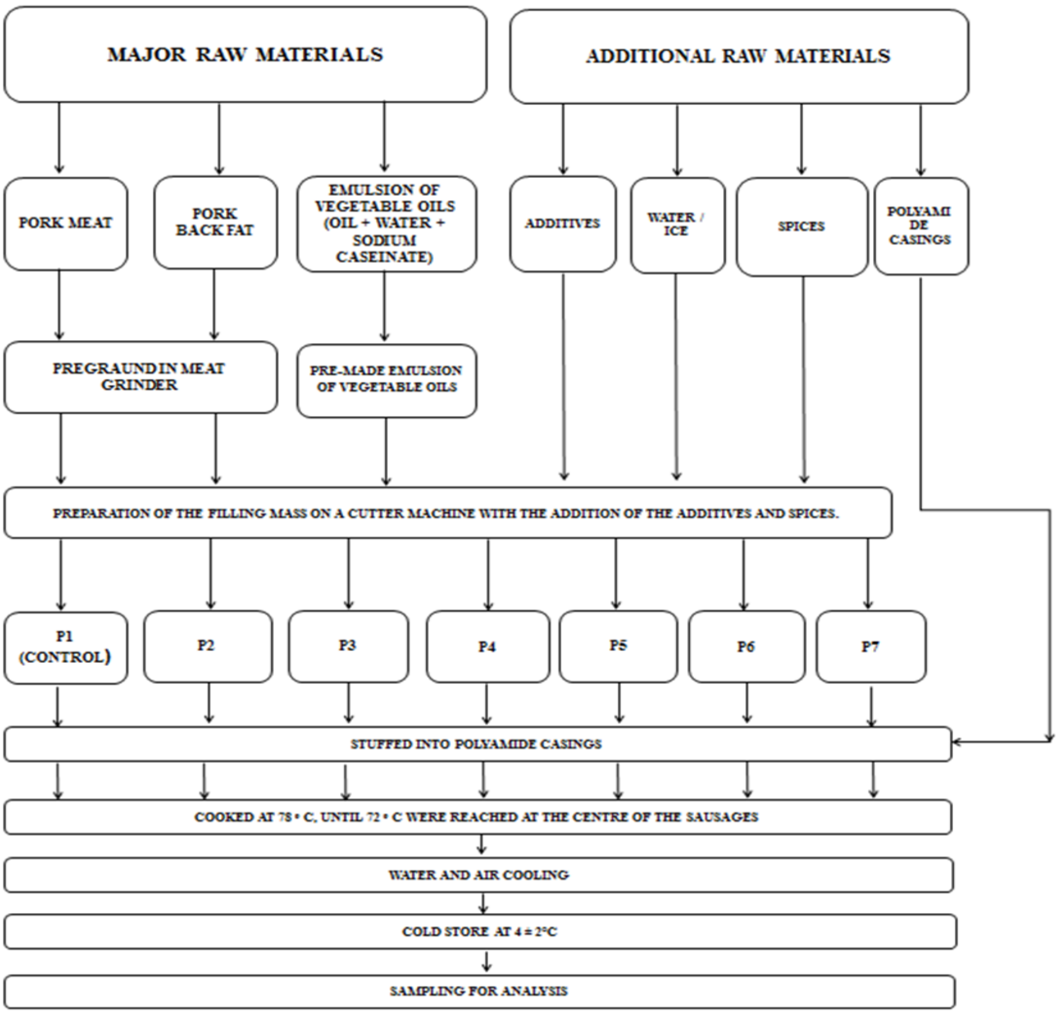

Fig. 1. Processing diagram of cooked sausages

Some authors [28] pointed out that the use of chia vegetable oil in reformulated sausages led to a rise in some of the texture parameters during storage. Other authors [29] reported that the use of vegetable oils as pork back fat substitutes in meat pâtés resulted in lower hardness values, perhaps due to the increased unsaturated fatty acid content in the vegetable oils. Based on previously published data about the fatty acid content of here investigated products [30], it could be concluded that the hardness values in our experiments were fully consistent with the above reports, and the value of sample P3, where 100 % of the animal fat had been replaced by grape seed oil emulsion, was the closest to and a little higher than that of the control sample. The lowest hardness value, statistically discernible ($P<0.05$) from the other samples, was measured for sample P6, where emulsions of both vegetable oils had been used. According to [31, 32], chewiness is a parameter that reflects the results connected with hardness since it is a secondary parameter dependent on hardness, and it provides information on the force or work needed for chewing the sample studied [25].

The studies demonstrated that the consumption of sample P4 was related to the greatest force needed for chewing, followed by sample P1. Resilience and gumminess provide information on the structural and mechanical properties of the tested products that affect their performance during consumption. The values measured in the reformulated sausages were closely related to the hardness and homogeneity values. The gumminess parameter showed higher values in sample P4, followed by the control sample, and they were statistically different ($P<0.05$) both from each other and from the other samples. As regards the springiness parameter, the use of chia and grape seed vegetable oils in emulsion form led to higher values in the experimental samples compared to the control sample ($P<0.05$), which could be attributed to the use of a non-meat protein as emulsifier, which, according to [33], improves the structural properties, jellifying capacity and springiness in the meat system. Adhesiveness expresses the degree of adhesion of the product to the working organ, i.e., the teeth, in its movement to the original position on completion of the first cycle. In view of the considerable differences in the adhesiveness (stickiness) of a product observed in the different samples, the effect of the two vegetable oil emulsions, from chia and grape seeds, needs to be taken into account. The adhesiveness of the experimental samples was found to decrease with the exception of sample P6, where emulsions of both vegetable oils had been used as pork back fat substitutes, all samples being statistically discernible ($P<0.05$) from the control sample.

One of the main thermal characteristics of lipids is the Solid Fat Index (SFI), which shows the part of the fat that is still in crystalline state at a curtain temperature. SFI is responsible for many of the fundamental characteristics of fatty foods, such as physical appearance, organoleptic properties and spreadability, also influencing the plasticity of an edible oil product [34]. The SFIs for the oil raw material (chia vegetable oil, grape seed oil and pork back fat) and for the sausages investigated are presented in Fig. 2. The SFI decreased most rapidly in the grape seed oil, and it was practically zero at temperatures above 0 °C. Its behavior was similar in the chia vegetable oil: it was higher at negative temperatures and dropped at positive temperatures. In comparison, the SFI in the pork back fat was the highest at positive temperatures. The SFI temperature dependence is strongly influenced by the fatty acid composition of fats, being lower for unsaturated fatty acids, which melt at negative temperatures.

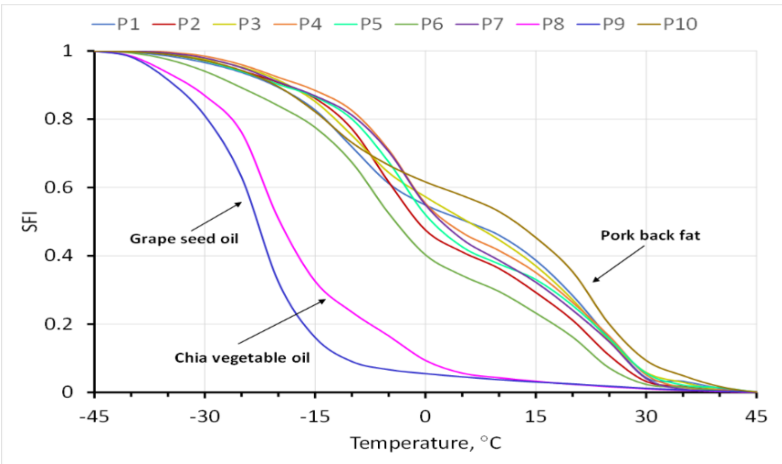

Fig. 2. SFI of the raw materials and sausages

Table 2. SFI of cooked sausage samples at 15 °C, texture parameters, and correlations between the SFI and the texture parameters

Sample	SFI (15°C)	Hardness (N)	Springiness	Homogeneity	Chewiness (N)	Resilience	Gumminess	Adhesiveness (Nmm)
P1	0.3870	24.23±2.39^{d}	0.91±0.03^{a}	0.57±0.03^{b}	12.48±1.19^{d}	0.45±0.02^{a}	13.73±1.29^{d}	-0.31±0.06^{b}
P2	0.2925	20.43±2.29^{b}	0.96±0.02^{c}	0.58±0.04^{b}	11.34±1b^{cd}	0.46±0.02^{a}	11.82±0.95^{b}	-0.14±0.03^{d}
P3	0.3702	22.84±2.7^{cd}	0.92±0.04^{ab}	0.58±0.05^{b}	12.13±2.08^{cd}	0.46±0.06^{a}	13.21±1.94^{cd}	-0.12±0.02^{d}
P4	0.3509	28.75±4.37^{e}	0.93±0.01^{ab}	0.53±0.03^{a}	14.01±2.07^{e}	0.44±0.04^{a}	15.1±2.18^{e}	-0.16±0.03^{d}
P5	0.3302	20.59±3.58^{b}	0.92±0.04^{ab}	0.55±0.03^{ab}	10.53±2.05^{ab}	0.46±0.04^{a}	11.4±2.21^{ab}	-0.27±0.05^{c}
P6	0.2322	18.21±1.32^{a}	0.92±0.04^{ab}	0.56±0.03^{b}	9.38±0.98^{a}	0.45±0.03^{a}	10.24±0.92^{a}	-0.38±0.07^{a}
P7	0.3225	21.1±2.56^{bc}	0.93±0.03^{bc}	0.57±0.04^{b}	11.28±1.47^{bc}	0.47±0.04^{a}	12.09±0.63^{bc}	-0.09±0.02^{e}
R*		0.6981	-0.3517	-0.0018	0.7601	-0.0622	0.7968	0.3516
P**		0.0811	0.4391	0.9970	0.0473	0.8943	0.0319	0.4395

$^{a-e}$-values within the same column bearing a common superscript did not differ statistically (P > 0.05)
R*- correlation between the texture parameters and SFI
P**- uncertainty level of the correlations

The lowest values of the index across the whole temperature range for the sausages studied were observed for sample P6, which contained the vegetable oils emulsions in equal proportions, with no pork back fat added. However, the values were higher than those of the vegetable oils used since the sample contained pork and, respectively, the animal fat included in it. The same sample showed the lowest hardness, chewiness and gumminess values, but also the highest adhesiveness values. The highest SFI was detected for the control sausage (P1), which contained pork back fat only. It ranked second with regard to the texture parameters. The full replacement of the pork back fat with chia oil emulsion (P2) resulted in very soft texture and a low SFI (15°C). The replacement of the pork back fat with GSO emulsion (P3) led to a high SFI (15°C) and moderate texture parameters. The hardest sausage (P4: pork back fat + chia oil emulsion) had a moderate SFI (15°C). The mixing of pork back fat with chia emulsion (P5) reduced the SFI (15°C) and the texture parameters. The equilibrium mixture (P7) of the fat components showed a high SFI (15°C) with moderate texture parameters and very low adhesiveness. It was interesting to note that the sausages prepared with fat mixtures (sample P4, P5 and P6) were characterised by lower SFIs than the pure fats. A possible reason could be the different morphology of the crystalline phase in the fat blends. In mixtures of materials that cannot co-crystallise, a more defective fine crystalline structure usually occurs, which is characterised by a lower melting point; hence, the SFI decreases [35]. In order to look for the interrelationships between the SFI at 15°C (Table 2) and the texture parameters, a correlation analysis was performed. It showed strong correlations with a meaningful uncertainty level between SFI: hardness (R=0.6981, P=0.0811), SFI: chewiness (R=0.7601, P=0.0473) and SFI: gumminess (R=0.7968, P=0.0319) (Table 2).

The SFI decrease led to a decrease in the hardness, chewiness and gumminess rheological parameters. Very similar results were reported by Dreher *et al*. [36, 37], who investigated the texture, appearance and sensory characteristics of plant-based salami analogues. He explained the observed correlations with the structure of the different fat particles, which affected the salami texture. [38] associated the change in texture with the degree of fatty acid saturation and the lower melting point of unsaturated fatty acids inherent to vegetable fats.

CONCLUSION

The use of vegetable oils in emulsion form as animal fat substitutes and their quantity in cooked sausages affected the texture parameters of the sausages. Sample P4, which contained equal amounts of chia vegetable oil emulsion and pork back fat, was characterised by the largest increase in the texture parameter values, except for homogeneity and resilience, compared to the control sample and the rest of the experimental samples. The lowest and statistically discernible values (P<0.05) for the control sample and the other samples were those for sample P6. The differences in the texture parameters were closely related to the decrease in the concentration of the fraction of fats in crystalline phase as indicated by the lower solid fat index (SFI).

Acknowledgements: *This study was funded by the Scientific Research Fund, the competition for fundamental scientific research of young scientists and post-doctoral students 2020, under project KP-06 M47/4 of 27 November 2020 "Vegetable oils and/or flours as new substitutes for animal fats,*

wholesome bioactive sources for the reformulation of emulsified meat sausages. Effects on the lipid profile, quality characteristics and technological properties",

REFERENCES

1. C. V. B. Souza, E. R. B. Bellucci, J. M. Lorenzo, A. C. D. S. Barretto, *Food Sci. Technol.,* **39**, 295 (2019).
2. M. A. D. Nobile, A. Conte, A. L. Incoronato, O. Panza, A. Sevi, R. Marino, *Meat Sci.*, **81**, 263 (2009).
3. Y. C. Trevisan, C. V. Bis, J. M. Henck, A. C. S. Barretto, *Braz. J. Food Technol.,* **19** (2016).
4. M. S. Rahman, J. K. Seo, M. A. Zahid, J. Y. Park, S. G. Choi, H. S. Yang, *Meat Sci*., **151**, 89 (2019).
5. Y. S. Choi, J. H. Choi, D.J. Han, H. Y. Kim, M. A. Lee, J. Y. Jeong, H. J. Chung, C. J. Kim, *Meat Sci*., **84**, 557 (2010).
6. D. Álvarez, M. Castillo, F. A. Payne, M. D. Garrido, S. Bañón, Y. L. Xiong, *J, Food Eng*., **82**, 310 (2007)
7. Y.S. Choi, J. H. Choi, D. J. Han, H. Y. Kim, M. A. Lee, H.W. Kim, J. Y. Jeong, C. J. Kim, *Meat Sci*., **82**, 266 (2009).
8. J. S. Lee, H. G. Kim, M. J. Choi, Y. J. Cho, *Food Sci. Anim. Resour.,* **40**, 262 (2020).
9. C. F. Rodrigues, W. Salgueiro, M. Bianchini, J. C. Veit, R. L. Puntel, T. Emanuelli, C. C. Dernadin, D. S. Ávila, *Nutr. Metab*., **15**, 1 (2018).
10. F. B. Shinagawa, F. C. D. Santana, L. R. O. Torres, and J. Mancini-Filho, *Food Sci. Technol*., **35**, 399 (2015).
11. Y. S. Choi, J. H. Choi, D. J. Han, H. Y Kim, M. A Lee, H. W. Kim, J. W. Lee, H. J. Chung, C. J. Kim, *Meat Sci*., **84**, 212 (2010).
12. E. Antonini, L. Torri, M. Piochi, G. Cabrino, M. A. Meli, R. D. Bellis, *Meat Sci*., **161**, (2020).
13. W. M. Willis, R. W. Lencki, A. G. Marangoni, *Crit. Rev. Food Sci. Nutr*., **38,** 639 (1998).
14. I. C. Pappa, J. G. Bloukas, I. S. Arvanitoyannis, *Meat Sci.*, **56**, 81 (2000)
15. E. J. C. Ospina, C. A. Sierra, O. Ochoa, J. A. Pérez-Álvarez, J. ez-López, *Crit. Rev. Food Sci. Nutr*, **52**, 113 (2012).
16. B. Kılıç, C. O. Özer, *Meat Sci.*, **148**, 206 (2019).
17. T. K. Kim, H. I. Yong, S. Jung, Y. B. Kim, Y. S. Choi, *Meat sci*., **163**, 108079 (2020).
18. M. Vargas-Ramella, P. E. Munekata, M. Pateiro, D. Franco, P. C. Campagnol, I. Tomasevic, R. Domínguez, J. M. Lorenzo, *Foods*, **9**, 571 (2020).
19. E. Muguerza, O. Gimeno, D. Ansorena, J. G. Bloukas, I. Astiasarán, *Meat Sci.*, **59**, 251 (2001).
20. R. T. Heck, E. Saldaña, J. M. Lorenzo, L. P. Correa, M. B. Fagundes, A. J. Cichoski, C. R. de Menezes, R. Wagner, P. C. B. Campagnol, *Meat Sci.*, **156**, 174 (2019).
21. D. J. Bishop, D. G. Olson, C. L. Knipe, *J. Food Sci*., **58**, 484 (1993).
22. E. Muguerza, O. Gimeno, D. Ansorena, J. G. Bloukas, I. Astiasarán, *Meat Sci.,* **59**, 251 (2001).
23. D. J. Bishop, D. G. Olson, C. L. Knipe, *J. Food Sci.* **58**, 484 (1993).
24. M. C. Bourne, *Food Technol*., **32**, 62 (1978).
25. M. Bourne, Food Texture and Viscosity: Concept and Measurement, 2nd edn. London, Academic Press, Elsevier, 2002.
26. E. J. Kim, V. K. Corrigan, D. I. Hedderley, L. Motoi, A. J. Wilson, M. P. Morgenstern, *J. Texture Stud*., **40**, 457 (2009).
27. J. W. Litwinenko, A. M. Rojas, L. N. Gerschenson, A. G. Marangoni, *J. Am. Oil Chem. Soc.*, **79**, 647 (2002).
28. F. A. L. de Carvalho, P. E. Munekata, M. Pateiro, P. C. Campagnol, R. Domínguez, M. A. Trindade, J. M. Lorenzo, *LWT.*, **122**, 109052 (2020).
29. D. Martin, J. Ruiz, R. Kivikari, E. Puolanne, *Meat Sci.,* **80**, 496 (2008).
30. M. Momchilova, M. Marudova, D. Gradinarska-Ivanova, *Bulletin of University of Agricultural Sciences and Veterinary Medicine Cluj-Napoca: Food Science and Technology*, **79**, 67 (2022).
31. M. D. Selgas, E. Cáceres, M. L. García, *FSTI*., **11**, 41 (2005).
32. N. Ktari, S. Smaoui, I. Trabelsi, M. Nasri, R. B. Salah, *Meat Sci*., **96**, 521 (2014).
33. G. Heinz, P. Hautzinger, *FAO*, Bangkok. (2007).
34. M. T. D. Santos, V. Gerbaud, G. A. C. Le Roux, *J. Food Eng*., **12**6, 198 (2014).
35. L. Zhao, X. Peng, X. Liu, Y. Wang, S. Qin, J. Zhang, *Polym. J.,* **45**, 929 (2013).
36. J. Dreher, M. Weißmüller, K. Herrmann, N. Terjung, M. Gibis, J. Weiss, *Int. Food Res. J.*, **145**, 110416 (2021).
37. J. Dreher, M. König, K. Herrmann, N. Terjung, M. Gibis, J. Weiss, *LWT.*, **143**, 111140 (2021).
38. T. Uzlaşır, N. Aktaş, K. E. Gerçekaslan, *Food Sci. Anim. Resour*., **40**, 551 (2020).

Bulgarian Chemical Communications, Volume 55, Issue 4 (pp. 424-429) 2023 *DOI: 10.34049/bcc.55.4.5572*

Evaluation of *in vitro* antioxidant activities of traditional fermented non-alcoholic beverages from Turkey

B. Ceylan*

Department of Pharmacognosy, Faculty of Pharmacy, Harran University, 63050 Haliliye-Sanlıurfa, Turkey

Recеıved: April 24, 2023; Revised: December 01, 2023

The aim of this study was to evaluate the *in vitro* potential of different solvent extracts of shalgam juice, hardaliye, boza, ayran (yoghurt drink) and kefir as natural antioxidants. The originality of this study was that different solvents were used for extraction, and according to the extraction yields, total phenolic and flavonoid contents of the extracts and antioxidant activity was determined. Liquid-liquid extraction was applied for sample preparation, which is the preferred extraction technique today due to its simple, fast and efficient procedure to determine antioxidant capacity. The antioxidant capacities of the acetone, ethanol and water extracts of traditional fermented non-alcoholic beverages were estimated using different antioxidant tests, including lipid peroxidation, 1,1-diphenyl-2-picrylhyrazyl (DPPH$^{•}$) free radical scavenging, superoxide anion radical scavenging, 2,2$^{'}$-azino-bis(3-ethylbenzothiozoline-6-sulfonic acid) diammonium salt (ABTS$^{•+}$) cation scavenging activity, hydrogen peroxide scavenging activity and cupric reducing capacity. Results showed that the highest contents of the target components including phenols and flavonoids were found in the water extract. The latter was found to be richer in antioxidant phytochemicals such as phenolics (189.33±2.77 mg PEs/g FW) and flavonoids (321.77±4.03 mg QEs/g FW). This study verified that the water extract with its high level of phenolics and flavonoids can be used as a source of potential antioxidants or functional food materials.

Keywords: Antioxidant activity, Fermented beverages, Phenolic compound, Scavenging activity, Food antioxidant

INTRODUCTION

Free radicals are one of the most important causes of deterioration of food products during processing and storage and are claimed to play an important role in affecting human health by causing many diseases (such as cancer, hypertension, heart attack and diabetes) [1-3]. Dietary intake of phenolic compounds and fermented food products is associated with these diseases and is protective in many health-related properties such as antioxidant, anticancer, antiviral, anti-Alzheimer, antidiabetic and anti-inflammatory activities [4]. Vegetable products and fermented food products are rich sources of antioxidants and are used as food additives to prevent oxidative degradation of fats and oils in processed foods and are compounds that increase shelf life and delay the lipid peroxidation process [5, 6].

Fermentation is one of the oldest (humans consumed 'sour milk' about 2000 years ago) and one of the most economical methods used in food preservation. The beneficial health effects of fermented foods and dairy products on humans are: increased mineral bioavailability, digestibility of proteins and carbonhydrates [7]. In accordance with the awareness of consumers, the trend towards Turkish fermented non-alcholic beverages (shalgam juice, hardaliye, boza, ayran and kefir) has increased, with natural (or slightly processed), high nutritional (due to probiotic properties) and health promoting value. The former ones (shalgam juice, hardaliye and boza) are obtained from vegetables, fruits and cereals, and the latter two (ayran and kefir) are made of milk. Shalgam juice, hardaliye and ayran are produced by lactic fermentation. In boza and kefir, both alcoholic and lactic fermentation occur [8].

In this study the antioxidant activities of acetone, ethanol and water extracts of non-alcoholic beverages (shalgam juice, hardaliye, boza, ayran and kefir) which can be an alternative to synthetic antioxidants (BHA, BHT and α-tocopherol) used in removing free radicals, were investigated using different methods (β-carotene/linoleic acid bleaching assay, ABTS$^{•+}$ cation radical scavenging, DPPH$^{•}$ free radical scavenging assays, superoxide anion radical scavenging, hydrogen peroxide scavenging activity, cupric reducing antioxidant capacity assay). In addition, the extraction method (liquid-liquid extraction) used provides superiority compared to previous studies because it is simple, fast and highly efficient. This study can help in food industry as a natural compound for antioxidant activity, which might be used as an alternative to synthetic antioxidants since it is environmentally friendly and safe for consumption.

* To whom all correspondence should be sent:
E-mail: b.ceylan022@gmail.com

EXPERIMENTAL

Chemicals and reagents

Linoleic acid, α-tocopherol, potassium persulfate, nicotinamide adenine dinucleotide (NADH), butylated hydroxyanisole (BHA), butylated hydroxytoluene (BHT), nitroblue tetrazolium (NBT), phenazine methosulfate (PMS), 1,1-diphenyl-2-picrylhydrazyl (DPPH), pyrocatechol, quercetin and 3-(2-pyridyl)-5,6-*bis*(4-phenyl-sulfonic acid)-1,2,4-triazine (ferrozine) were obtained from Sigma-Aldrich GmbH, Sternheim, Germany.

Ammonium thiocyanate, ferrous chloride, polyoxyethylenesorbitan monolaurate (Tween-20), tricholoroacetic acid (TCA), ethanol (EtOH) and acetone were purchased from Merck. All other chemicals used were of analytical grade, obtained from either Sigma-Aldrich or Merck. Water was puridifed by Human (Japan) ultrawater purification system.

Material and extraction procedures

Fermented non-alcoholic beverages were purchased from local stores. Since the beverages are in liquid form, they were homogenized (by shaking) before use and used directly without any other pre-treatment. For the preparation of the extracts, 25 mL of the beverage (shalgam juice, hardaliye, boza, ayran and kefir) was incubated in 500 mL of solvent (acetone, ethanol and water) at room temperature (25 ºC) at 100-150 rpm in a shaking water bath for 3 hours. The obtained extracts were filtered through filter paper (Whatman No.1 paper) and the solvents of the filtrates (acetone and ethanol) were evaporated in a rotary evaporator (Büchi R-200, Switzerland) at 40-80 ºC. The resulting water extracts were filtered through filter paper and the filtrate was lyophilized (at 5 µm Hg pressure at – 50 ºC [Labconco, Freezone 1 L]). All extracts were kept at -20 ºC and dissolved in water or solvent before use.

Total phenolic and flavonoid contents

The total phenolic [9] and flavonoid [10] contents of the analysed samples were calculated as equivalent to pyrocatechol and quercetin, respectively. The following equations were used to calculate the total phenolic and flavonoid contents of fermented non-alcoholic beverage extracts:

Absorbance = 0.0413x + 0.0440 pyrocatechol (µg) ($r^2 = 0.9975$)
Absorbance = 0.0362x + 0.0172 quercetin (µg) ($r^2 = 0.9975$)

Antioxidant activity

In order to determine the antioxidant activity of the sample six methods were applied: β-carotene/linoleic acid bleaching assay [11], ABTS cation radical scavenging [12], DPPH free radical scavenging assay, superoxide anion radical scavenging [13], hydrogen peroxide scavenging activity [14], CUPRAC (Cupric reducing antioxidant capacity) assay [15]. In oder to calculate IC_{50} (50% inhibition) values of the samples 100, 50, 25 and 10 µg/mL of their concentrations were prepared. The smallest concentration value (10 µg/mL) is the minumum IC_{50} value that can be calculated. That is, at concentrations lower than the smallest concentration (10 µg/mL), the IC_{50} cannot be calculated. In these six antioxidant test methods, BHA, BHT and α-tocopherol were used as standards.

Statistical analysis

Power analysis was performed to determine the number of fermented non-alcoholic beverage extracts. The outcomes were presented as means ± standard deviation (n=3 per each test sample).

RESULTS AND DISCUSSION

Extraction yield, total phenolic and flavonoid contents

The percentage yields of fermented non-alcoholic beverage extracts are shown in Table 1. The highest extraction efficiency was observed in water extracts. The percent extraction yields of the water extracts varied between 38.65% and 30.26%. So the water extract resulted in a higher amount of total extractable compounds. Phenolics or polyphenols are food secondary metabolites and are important by virtue of their antioxidant acitivty by chelating redox-active metal ions, inactiating lipid free radical chains and preventing hydroperoxide conversions into reactive oxyradicals. Polyphenols are known as markers of the nutritional quality of foods. Polyphenols are known for their antioxidant activity as radical scavengers having possible beneficial roles in human health, such as reducing the risk of cancer, cardiovascular disease, and other pathologies. Fermented non-alcoholic beverages containing high amounts of phenolic compounds can be a good source of antioxidants. For this reason, this information has led to the determination of the total phenolic content of the sample under study [16]. The total phenolic content of the ethanol extracts varied between 163.61±0.94 and 110.63±1.58 µg PEs/mg extract. The highest total phenolic content of ethanol extracts was found in shalgam juice extract (163.61±0.94 µg PEs/mg extract).

Flavonoids are natural phenolic compounds and well known antioxidants. Therefore, dietary intake of flavonoid-containing foods was suggested to be beneficial for preservation from free radical damage. Total flavonoid content of acetone extracts ranged from 210.18±1.83 to 171.90±2.28 µg QEs/mg extract. The highest total flavonoid content of acetone extracts was found in hardaliye extract (210.18±1.83 µg QEs/mg extract). These amounts were comparable with the results described in the literature for other extracts of plant and fruit products [17].

Antioxidant activity

Total antioxidant activity determination

Total antioxidant activity of fermented non-alcoholic beverage extracts was determined by the thiocyanate method (β-carotene/linoleic acid bleaching assay [11]). Fermented non-alcoholic beverages water extracts (shalgam juice, hardaliye, boza ayran and kefir) exhibited effective antioxidant activity.

The effect of the same amounts of water extracts of fermented non-alcoholic beverages (100 µg/mL) on the peroxidation of β-carotene-linoleic acid emulsion are shown in Fig. 1. The effects on lipid peroxidation (IC_{50} value) of linoleic acid emulsion of extracts and standards decreased in the order: KFW (6.78±0.79) > BZW (8.81±1.10) > AYW (11.63±1.40) > HRW (14.66±1.88) > SHW (15.38±1.72) > α-tocopherol (30.34±2.20) > BHT (33.96±2.58) > BHA (35.37±2.08). In previous studies, Ertaş *et al.* reported that the water extract (153.05±0.21) exhibited very strong activity in the β-carotene/linoleic acid bleaching assay [18]. But our results showed stronger activity than this value. The total antioxidant activitiy of fermented non-alcoholic beverages water extracts may be attributed to their chemical composition and the phenolic acid content demonstrated that some bioactive compounds and milk products present in raw materials possessed high total antioxidant activity which was due to the presence of phenolics, carotenoids and flavonoids.

Table 1. Extraction yields and contents of total phenols, total flavonoids in fermented non-alcoholic beverage extracts

Fermented non-alcoholic beverage	Extraction solvent	Abbreviation	Extraction yield (%)	Total phenolic content (µg PEs/mg extract)[a]	Total flavonoid content (µg QEs/mg extract)[b]
Shalgam juice	Acetone	SHA	12.63	133.84±2.82	196.36±2.61
	Ethanol	SHE	21.56	163.61±0.94	284.13±3.93
	Water	SHW	32.44	154.13±1.32	314.43±3.86
Hardaliye	Acetone	HRA	14.38	122.54±2.12	210.18±1.83
	Ethanol	HRE	19.23	145.80±1.38	261.16±3.55
	Water	HRW	38.65	189.33±2.77	321.77±4.03
Boza	Acetone	BZA	11.36	102.29±1.18	188.59±1.99
	Ethanol	BZE	20.88	152.55±3.82	280.69±2.80
	Water	BZW	34.10	177.59±2.43	311.66±3.23
Ayran	Acetone	AYA	10.83	98.35±0.71	171.90±2.28
	Ethanol	AYE	17.68	110.63±1.58	252.90±2.94
	Water	AYW	30.26	146.24±3.40	303.97±3.52
Kefir	Acetone	KFA	13.71	118.66±0.79	202.40±2.12
	Ethanol	KFE	22.16	151.37±1.74	296.33±4.40
	Water	KFW	33.75	166.21±0.87	318.39±2.41

[a]Phenolic content equivalent to pyrocatechol (y=0.021x+0.0396 R^2=0.9993)
[b]Flavonoid content equivalent to quercetin (y=0.021x+0.0396 R^2=0.9993)

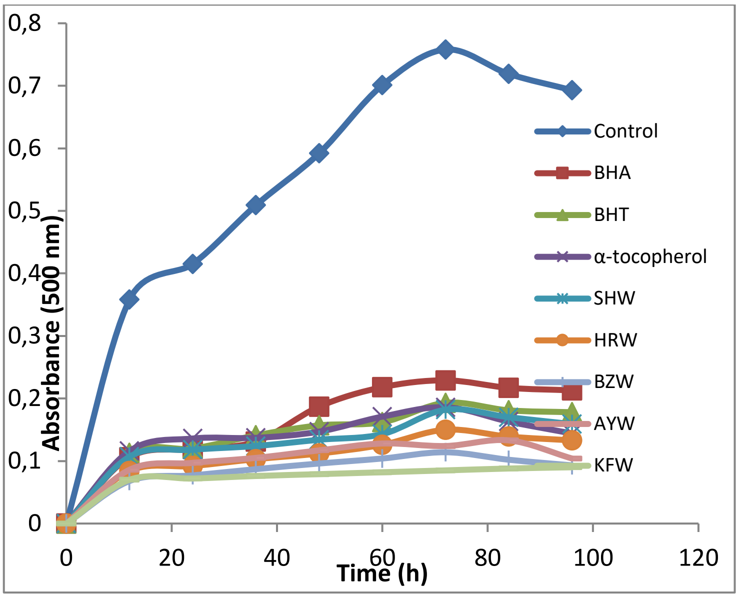

Fig. 1. Inhibitory effect of the water extracts from fermented non-alcoholic beverages on lipid peroxidation. BHA, BHT and α-tocopherol were used as reference antioxidants. Values are means ± SD (n=3)

Table 2. IC_{50} values of DPPH$^{\bullet}$ free radical scavenging activity, ABTS$^{\bullet+}$ cation radical scavenging activity, hydrogen peroxide scavenging activity and superoxide anion scavenging activity of fermented non-alcoholic beverage water extracts (100 µg/mL)

		IC_{50} (µg/mL)		
Extracts and standards	Scavenging ability on DPPH$^{\bullet}$ free radicals	Scavenging ability on ABTS$^{\bullet+}$ cation radicals	Scavenging ability on hydrogen peroxide	Scavenging ability on superoxide anions
SHW	27.84±1.52	17.19±0.13	40.56±3.66	33.15±1.14
HRW	33.67±1.33	12.95±1.10	45.31±2.93	35.88±1.29
AYW	30.88±2.11	14.42±0.06	43.18±2.47	37.60±1.34
BZW	36.45±0.49	21.23±1.75	47.24±2.18	31.27±2.13
KFW	34.35±1.48	22.30±2.01	44.61±3.41	34.83±1.58
BHA	45.80±2.53	38.27±1.49	60.19±2.30	50.24±2.89
BHT	48.28±2.45	40.33±2.52	61.73±1.22	52.33±2.21
α-tocopherol	51.53±3.19	42.81±2.85	64.60±2.32	55.20±2.55

Values are given as the mean and standard deviation of three parallel measurements.

Table 3. CUPRAC test assay of the fermented non-alcoholic beverage water extracts and standards

	Concentrations			
Extracts and standards	10 µg/mL	25 µg/mL	50 µg/mL	100 µg/mL
SHW	0.150±0.030	0.318±0.085	0.463±0.120	0.808±0.170
HRW	0.123±0.028	0.333±0.074	0.452±0.142	0.826±0.186
AYW	0.135±0.034	0.328±0.060	0.473±0.134	0.859±0.191
BZW	0.142±0.041	0.311±0.077	0.488±0.125	0.840±0.193
KFW	0.130±0.022	0.320±0.091	0.424±0.121	0.820±0.172
BHA	0.352±0.064	0.501±0.110	0.716±0.142	1.215±0.221
BHT	0.385±0.067	0.516±0.119	0.755±0.153	1.236±0.210
α-tocopherol	0.321±0.072	0.511±0.128	0.747±0.150	1.225±0.213

Values are given as the mean and standard deviation of three parallel measurements.

$ABTS^{\bullet+}$ cation scavenging activity

The $ABTS^{\bullet+}$ method is widely employed for measuring the relative radical scavenging activity of hydrogen donating and chain breaking antioxidants in many food extracts. $ABTS^{\bullet+}$ cation scavenging activity is best presented by IC_{50} value, defined as the concentration of the antioxidant needed to scavenge 50% of $ABTS^{\bullet+}$ cation present in the test solution (Table 2). A higher $ABTS^{\bullet+}$ cation radical scavenging activity is associated with a lower IC_{50} value. IC_{50} values for SHW, HRW, AYW, BZW, KFW, BHA, BHT and α-tocopherol on $ABTS^{\bullet+}$ radical scavenging activity were found as 17.19, 12.15, 14.42, 21.23, 22.30, 38.27, 40.33, 42.81 µg/mL, respectively. In previous studies, Kolak *et al*. found the IC_{50} value of the $ABTS^{\bullet+}$ cation radical scavenging activity of the compounds they isolated as 78.68±1.32 µg/mL [20]. Fermented non-alcoholic beverages water extracts showed similar $ABTS^{\bullet+}$ cation radical scavenging acitivites compared to the $ABTS^{\bullet+}$ cation radical scavenging activity of the standards.

$DPPH^{\bullet}$ free radical scavenging assay

Antioxidant properties, especially radical scavenging activites, are very important due to the deleterious role of free radicals in foods and in biological systems. Excessive formation of free radicals accelerates the oxidation of lipids in foods and decreases food quality and consumer acceptance. The model of scavenging the stable $DPPH^{\bullet}$ is that the stable free radical accepts an electron or hydrogen radical to become a stable diamagnetic molecule.

$DPPH^{\bullet}$ free scavenging activity is best presented by the IC_{50} value, defined as the concentration of the antioxidant needed to scavenge 50% of $DPPH^{\bullet}$ present in the test solution (Table 2). A higher $DPPH^{\bullet}$ radical scavenging activity was associated with a lower IC_{50} value. IC_{50} values for SHW, HRW, AYW, BZW, KFW, BHA, BHT and α-tocopherol on $DPPH^{\bullet}$ free radical scavenging activity were found as 27.84, 33.67, 30.88, 36.45, 34.35, 45.80, 48.28, 51.53 µg/mL, respectively. In previous studies, Mavi *et al.* reported that *S. sempervivoides* showed very strong activity - 88.0% inhibition in the $DPPH^{\bullet}$ free radical scavenging assay method at 200 µg/mL concentration [19]. Fermented non-alcoholic beverage water extracts showed similar $DPPH^{\bullet}$ free radical scavenging acitivites compared to the $DPPH^{\bullet}$ free radical scavenging activity of the standards.

Hydrogen peroxide scavenging activity

Hydrogen peroxide itself is not very reactive, but it can sometimes be toxic to cells, since it may rise to hydroxyl radicals inside the cell. IC_{50} values for SHW, HRW, AYW, BZW, KFW, BHA, BHT and α-tocopherol on hydrogen peroxide scavenging activity were found as 40.56, 45.31, 43.18, 47.24, 44.61, 60.19, 61.73, 64.60 µg/mL, respectively (Table 2). In previous studies, Yeşiloğlu *et al*. reported that the water extract (78.89±1.3%) exhibited very strong activity in hydrogen peroxide scavenging [21]. Our results are in agreement with previous studies. Fermented non-alcoholic beverages water extracts showed similar hydrogen peroxide radical scavenging acitivites compared to the hydrogen peroxide scavenging activity of the standards.

Superoxide anion radical scavenging activity

Superoxide is a reactive oxygen species, which can cause damage to cells and DNA,bthus leading to various diseases. It was, therefore, proposed to measure the comparative interceptive ability of the antioxidant extracts to scavenge the superoxide radical. IC_{50} values for SHW, HRW, AYW, BZW, KFW, BHA, BHT and α-tocopherol on superoxide anion radical scavenging activity were found as 33.15, 35.88, 37.60, 31.27, 34.83, 50.24, 52.33, 55.20 µg/mL, respectively (Table 2).

In previous studies, Yeşiloğlu *et al*. reported that the water extract (18.2%) exhibited moderate activity in hydrogen peroxide scavenging [22]. Our results showed very high activity, compared to previous studies. Fermented non-alcoholic beverages water extracts showed similar superoxide radical scavenging acitivites compared to the superoxide anion radical scavenging activity of the standards.

CUPRAC (Cupric reducing antioxidant capacity) assay

The CUPRAC antioxidant determination method was studied at four different concentrations (10, 25, 50, 100 µg/mL) (Table 3). An increase in activity was observed in direct proportion to the increase in concentration. It was found that the water extracts showed moderate activity than the standards. But showed very strong activity compared to other studies. In previous studies, Orak *et al.* found the results of the cupric reducing antioxidant capacity method of dichloromethane, ethanol and methanol extracts of *A. muricata* L. at 100 µg/mL concentration as 0.143±0.020, 0.136±0.060 and 0.063±0.040, respectively [23].

CONCLUSION

Natural antioxidants in fermented products can be used to reduce the harmful effects of free radical species. Synthetic antioxidants such as BHA and BHT can be used, but the use of these molecules is risky. Therefore, in recent years, restrictions have been imposed on the use of synthetic antioxidants in many countries. Therefore, interest in natural antioxidants has increased and related research has gained momentum. The water extracts of fermented non-alcoholic beverages exhibited different levels of antioxidant activity in all the models studied. In the β-carotene/linoleic acid bleaching assay, SHW (15.38±1.72) showed the closest activity to the standards. In the $ABTS^{\bullet+}$ cation scavenging activity assay, KFW (22.30±2.01) showed the closest activity to the standards. BZW extract showed the highest activity compared to other extracts in DPPH free radical scavenging assays, superoxide anion radical scavenging, and hydrogen peroxide scavenging activity experiments. In the CUPRAC assay, all extracts showed moderate activity compared to the standards. The results revealed that the fermented non-alcoholic beverages had significant antioxidant activity and free radical scavenging activity. The free radical scavenging property may be one of the mechanisms by which these products or beverages are useful as foodstuffs, as well as traditional medicines. However, further investigation of individual compounds, their *in vivo* antioxidant activities and participation in different antioxidant mechanisms is needed. It was concluded that fermented non-alcolic beverages can be used as natural antioxidant sources.

REFERENCES

1. B. Halliwell, *Cardiovascular Res.,* **73**, 341 (2007).
2. J. Kubola, S. Siriamornoun, *Food Chem.,* **110**, 881 (2008).
3. S. M. Mohsen, A. S. M. Ammar, *Food Chem.,* **112**, 595 (2009).
4. H. O. Boo, B. G. Heo, S. Gorinstein, S. U. Chon, *Plant Sci.,* **181**, 479 (2011).
5. I. S. Young, J. V. Woodside, *J. Clin. Pathol.,* **54**, 176 (2001).
6. E. Bombardelli, P. Morazzonni, *Fitoterapia,* **66**, 291 (1995).
7. A. S. Naidu, W. R. Bidlack, R.A. Clemens, *Crit. Rev. Food. Sci. Nutr.,* **38**, 13 (1999).
8. H. Tangüler, H. Erten, *J. Food. Qua.,* **35**, 298 (2012).
9. M. I. N. Moreno, M. I. Isla, A. R. Sampietro, M. A. Vattuone, *J. Ethnopharmacol.,* **71**, 109 (2000).
10. K. Slinkard, V. Singleton, *AJEV,* **28**, 49 (1977).
11. H. Miller, *J. Am. Oil. Chem. Soc.,* **48**, 91 (1971).
12. R. Re, N. Pellegrini, A. Proteggente, A. Pannala, M. Yang, C. Rice-Evans, *Free Radic. Biol. Med.,* **26**, 1231 (1999).
13. Q. Liu, G. Zhu, P. Huang, *Zhong. Zhong Yao Za Zhi* (*China Journal of Chinese Materia Medica),* **161**, 50 (1991).
14. R. J. Ruch, S. J. Cheng, J. F. Klauning, *Carcinogen.*, **10**, 1003 (1989).
15. R. Apak, K. Güçlü, M. Özyürek, S. E. Karademir, *J. Agric. Food. Chem.,* **52**, 7970 (2004).
16. S. Selappan, C. C. Akoh, G. Krewer, *J. Agric. Food Chem.,* **50**, 2432 (2002).
17. B. Ceylan, Y. Yeşiloğlu, *Rev. Roum. Chim,* **67**, 343 (2022).
18. A. Ertaş, M. Boğa, M. A. Yılmaz, Y. Yeşil, N. Haşimi, M. Ş. Kaya, H. Temel, U. Kolok, *J Agric. Food Chem,* **62**, 4601 (2014).
19. A. Mavi, Z. Terzi, U. Ozgen, A. Yıldırım, M. Coşkun, *Biol. Pharm. Bull.,* **27**, 702 (2004).
20. U. Kolak, I. Hacıbekiroğlu, M. Öztürk, F. Gökçe, G. Topçu, *Turkish J. Chem.* **33**, 813 (2009).
21. Y. Yeşiloğlu, L. Şit, I. Kılıç, *Asian J. Chem,* **25**, 8311 (2013).
22. Y. Yeşiloğlu, S. Gülen, *Bulgarian Chem. Commun,* **48**, 9 (2016).
23. H. H. Orak, I. S. Bahrisefit, T. Sabudak, *Pol. J. Food Nutr. Sci.* **69**, 359 (2019).

Bulgarian Chemical Communications, Volume 55, Issue 4 (pp. 430-433) 2023 DOI: 10.34049/bcc.55.4.5590

Catalytic effect of sodium dodecyl sulfate on the oxidation of propanal by potassium permanganate in acidic medium

D. F. Latona*

Department of Pure & Applied Chemistry, College of Science, Engineering & Technology, Osun State University, Osogbo, Nigeria

Received: July 14, 2023; Revised: October 03, 2023

The effect of anionic micelles of sodium dodecyl sulfate (SDS) on the oxidation of propanal by potassium permanganate in acidic medium was spectrophotometrically investigated. The oxidation reaction showed first order to each [$KMnO_4$], [propanal] and fractional order to [H^+]. The surfactant micelles catalyzed the reaction. The catalysis increased with increase in [SDS] and reached a maximum. Activation parameters were obtained from Eyring's equation as 20.41 kJ mol^{-1}, -0.23 kJ K^{-1} mol^{-1} and 88.95 kJ mol^{-1} for $\Delta H^{\#}$, $\Delta S^{\#}$ and $\Delta G^{\#}$, respectively. Quantitative kinetic analysis of $k\psi$ –[SDS] data was performed based on the pseudo-phase model by Menger-Portnoy and the Piszkiewicz cooperativity model.

Keywords: Propanal, activation parameters, sodium dodecyl sulfate (SDS), thermodynamics.

INTRODUCTION

The effect of surfactant micelles on chemical reactions has received great attention over the years. The use of cationic, anionic, neutral and zwitterionic micelles [1-10] has been reported. The chemistry of the micellar effect has been explained *via* electrostatic and hydrophobic interactions between the micelles and the substrates. Several models like the Menger-Portnoy pseudo-phase model, Piszkiewicz cooperativity model and Raghvan-Srinivasan model have been used to explain the mechanism of influence of surfactants on chemical reactions. Interaction of surfactant molecules with substrates can either catalyze or inhibit a chemical reaction. The oxidation of propanal is a very important reaction which has not been reported in the micellar system using $KMnO_4$ as oxidant. Therefore, this paper seeks to investigate the influence of SDS on the oxidation of propanal by potassium permanganate in acidic medium. Studies of the micellar effect on the oxidation of aldehydes using various oxidants like Cr (VI), N-bromophthalimide, and bromate [11-14] have been reported with the exception of $KMnO_4$. Potassium permanganate is a versatile oxidant used in various organic and inorganic redox reactions, which prompted the need to investigate its oxidation effect on propanal in the micellar system.

EXPERIMENTAL

Materials

Propanal (Merck, India), SDS (Fluka, Switzerland), H_2SO_4 (Merck, India), KNO_3, $KMnO_4$ (BDH) were of Analar grade and used without further purification. All solutions were prepared in mole litre^{-1} using doubly distilled CO_2-free water. The results were obtained in duplicate.

Kinetic runs

Requisite volumes of SDS, KNO_3, H^+, propanal and distilled water except $KMnO_4$ were placed in the reaction vessel fitted with a double-wall spiral condenser to check evaporation in a water bath thermostat. Furthermore, at constant temperature of the mixture in the reaction vessel, $KMnO_4$ solution thermostated at the same temperature was transferred to the mixture in the reaction vessel. For the purpose of this study, aliquots of the reaction mixtures were withdrawn at definite time intervals, quenched in ice bath and absorbance was taken. The progress of the reaction was monitored by measuring the decrease in absorbance of the reaction mixture at 525 nm using a double-beam Unicam-1800 Schimadzu spectrophotometer equipped with a thermo-regulated cell compartment. The pseudo-first order rate constants k_{ψ} (s^{-1}) were calculated from the slope of the plot of log absorbance *versus* time.

* To whom all correspondence should be sent:
E-mail: dayo.latona@uniosun.edu.ng

RESULTS AND DISCUSSION

The observed pseudo first-order rate constants (k_ψ) at various initial concentrations of the reactants are shown in Table 1. The log k_ψ *versus* log [X] where X = $KMnO_4$, propanal and H^+ showed first-order dependence to each [$KMnO_4$] and [propanal] and fractional order to [H^+] with no effect on the ionic strength of the mixture suggesting the presence of a neutral molecule in the rate-determining step.

Table 1. Effect of [Reactants]

10^5[$KMnO_4$] (mol dm^{-3})	10^3[Propanal] (mol dm^{-3})	10^3[H^+] (mol dm^{-3})	$10^2 k_\psi$/s^{-1}
1.00	3.00	1.00	0.15
2.00	3.00	1.00	0.54
3.00	3.00	1.00	0.79
4.00	3.00	1.00	1.00
5.00	3.00	1.00	1.29
6.00	3.00	1.00	1.46
7.00	3.00	1.00	1.67
3.00	1.00	1.00	0.08
3.00	2.00	1.00	0.19
3.00	3.00	1.00	0.25
3.00	4.00	1.00	0.35
3.00	5.00	1.00	0.45
3.00	6.00	1.00	0.53
3.00	7.00	1.00	0.61
3.00	3.00	1.00	0.25
3.00	3.00	2.00	0.33
3.00	3.00	3.00	0.43
3.00	3.00	4.00	0.52
3.00	3.00	5.00	0.58
3.00	3.00	6.00	0.68
3.00	3.00	7.00	0.75

At fixed ionic strength μ= 0.05 mol dm^{-3} maintained by KNO_3, [SDS] 3 ×10^{-2} mol dm^{-3} at 298K

Activation parameters obtained from the temperature-dependent study using equations (1) and (2) are shown in Table 2.

$$In\left(\frac{k}{T}\right) = \frac{-\Delta H^{\#}}{RT} + In\left(\frac{K^{/}}{h}\right) + \left(\frac{\Delta S^{\#}}{R}\right) \quad (1)$$

where $In\left(\frac{K^{/}}{h}\right) = 23.76$

$$\Delta G^{\#} = \Delta H^{\#} - T\Delta S^{\#} \quad (2)$$

k = rate constant; T= temperature; $\Delta H^{\#}$ = enthalpy of activation; $\Delta S^{\#}$ = entropy of activation; $\Delta G^{\#}$ = free Gibbs energy of activation; R = molar gas constant; $k^{/}$ = Boltzmann's constant; h= Plank's constant.

Table 2. Activation parameters

Substrate	$\Delta H^{\#}$/kJ mol^{-1}	-$\Delta S^{\#}$/kJ K^{-1} mol^{-1}	$\Delta G^{\#}$/kJ mol^{-1}
Propanal	20.41	0.23	88.95

[$KMnO_4$] = 3 × 10^{-5} mol dm^{-3}, [propanal] = 3 × 10^{-3} mol/dm^{-3}, [H^+] = 1 × 10^{-3} mol dm^{-3}, μ = 0.05.

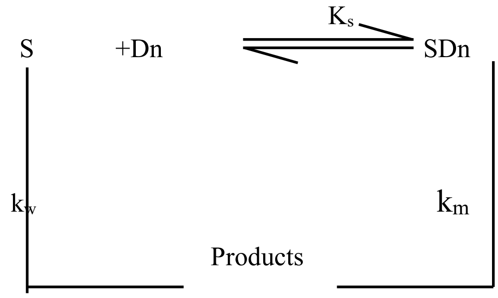

Scheme 1. Menger-Portnoy model (D_n= micellar SDS surfactant; S = free substrate; SD_n= associated substrate)

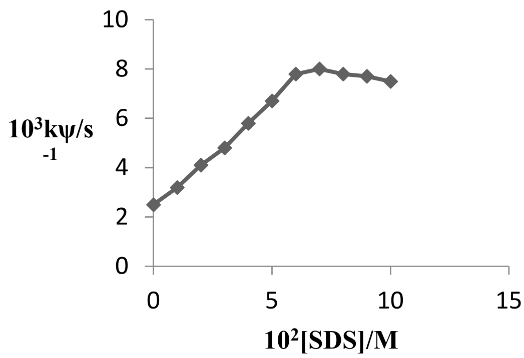

Fig. 1. Plot of k_ψ *versus* [SDS] Menger-Portnoy model.

A pseudo-phase kinetic model proposed by Menger and Portnoy was used to interpret the catalytic activity of sodium dodecyl sulfate and to evaluate the binding constant between the substrate and the surfactant.

$$k_\psi = \frac{(k_w + k_m K_s[D_n])}{(1 + K_s[D_n])} \quad (3)$$

The critical micelle concentration (CMC) of SDS in the reaction mixture is 8.20 × 10^{-3} mol dm^{-3} [15, 16]. k_w is the pseudo-first order rate constant in aqueous phase; k_m is the pseudo-first order rate constant in micellar phase; Ks is the binding constant of the substrate with the surfactant; [D_n] is the concentration of the micelle surfactant; $[D]_T$ is the stoichiometric concentration of the surfactant.

$[D_n] = ([D]_T – CMC)$

Rearrangement of equation (3) gives:

$$\frac{1}{(k_\psi - k_w)} = \frac{1}{(k_m - k_w)} + \frac{1}{(k_m - k_w)K_s[D_n]} \qquad (4)$$

Fig. 2 shows the validity of Menger-Portnoy pseudo-phase model. The obtained value of k_m was 7.45×10^{-3} s^{-1}.

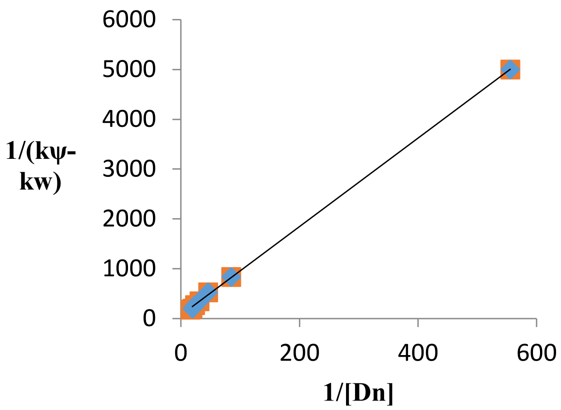

Fig. 2. Validity of Menger-Portnoy model

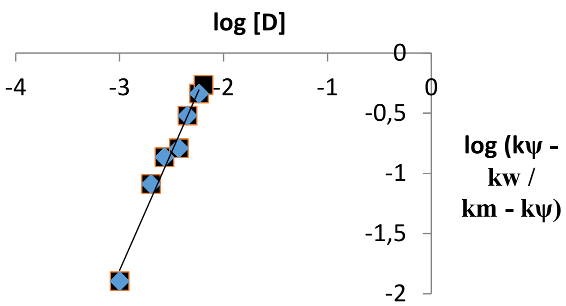

Fig. 3. Plot of $log\frac{(k_\psi - k_w)}{(k_m - k_\psi)}$ *versus* log[D]

Piszkiewicz cooperativity model

Piszkiewicz cooperativity model which is analogous to Hill model applied to enzyme-catalyzed reactions helps to explain the reactions in micellar systems. It gives a more accurate dependence of the observed rate constants on surfactant concentrations at low concentrations as shown in Scheme 2.

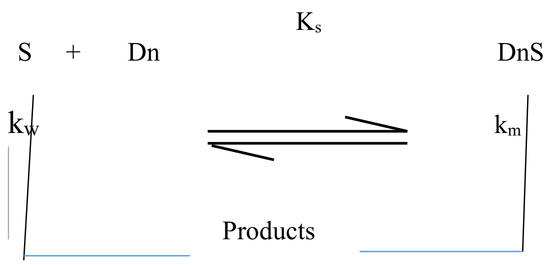

Scheme 2. Piszkiewicz cooperativity model

Piszkiewicz cooperative model shows that:

$$k_\psi = k_m[D]^n + \frac{K_D k_w}{K_D + [D]^n} \qquad (5)$$

Re-arranging Equation 5:

$$\log\frac{(k_\psi - k_w)}{(k_m - k_\psi)} = n\log[D] - \log K_D \qquad (6)$$

K_D is the dissociation constant of micellized substrate back to its free components; K is the association constant of the micelle-substrate complex.

Applying Equation 6 and using the earlier obtained value of k_m from Menger-Portnoy model, the plot of $log\frac{(k_\psi - k_w)}{(k_m - k_\psi)}$ *versus* log[D] was linear for this reaction.

Sodium dodecyl sulfate (SDS) micelles catalyzed the oxidation reaction, the plot of kψ *vs* [SDS] shows a rate maximum at [SDS] 7×10^{-2} mol dm^{-3}, increase in [SDS] > 7×10^{-2} mol dm^{-3} led to a decrease in the reaction rate as shown in Fig. 1. The kψ *vs* [SDS] profile can be explained using the pseudo-phase model proposed by Menger and Portnoy. The overall increment of rate constant at low [SDS] can be attributed to the fact that the reactants get associated /incorporated at the stern layer of the micellar phase. Consequently, the decrease in kψ beyond [SDS] greater than 7×10^{-2} mol dm^{-3} can be explained as follows: At higher [SDS] all the substrate has been incorporated into the micellar phase. When bulk of the substrate is incorporated into the micelle, addition of more SDS generates more SDS and more Na^+ counter-ions in the Guoy-Chapman layer of the micelles. The overall increase in the positive charge in the Guoy-Chapman layer of the micelles results in the repulsion of the positively charged substrates and thereby inhibiting the partitioning of the substrate into the stern layer of the micelle. The dissociation constant of the micellized surfactant back to its component (K_D) and the index of cooperativity (n) were obtained by the Piszkiewicz model. The value of Ks was 7.09, n was 2 which is greater than unity and suggests positive cooperativity. This means that the binding of the first molecule of a substrate allows subsequent molecules to bind easily [17]. The value of n is far less than the number of surfactant molecules in the micelle, hence the existence of premicellar aggregates cannot be ignored. K_D was obtained to be 9.68×10^{-5}.

Acknowledgement: *The author is indebted to the members of the staff of the Central Science Laboratory at the Obafemi Awolowo University, Ile-Ife for their technical assistance.*

Disclosure and conflict of interest: *The author declares no conflict of interest.*

REFERENCES

1. A. Raducan, A. Olteanu, M. Puiu, D. Oancea, *Centr. Eur. J. Chem.,* **6(1**), 89 (2008).
2. B. Samiey, A. R Toosi, *Bull. Korean Chem. Soc.,* **30(9),** 2051 (2009).
3. M. A. Safarpour, A. A. Rafati, H. Gharibi, R. Sameti, *Journal of Chinese Chemical Society,* **46**, 983 (1999).
4. I. Johnson, G. Olofsson, *Journal of Colloid and Interface Science,* **115(1)**, 56 (1987).
5. S. Satchawan, W. Naksata, C. Rattanakawin, S. Thiansem, P. Panya, P, Sooksamiti, P. J. Scales, O. Arqueropanyo, *Korean J. Chem. Eng.,* **31(6)**, 1076 (2014).
6. G. M. Forland, J. Samseth, M. Gjerde, H. Hoiland, A. O. Jensen, K. Mortensen, *Journal of Colloid and Interface Science,* **203**, 328 (1998).
7. A. Bhattarai, H. W. Wachnik, M. Grzegorek, *American Journal of Pharmacology and Pharmacotherapeutics,* **4(3)**, 8 (2017).
8. M. A. Motin, M. A. Hafiz Mia, A. K. M. Nasimul Islam, K. M. Salim Reza, M. A. Yousuf, *Journal of Bangladesh Chemical Society*, **25(2)**, 110 (2012).
9. S. Kumar, T. J. Kirha, T. Thonger, *Journal of Chemical and Pharmaceutical Research*, **6(5)**, 1488 (2014).
10. D. Myers, Surfactant Science and Technology, John Wiley and Sons, Hoboken, NJ, USA, 2006.
11. S. Melik, A. Ghosh, P. Sar, M. H. Mondal, K. Mahati, B. Saha, *J. Chem. Sci.,* **129(5**). 637 (2017).
12. S. Chowdhury, A. Rakshit, A. Acharjee, B. Saha, *Journal of Molecular Liquids*, **310**, 113224 (2020).
13. Y. Katre, R. Sharma, G. K. Joshi, A. K. Singh, *Journal of Dispersion Science and Technology*, **33(6)**, 863 (2012).
14. F. Ahmed, M. A. Siddiqui, R. Singh, R. F. H. Khan, *Asian Journal of Chemistry*, **23(10)**, 4245 (2011).
15. R. J. Williams, J. W. Phillips, K. J. Mysel, *Trans. Faraday Soc.,* **51**, 728 (1985).
16. P. Mukerjee, K. J. Mysels, Critical Micelle Concentration of Aqueous Surfactant System, NSRDS-NBS, US Government Printing Office, Washington D.C., 2006, p. 34.
17. M. Akram, A. Adel, M. Saeed, K. Kabir-ud-Din, *Eur. Chem. Bull.,* **3(2)**, 119 (2014).

The evolution of hydrogen technologies: paving the way to a sustainable hydrogen economy

M. Pandev[1,2*], V. Terziev[1], B. Abrashev[1]

[1]*Acad. Evgeni Budevski Institute of Electrochemistry and Energy Systems, Bulgarian Academy of Sciences, Acad. G. Bonchev Str., Bl. 10, 1113 Sofia, Bulgaria*

Joint Innovation Centre of the Bulgarian Academy of Sciences, Acad. G. Bonchev Str., Bl. 26 B, 1113 Sofia, Bulgaria

Received: August 24, 2023; Revised: October 01, 2023

Nowadays, there are growing concerns about pollution, climate change and the emerging depletion of fossil fuels. The focus is on the research and development of alternative and renewable energy sources (RES). Hydrogen is emerging as a promising energy carrier to reshape the energy landscape. Fuel cell and hydrogen (FCH) technologies combine various innovations that can change the way we produce and store energy, the way we power our vehicles and mitigate the impact on the environment in general. This brief overview gives an insight into their applications, added value, potential challenges and policy initiatives, highlighting their key role for a sustainable future.

Keywords: Hydrogen, fuel cell, metal hydrides, hydrogen economy, environment

INTRODUCTION

Hydrogen has remarkable properties that make it an attractive energy carrier. Its high energy content per unit mass and zero-emission combustion properties set the stage for its various applications. The most common methods of hydrogen production include methane steam reforming, electrolysis and biomass gasification. Electrolysis, which involves splitting water molecules using electricity, is particularly notable for its potential to harness renewables such as solar and wind power, thereby making hydrogen production inherently greener. Hydrogen is usually categorized into several different colors that reflect the sources through which it is produced and processed (Fig. 1).

One of the main applications of hydrogen technology is the mobility sector. Hydrogen fuel cell vehicles (FCVs) are an environmentally friendly alternative to vehicles with internal combustion engines, as FCVs emit only water vapour as a by-product. In addition, hydrogen can also be used in the aviation and marine industries, addressing the challenges of decarbonizing these sectors with a traditionally high carbon footprint.

Another major application of hydrogen is for energy storage and grid management. RES such as solar and wind are intermittent in nature, which poses challenges to grid stability. Hydrogen can be stored and later converted into electricity *via* fuel cells during peak demand, effectively acting as a buffer to balance fluctuations in energy supply. This approach promotes the integration of renewable sources into the energy mix, making the grid more reliable and sustainable. Nevertheless, the road to widespread hydrogen adoption is not without its challenges. Infrastructure remains a significant hurdle, as building a robust hydrogen refueling network for vehicles and integrating hydrogen storage into existing energy systems requires significant investment. In addition, the efficiency of hydrogen production methods, especially electrolysis, needs improvement to make hydrogen competitive with other energy carriers in terms of profitability [2].

The development of hydrogen technologies also raises concerns about the sustainability of production methods [3]. While electrolysis powered by renewable energy is a clean process, the current dominant method of steam methane conversion relies on fossil fuels, releasing greenhouse gases without using carbon capture and storage (CCS). In order to truly exploit the potential of hydrogen as a green energy carrier, switching to electrolysis with the use of renewable energy is imperative.

In summary, hydrogen technologies present an entirely new model for producing and storing energy and managing the entire grid system. Combined with its potential to significantly reduce greenhouse gas emissions, hydrogen is positioned as a major player in the transition to a sustainable energy future. However, it is crucial to meet the challenges of building the necessary infrastructure and reducing production costs. With continued research, innovation and collaborative efforts, hydrogen technologies have the capacity to change the energy landscape and contribute to a cleaner and greener planet.

* To whom all correspondence should be sent:
E-mail: pandeff@gmail.com

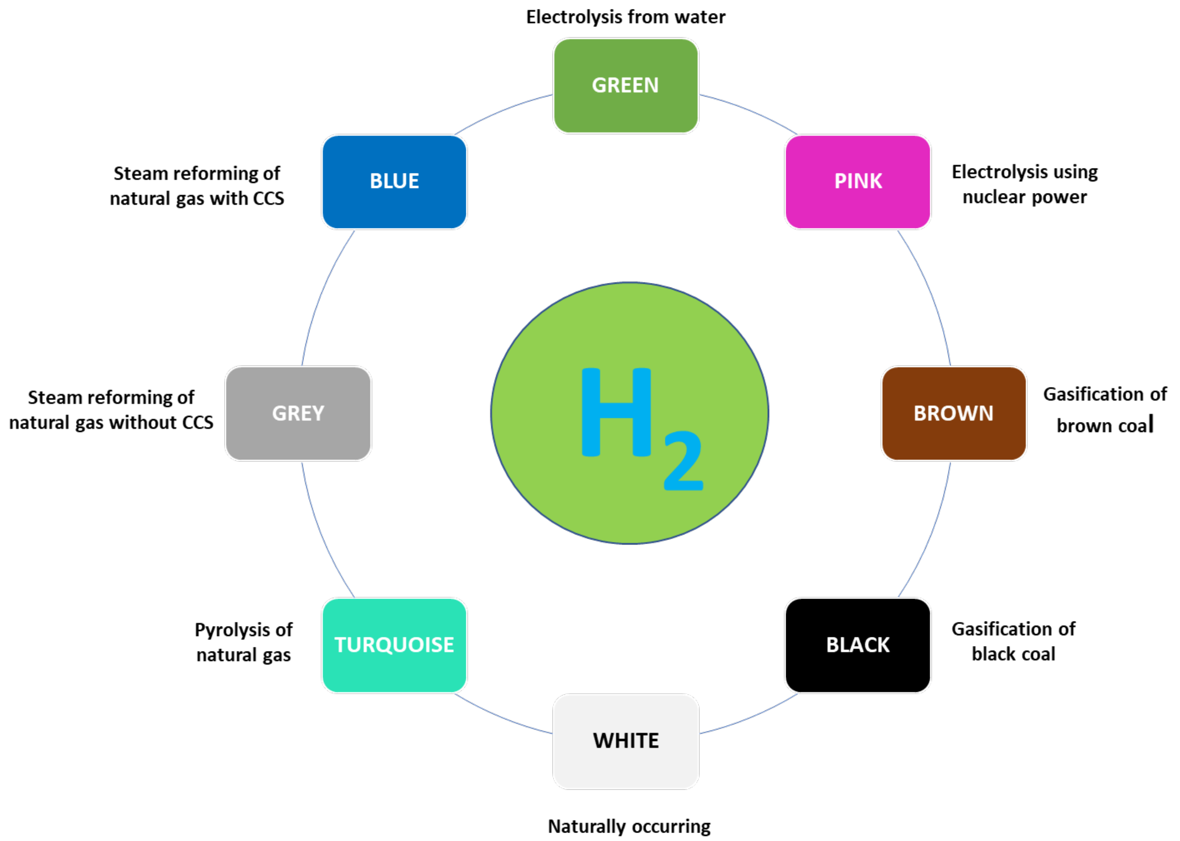

Figure 1. Colors of hydrogen by production [1]

Hydrogen Technologies and Policies across European Union Member States

The European Union (EU) has recognized the potential of hydrogen technologies to achieve its ambitious climate and energy goals, and Europe has already adopted its Hydrogen Strategy. The European Commission positions hydrogen as a core element in its clean energy policy framework. As a significant step towards this vision, the Commission unveiled a strategic proposal in July 2020 designed to accelerate the progress of green hydrogen generated from renewable sources. This strategic push aims to seamlessly integrate green hydrogen into the European energy landscape by 2050. Currently, hydrogen makes up a modest 2% of the EU's energy mix, with a significant majority, approximately 95%, derived from brown hydrogen [4, 5]. In particular, brown hydrogen is produced from natural gas or oil, resulting in annual emissions of 70-100 million tons of carbon dioxide. The paradigm shift to green hydrogen, used through electrolysis powered by renewable electricity, has the potential to revolutionize this landscape. Forecasts indicate that by 2050, ecological hydrogen could cover up to 20% of the EU's energy supply, significantly contributing to meeting the energy needs of the transport sector (20-50% of demand) and the industrial sector (5-20% of demand) [6-8].

The key elements in the European Hydrogen Strategy are as follows:

✓ *Production Methods and Green Hydrogen*: Green hydrogen, produced through electrolysis powered by renewable energy, is seen as the most environmentally friendly option. Scalability, cost-effectiveness, and availability of RES for large-scale green hydrogen production still remain as potential issues.

✓ *Infrastructure Development*: Establishing a hydrogen infrastructure for production, storage, distribution, and consumption is a significant challenge. Developing the necessary infrastructure requires substantial investment, including building new hydrogen production facilities, retrofitting existing pipelines, and/or setting up distribution networks.

✓ *Technology and Innovation*: Research, development and innovation in hydrogen technologies are crucial for improving efficiency, reducing costs, and enhancing the overall viability of hydrogen as an energy carrier. This includes advancements in electrolysis technology, fuel cells, storage solutions, and transportation methods.

✓ *Regulatory Framework*: Creating a supportive regulatory framework that addresses safety, quality, and environmental standards for hydrogen production, distribution, and usage is essential. Harmonizing regulations across EU member states and ensuring consistency with international standards are important considerations.

- ✓ *Market Development and Demand*: Stimulating demand for hydrogen across various sectors, such as industry, transport, and power generation, is a key challenge. Developing incentives, subsidies, and market mechanisms to promote the adoption of hydrogen-based solutions is of essential importance.
- ✓ *Investment and Financing*: The successful implementation of the European Hydrogen Strategy requires substantial financial resources and is directly linked to securing public and private investments to fund research, infrastructure development, and commercial deployment of hydrogen technologies.
- ✓ *Global Collaboration*: Ensuring international collaboration and cooperation in the development of hydrogen technologies and markets is a priority. This involves close collaboration with third countries, sharing best practices, and creating a global hydrogen market.
- ✓ *Supply Chain and Raw Materials*: Hydrogen production requires raw materials, such as water and metals for electrolysis, which could raise concerns about resource availability, sustainability, and potential environmental impacts.
- ✓ *Skills and Workforce Development*: Building a skilled workforce to support the hydrogen sector, including engineers, technicians, and other professionals, is considered important for the successful implementation of the strategy [6, 9].

Member states have been actively pursuing various hydrogen-related initiatives, demonstrating a diverse range of applications and policy approaches [10]. In their national programs and policies, the leading EU countries focus on various aspects related to the large-scale application of hydrogen technologies:

Germany has positioned itself as a frontrunner in hydrogen technology adoption. The country's National Hydrogen Strategy, unveiled in June 2020, outlines a comprehensive roadmap for hydrogen deployment across various sectors. The strategy emphasizes both green hydrogen production through renewable-powered electrolysis and blue hydrogen through carbon capture and storage. Germany aims to have 5 GW of electrolysis capacity by 2030 and has committed significant funding to research, development, and infrastructure expansion for hydrogen technologies [11].

France is focusing on integrating hydrogen into its public transportation system. The country has launched pilot projects to test hydrogen-powered buses and trains, with the aim of decarbonizing local transport. For instance, the "Hydrogen Mobility Ecosystem" project in the Auvergne-Rhône-Alpes region involves deploying hydrogen fuel cell buses and establishing refueling infrastructure. France's approach highlights the potential of hydrogen in reducing emissions in urban mobility [12].

The Netherlands is leveraging its expertise in offshore wind energy to produce green hydrogen. The Dutch government has set targets for installing gigawatts of offshore wind capacity by 2030, which will be used to power electrolysers for hydrogen production. The "North Sea Wind Power Hub" initiative envisions a cooperative approach among North Sea countries to produce hydrogen from offshore wind farms and distribute it across the region [13].

Spain is focusing on the development of hydrogen industrial clusters to foster collaboration among industries, research institutions, and public entities. The country's "Hydrogen Roadmap" outlines plans to create these clusters in regions with existing industrial infrastructure. These clusters aim to integrate renewable hydrogen in industries such as steel, chemicals, and transport, contributing to sectoral decarbonization [14].

Belgium is working on cross-border hydrogen infrastructure to facilitate the transport and distribution of hydrogen within the Benelux region. The "Hydrogen for the Future" project aims to build an integrated hydrogen network connecting production, storage, and consumption facilities across Belgium, the Netherlands, and Luxembourg. This approach highlights the importance of collaboration for creating a pan-European hydrogen market [15].

In conclusion, hydrogen technologies are gaining momentum across the EU, with member states adopting diverse approaches to harness their potential. From national strategies to sector-specific projects, these initiatives demonstrate the commitment of EU countries to transition towards a cleaner and more sustainable energy future. As the technology matures and international collaboration grows, hydrogen is to play a vital role in achieving the EU's carbon neutrality goals. Furthermore, not only the EU has put efforts and funding for the development and implementation of FCH technologies. Currently, the global hydrogen market is valued at 242.7 billion USD as of 2023 and is expected to reach 410.6 billion USD by 2030. That actually presents an annual growth rate of about 7-8% during the forecast period. The growth in hydrogen demand during the recent years is due to the increasing policy measures for achieving hydrogen-based economies and the notable investment in hydrogen infrastructure. The market for hydrogen is expected to benefit greatly from the rising use of low-emission fuel [16]. In Japan, for instance, establishing an H_2 system is identified as a key aim for Japan's future technology portfolio and the government has launched different policies in order to contribute to the realization of a low-carbon society. The share of hydrogen is expected to be 13% of the total primary energy supply in the country by 2050 under severe environmental constraints [17].

Hydrogen Production: Electrolysis and Steam Methane Reforming

Electrolytic hydrogen production involves the splitting of water molecules (H_2O) into hydrogen (H_2) and oxygen (O_2) using an electrical current. This reaction occurs at the electrode surfaces:

$$2H_2O \rightarrow 2H_2 + O_2.$$

Electrolysis can be powered by RES, ensuring "green hydrogen" production with minimal carbon footprint.

In Steam Methane Reforming, natural gas (methane, CH_4) reacts with steam (H_2O) to produce hydrogen and carbon dioxide (CO_2):

$$CH_4 + H_2O \rightarrow CO_2 + 3H_2.$$

This is the most common method for industrial hydrogen production but results in CO_2 emissions unless carbon capture and storage are implemented [18].

Hydrogen Storage: Metal Hydrides and Compression. Metal Hydrides Storage Systems for RES

The conventional methods of storing and transporting hydrogen are in the form of high-pressure gas and liquid hydrogen [19]. The technically easiest way to store hydrogen is as a pressurized gas. Modern hydrogen storage containers are constructed from new composite materials that allow the weight of the container to be reduced to normal limits. However, containers take up a large volume, which is why this method is more applicable to larger vehicles such as buses and vans. Liquid hydrogen occupies a relatively small volume. Moreover, this method is characterized by the highest weight storage capacity. In order to liquefy hydrogen, however, it must be cooled to -253°C, which requires energy equal to about 1/3 of its own energy content. The tanks have expensive insulation, with a wall thickness of about 3 cm. However, a certain amount of hydrogen (about 1-3% per day) is irreversibly lost due to heating and evaporation. In addition to being too expensive due to the high unproductive consumption of energy for compression (up to 35%) and liquefaction (up to 60%), both methods carry the risk of accidents and require serious safety measures.

The alternative of the above-mentioned methods is the storage of hydrogen in the form of metal hydrides [20]. Certain metals (e.g. Pd, Mg) and alloys (e.g. $LaNi_5$, FeTi) can form hydrides by absorbing hydrogen, creating a solid-state storage solution. This reversible reaction allows for hydrogen absorption and release, aiding in safe and efficient storage:

$$M + H_2 \rightleftharpoons MH_2.$$

The desorption reaction is endothermic, requiring heat input [21]. When the hydride is heated, the reaction proceeds in the reverse direction. Despite the fact that a certain amount of energy is required for the release of hydrogen, in principle this ensures stability and safety - in the event of a collision, the supplied heat stops and the release of hydrogen ceases. In addition, hydrides can store about 60% more hydrogen by volume than liquid hydrogen tanks. So far, ternary metal hydrides of AB_5 and AB_2 alloys have found practical application [20]. Special units are filled with them, from which, on demand, the hydrogen is supplied to fuel cells or heating installations [22].

The advantages of the metal hydrides storage systems can be summarized as follows:

- ✓ Safe and Compact Storage: Metal hydride storage systems provide a safe and compact method of hydrogen storage compared to high-pressure gas or cryogenic liquid storage methods.
- ✓ High Energy Density: Metal hydrides can store a significant amount of hydrogen by weight, resulting in a high energy density storage solution.
- ✓ Thermal Energy Storage: The heat released during hydrogen absorption can be utilized for thermal energy storage applications, enhancing system efficiency.
- ✓ Reduced Hydrogen Loss: Metal hydrides have a relatively low rate of hydrogen loss during storage compared to other storage methods.
- ✓ Integration with RES: Metal hydrides storage systems can play a crucial role in integrating RES into the energy mix.
- ✓ Energy Storage: Excess energy generated from RES can be used to power the hydrogen desorption process, storing the energy as hydrogen in metal hydrides during periods of high renewable energy production.
- ✓ Energy Release: When renewable energy generation is low, stored hydrogen can be released

through the desorption process to generate electricity *via* fuel cells or combustion, contributing to a stable energy supply.

Challenges that metal hydride storage systems face are:

✓ Kinetics: The absorption and desorption reactions can be relatively slow, affecting the system's responsiveness to changes in energy demand.

✓ Heat Management: Effective heat management is crucial to ensure efficient hydrogen release.

✓ Cost: Developing efficient and cost-effective metal hydride materials remains a challenge, impacting the economic viability of these systems.

In conclusion, metal hydride storage systems offer a promising way for efficiently storing and utilizing renewable energy in the form of hydrogen. With ongoing research and development efforts focused on improving reaction kinetics, material performance, and system integration, metal hydrides have the potential to contribute significantly to a more sustainable and secure energy future.

In the context of RES, metal hydrides can play a key role. For example, during periods of excess renewable energy production, the hydrogen desorption reaction can be driven by the surplus energy, storing hydrogen within the metal hydrides. When energy demand exceeds renewable energy generation, the stored hydrogen can be released through the hydrogen desorption reaction to generate electricity *via* fuel cells or other conversion technologies.

Hydrogen Utilization: Fuel Cells vs. Combustion

When hydrogen is burned in the presence of oxygen, it releases heat energy and forms water vapor:

$$2H_2 + O_2 \rightarrow 2H_2O.$$

The more sophisticated way for hydrogen utilization, however, is in fuel cells, which convert hydrogen and atmospheric oxygen into electricity, with water as the only byproduct. The anode reaction involves hydrogen oxidation:

$$2H_2 + 4OH^- \rightarrow 4H_2O + 4e^-.$$

Although they were discovered and demonstrated already in the first half of the 19^{th} century, fuel cells found their first serious application only in the early 60s of the 20^{th} century when alkaline fuel cells developed by Bacon and perfected by Pratt and Whitney, have been used in manned flights of the US space program as sources of both electricity and water [19]. Since then, five varieties of hydrogen fuel cells - Alkaline fuel cells, Proton exchange membrane fuel cells, Fuel cells with phosphoric acid electrolyte, Carbonate melt fuel cells, and Solid oxide fuel cells, with different characteristics and possible applications have been developed [19].

Interaction with Materials: Hydrogen Embrittlement

Hydrogen can diffuse into metals, causing embrittlement and weakening of materials. This interaction is of concern in industrial applications and requires careful engineering to prevent structural failures.

Environmental Benefits and Challenges

Hydrogen offers a pathway to decarbonize sectors like transportation and industry. Hydrogen fuel cell vehicles emit only water vapor and provide longer ranges compared to battery electric vehicles. Hydrogen's versatility makes it suitable for applications like energy storage and grid balancing.

Green hydrogen production requires substantial electricity, potentially impacting grid stability. Ensuring sustainable production methods and addressing the efficiency of electrolysis are ongoing challenges. Furthermore, hydrogen's low energy density per unit volume requires advanced storage solutions for practical use.

International Collaboration and Research

Numerous research initiatives worldwide aim to enhance hydrogen production, storage, utilization efficiency, and safety. International collaboration is essential to address challenges and accelerate technological advancements.

The concept of a "hydrogen economy" envisions a transition from fossil fuels to hydrogen as a versatile energy carrier. This transformation necessitates interdisciplinary research in chemistry, materials science, engineering, and policy development.

Hydrogen technologies offer diverse opportunities to reshape energy systems while addressing environmental concerns. Scientific understanding of hydrogen's interactions, reactions, and material implications is crucial for realizing the full potential of this versatile element in building a sustainable energy future.

Integration of Hydrogen Technologies and RES

It may be pointed out that since 2010 the use of RES has notably increased as shown on Figure 2.

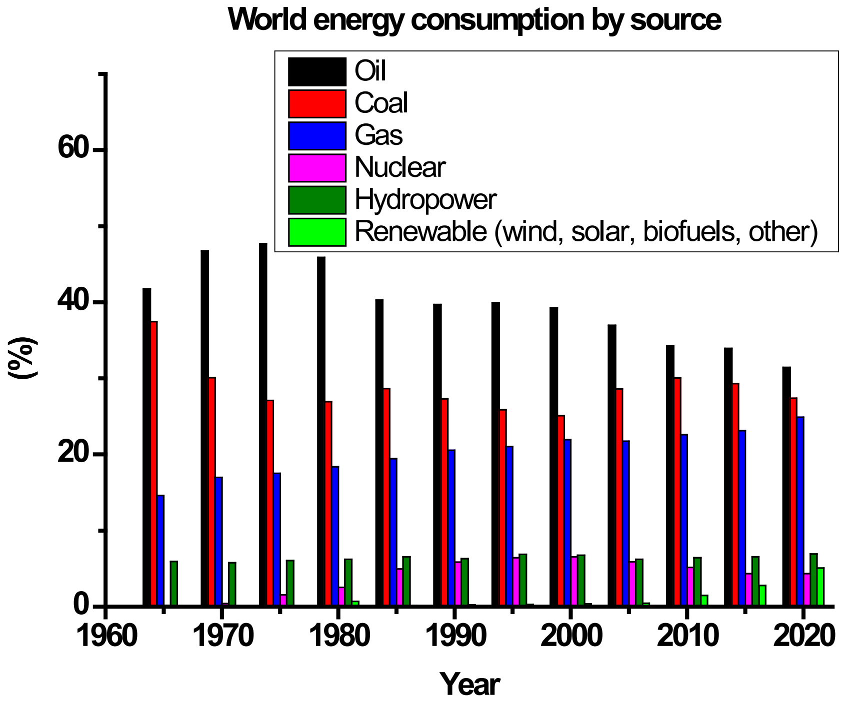

Figure 2. World energy consumption during the last six decades [23, 24]

The integration of hydrogen technologies with RES presents a powerful solution for addressing both energy demand and environmental sustainability. By harnessing the energy from renewable sources to produce, store, and utilize hydrogen, a symbiotic relationship can be established that contributes to a cleaner and more reliable energy system [25]. Here's a closer look at how hydrogen technologies and RES can be integrated [26-28]:

✓ Green Hydrogen Production: RES such as solar, wind, hydroelectric, and even geothermal power can be used to power electrolysers, splitting water into hydrogen and oxygen. This process yields hydrogen without any direct carbon emissions, resulting in a clean energy carrier.

✓ Intermittency Management: RES are often characterized by their intermittent nature, dependent on factors like weather and time of day. Hydrogen technologies can address this intermittency by storing excess energy generated during peak production periods as hydrogen. This stored hydrogen can later be converted back into electricity through fuel cells or combustion when renewable energy generation is low, helping to balance supply and demand on the grid.

✓ Seasonal Energy Storage: Unlike battery storage, hydrogen has the potential to store energy for longer durations, making it suitable for seasonal energy storage. Excess renewable energy generated during the summer months, for example, can be converted into hydrogen and stored until the winter when energy demand is higher.

✓ Transport and Power Generation: Hydrogen produced from RES can be used as fuel for various applications. Hydrogen fuel cell vehicles can provide zero-emission transportation, and hydrogen-powered generators can supply electricity during periods of high demand or low renewable energy availability.

✓ Grid Balancing and Flexibility: Hydrogen-based energy systems offer grid operators additional flexibility for managing energy supply and demand. By adjusting hydrogen production and utilization rates, grid stability can be maintained, reducing the need for fossil fuel-based backup power.

✓ Challenges and Considerations: While the integration of hydrogen technologies with RES holds immense promise, several challenges must be addressed:

a) Efficiency: The efficiency of converting renewable energy into hydrogen and then back into electricity needs improvement to ensure the overall viability of the process.

b) Cost: The cost of electrolysis, storage, and fuel cells can be prohibitive, making it necessary to drive down costs through technological advancements and economies of scale.

c) Infrastructure: Establishing a widespread hydrogen infrastructure, including production, storage, and distribution facilities.

d) Policy and Regulation: Clear policies and regulations are needed to incentivize the adoption of hydrogen technologies and ensure a level playing field with other energy sources.

In conclusion, the integration of hydrogen technologies with renewable energy sources presents a promising trajectory toward a sustainable energy future. By harnessing the complementary strengths of hydrogen and renewable energy, an interconnected energy ecosystem can emerge, effectively curbing carbon emissions, bolstering energy security, and propelling technological advancement. However, the successful realization of this synergy hinges upon the adept handling of technical intricacies, economic considerations, and regulatory frameworks.

The prospects for hydrogen technologies on the global stage hold immense potential, coinciding with the global pursuit of cleaner and more sustainable energy paradigms. As a versatile and adaptable energy carrier, hydrogen stands poised to assume a pivotal role in driving decarbonization efforts and navigating multifaceted energy dilemmas. This prospective future is characterized by strategic investments, rigorous research endeavours, and the pervasive adoption of hydrogen across diverse sectors. Impending landscape of hydrogen technologies exemplifies a shift toward heightened sustainability within energy systems. Prioritizing the proliferation of green hydrogen production, its application in industry, transportation, energy storage, and fostering international collaboration collectively underpin its transformative capacity. Thus, hydrogen emerges as an energy carrier, holding the potential to substantially contribute to a cleaner, more robust, and ultimately carbon-neutral energy landscape.

Acknowledgements: *The authors kindly acknowledge the financial support of project № BG05M2OP001-1.002-0014 „Center of Competence HITMOBIL - Technologies and Systems for Generation, Storage and Consumption of Clean Energy", funded by Operational Programme "Science and Education for Smart Growth" 2014-2020, co-funded by the EU from European Regional Development Fund.*

REFERENCES

1. https://www.nationalgrid.com/stories/energy-explained/hydrogen-colour-spectrum
2. M. Balla, M. Wietschel, *Int. J. Hydrog. Energy*, **34**, 615 (2009).
3. D. Santos, C. Sequeira, *Quim. Nova*, **36** (8) 1176 (2013).
4. A. Sgobbi, W. Nijs, R. Miglio, A. Chiodi, M. Gargiulo, C. Thiel, *Int. J. Hydrog. Energy*, **41**, 19 (2016).
5. N. Muradova, T. Veziroglu, *Int. J. Hydrog. Energy*, **33**, 6804 (2008).
6. https://energy.ec.europa.eu/topics/energy-systems-integration/hydrogen_en#eu-hydrogen-strategy
7. G. Kakoulaki, I. Kougias, N. Taylor, F. Dolci, J. Moya, A. Jäger-Waldau, *Energy Conversion and Management,* **228**, 113649 (2021).
8. T. Schmidt, *iScience*, **24** (2) 102045 (2021).
9. T. Tröndle, J. Lilliestam, S. Marelli, S. Pfenninger, *Joule*, **4** (9) 1929 (2020).
10. M. Kanellakis, G. Martinopoulos, T. Zachariadis, *Energy Policy*, **62** 1020 (2013).
11. https://www.bmwk.de/Redaktion/EN/Hydrogen/Dossiers/national-hydrogen-strategy.html
12. https://s3.production.france-hydrogene.org/uploads/sites/4/2023/01/VF-Executive-summary-FH-2022-EN-Web.pdf
13. https://www.offshorewind.biz/2023/03/20/the-netherlands-chooses-site-for-worlds-largest-offshore-wind-to-hydrogen-project
14. https://www.wfw.com/articles/the-spanish-hydrogen-strategy
15. https://www.waterstofnet.eu/_asset/_public/Publicaties/Final-Report-Benelux-H2- Project_FINAL.pdf
16. https://www.marketsandmarkets.com/Market-Reports/hydrogen-market-132975342.html
17. S. Iida, K. Sakata, *Clean Energy*, 1 (2018).
18. https://www.energy.gov/eere/fuelcells/hydrogen-production-natural-gas-reforming
19. M. Mitov, I. Kondev, Y. Petrov, St. Bliznakov, A. Popov, *Khimiya*, **12**, 455 (2003).
20. S. Bliznakov, E. Lefterova, M. Mitov, L. Bozukov, A. Popov, I. Dragieva, *New Trends in Intercalation Compounds for Energy Storage*, 601 (2002).
21. T. Somo, T. Maponya, M. Davids, M. Hato, M. Lototskyy, K. Modibane, *Metals*, **10**, 562 (2020)
22. J. Abe, A. Popoola, E. Ajenifuja, O. Popoola, *Int. J. Hydrog. Energy*, **44**, 15072 (2019).
23. https://www.bp.com/en/global/corporate/energy-economics/statistical-review-of-world-energy.html
24. https://ourworldindata.org/grapher/modern-renewable-energy-consumption
25. M. Shelyapina, Handbook of Ecomaterials, 775 (2019).
26. P. Brandon, Z. Kurban, *Phil. Trans. R. Soc.* **A**, **375** (2098) 1 (2017).
27. A. Pareek, R. Dom, J. Gupta, J. Chandran, V. Adepu, P. Borse, *Materials Science for Energy Technologies.* **3**, 319 (2020).
28. S. Hosseini, M. Wahid, *Renewable and Sustainable Energy Reviews,* **57**, 850 (2016).

Bulgarian Chemical Communications, Volume 55, Issue 4 (pp. 441-445) 2023 *DOI: 10.34049/bcc.55.4.5536*

New possibility to locally convert municipal waste into energy

D. N. Kolev*

Institute of Chemical Engineering, Bulgarian Academy of Sciences, Laboratory of Transfer Processes in Multiphase Media, Sofia, Bulgaria

Received: October 14, 2022; Revised: December 05, 2023

This article discusses a technology that enables the use of generated municipal waste near its receipt. This makes it possible to reduce the costs associated with the transport of waste and to reduce the associated greenhouse gas emissions. The use of energy generated by transforming waste into energy benefits the society that generated it. The proposed technology uses municipal waste directly and without the need for pre-treatment outside the plant. The technology provides solutions to avoid possibilities for environmental pollution and allows compliance with all European norms [7]. The proposed installation is designed for treatment of waste generated by a population of 30 to 70 thousand inhabitants.

Keywords: environmental protection, incineration, packed bed columns, gas cleaning, solid waste treatment

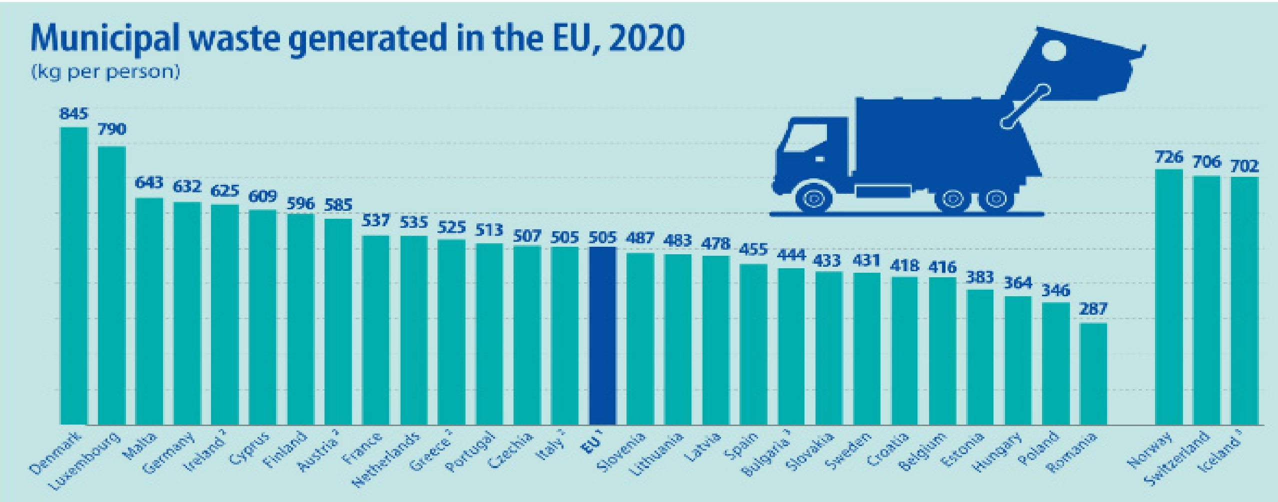

Figure 1. Household waste generated by a person per year in the countries of the European Union, 2020 [1]

INTRODUCTION

With the growing consumption in the recent years, the generation of waste on a European scale has also increased.

As can be seen from Fig. 1, the largest waste production per capita is in Denmark - 845 kg per year per person, and the lowest - 287 kg in Romania. Bulgaria has 444 kg, which is below the European average [1]. Unfortunately, there are no data to clarify the distinction between generation of household waste in cities and in villages.

This article focuses on the state of urban household waste for the city of Sofia. The waste, collected from Sofia, is transported to the Sadinata area near the village of Yana, where a mechanical and biological treatment plant for waste with production of RDF is located [8]. The distance from there to the center of Sofia is 22 km. Bulk density of waste varies from 250-350 kg/m^3, therefore, no more than 10 tons of household waste is collected in one garbage collection truck. The consumption rate of the transport trucks is about 27 l of diesel/per 100 km. On average, 387 467 tons of household waste are delivered to the processing plant annually. According to statistics, the population of Sofia is 1 221 172. If the above chart is considered, the amount of waste produced is 1 221 172 (the population) × 444 (kg waste per person) = 542 200 tons. From the reasoning done, it can be seen that there is difference of 154733 tons. It can be assumed that this amount has been previously separated and submitted for recycling. According to the data of the company that deals with this activity, they have fulfilled their commitments to recycle more than 60% of the packaging put into circulation on the market. The waste separated in the containers of the recycling company is not contaminated with food waste and is

* To whom all correspondence should be sent:
E-mail: d.kolev@iche.bas.bg

suitable for use for recycling.

The transportation of waste from Sofia to the primary processing plant requires 38 746 courses round, in the opposite direction the trucks are empty.

Calculation of required fuel: 38 746 courses × 44 km (both ways; total) × 0.27 l/km= 460 302 litres of diesel fuel. At the price of diesel of 1.53 EUR per litre, this is 706 346 EUR. Let's also calculate the carbon footprint of this transport. The burning of 1 litre of diesel produces 2.67 kg of CO_2, so it is 1 220 t of CO_2 .

What role does the household waste treatment plant play?

It reduces the moisture content of waste;
Obtained recyclate;
Obtained RDF fuel;
Obtained material for direct disposal.

We will briefly discuss the above items separately.

It reduces the moisture content of waste

Reduction of the moisture content of waste is carried out by means of aerobic fermentation of food waste. The food waste turns into earth, giving off heat. The heat is used to heat air that dries the waste. The moisture obtained during the drying process is condensed by means of coolers - water towers. The heat carried by the water vapor is not used, but is emitted into the atmosphere, causing thermal pollution. In this way, a large amount of energy is lost; if it had been used in the combustion process, it would be utilised for heating purposes.

Below is an estimate of the material and heat flows. The data used are for 2020.

Food and green waste in the product entering the plant is 38.9 % with approximately 72% water content [4]. Annually, they are 150 724 t or in dry condition 42 202 t. In the RDF product generated by the plant, the content of food waste is 5.68% and its humidity is 20%, the amount of RDF is 154 652 t. Calculated as a dry substance, this is 7 027 t. When we balance the drying process, as well as losses in the various separation processes, 64 984 t is obtained. Their energy evaporated 102 000 000 kg of water. If we equate the calorific value of dry food waste to carbohydrates (1 kg- 4000 kcal, 16.74 MJ), the energy carried in dry waste is 140 698 452 000 kcal (589 076 GJ). Evaporation of 1 kg of water requires about 700 kcal (2.93MJ). If we assume that the dry waste is burned in a cauldron with an efficiency of 80% (conservative assumption), 160 798 tons of water can be evaporated with this energy. The amount of energy that would be saved, recalculated as diesel (1 l diesel - 10 000 kcal, 41.86 MJ) is 4 115 860 kg (6 297 265 EUR). Its carbon footprint is 10 989 t of CO_2, respectively. At time of writing, the price of carbon emissions fluctuates between 70-90 EUR per ton, as shown in Fig. 2. For the calculation a significantly lower value of 50 Euros is assumed resulting in 549 467 Euros.

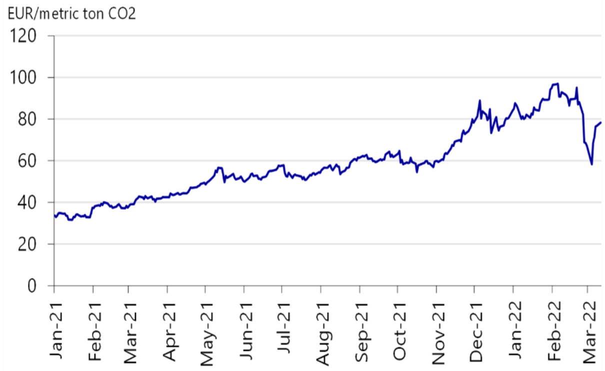

Figure 2. Average tender price of quota emission in Euro/t.CO_2 [2]

If a combustion installation is used, the shown effect could increase up to two times as the evaporated water will condense and heat the heating water.

Obtained recyclate

The annually received recyclate is 36 997 tons, which is 10.5% of the input material. In the process of separation, several products are separated. The price the Metropolitan Municipality receives for them is given below:

Mixed plastics 18 146 t - bid price 1.82 EUR/t
Glass 4628 t - bid price 1.68 EUR/t
Paper and cardboard 5908 t - bid price 3.82 EUR/t
Ferrous metals 6296 t - bid price 10.23 EUR/t
Nonferrous metals 578 t - bid price 306.9 EUR/t

Based on the above prices, the total revenue of the plant from separation of products is 305 343 EUR. Below is a figure showing the international average exchange prices in the European Union for waste products.

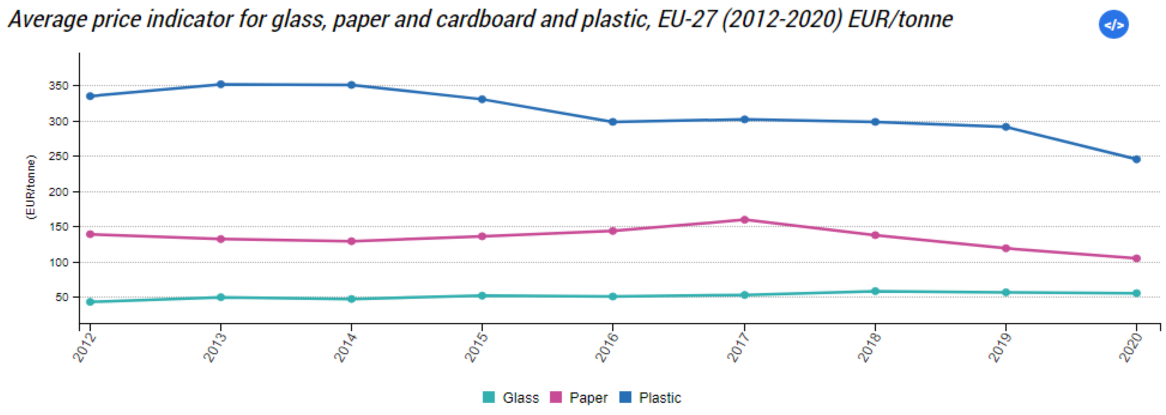

Figure 3. Average European prices of separated waste materials by year [1]

The values for 2020 are: glass 65 EUR, paper 120 EUR, plastics 270 EUR.

Calculating from the quantities received in the processing plant according to the data from Fig. 3, the result is 5 905 960 EUR. These prices are lower than the usual trade prices, mostly due to the contamination of food waste [9].

Obtained RDF fuel

The amount of RDF obtained is 154 652 t with an average calorific value of 3000-4000 kcal/kg (12.5-16.7 MJ). It should be noted that household waste is treated as a partially renewable source of energy. At the moment, there is no RDF incineration plant built in Sofia, which is why the processing plant is overflowed with material. According to data from the Ministry of Environment and Water, the plant currently pays 15 to 25 EUR per ton to licensed companies that can use it. Only 50 000 t are disposed of in this way, the rest is landfilled.

In the future, a waste incineration plant on the territory of the Sofia district heat and power station is planned to be built, which will be able to burn the entire amount of RDF produced by the plant and produce electricity, as well as heat the water for central heating.

The distance from the processing plant to the heat and power station site of Sofia is 23 km. And here, as above, we will calculate the fuel consumption for transportation of the waste, as well as its carbon footprint. The amount of fuel is 15 465 × 46 × 0.27 = 192 075 litres of diesel. Carbon footprint 192 075 × 2.67 = 512.8 t CO_2.

Obtained material for direct disposal

The amount of disposed waste is 52 072 tons. This amount is about 14 % of the supplied material. It most likely contains materials that, when burned, would give off an additional amount of heat. By burning this waste, its quantity would also be significantly reduced.

Health considerations

In the separation plant, all the household waste of Sofia is being mixed. Before the Covid-19 pandemic, this did not attract the attention of the specialists in the field, but now is already treated with caution. Dissociation and separation of waste is done mostly manually. Workers performing these activities are exposed to great risks, that is why burning of municipal waste without this treatment step is advantageous for the workers' health.

The alternative

Below in Figure 4 is presented a new technology (successfully patented [3]) for using urban household waste as a raw material to obtain electrical energy and heat for heating needs. The installation can be located in residential neighborhoods, so that the distance from which the waste is delivered does not exceed 3-5 km. To date, this technology has not been implemented. The feasibility studies for the implementation of the technology provided us with evidence that the necessary territory required for the construction of the waste treatment plant is a little over 4 000 m^2. The installation is intended for treatment (waste-to-heat process) of 50-100 tons of household waste per day without being previously processed. The energy characteristic of Sofia waste is 1300 kcal/kg (5.4 MJ) with a moisture content of 40% [4].

Operation processes

The arriving truck discharges the waste into a receiving bunker. After the bunker, the waste passes through a separation line where the following takes place: the bags are broken open, then waste passes through a scale and magnetic separator, and from there it is delivered into a shredder. After being so separated it is delivered into a day bunker or into a line stand-by bunker. The stand-by bunker has a capacity to take waste for 15 days.

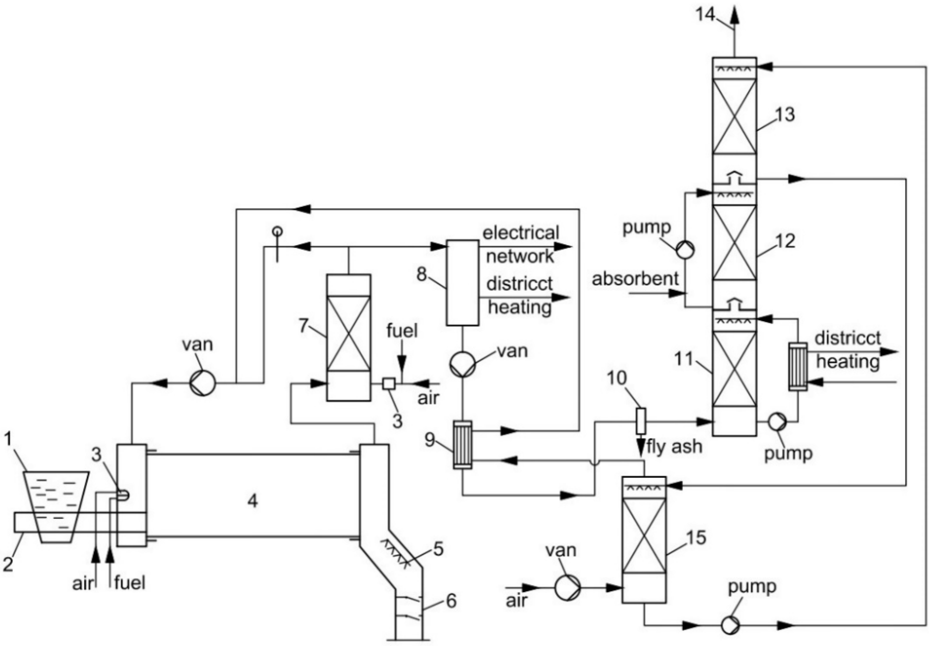

Figure 4. Installation for incineration of urban household waste. 1. day bunker, 2. feed auger, 3. burner, 4. rotary kiln, 5. water nozzle, 6. bottom ash extractor, 7. post combustor, 8. utilization unit, 9. recuperation unit, 10. beg filter, 11. contact economizer I, 12. absorber, 13. contact economizer II, 14. chimney, 15. direct heater and humidifier

From the daily bunker, the waste is delivered to the rotating combustion chamber (rotary kiln). The downtime therein is around 30 minutes. The length of the rotary kiln is 15 m. The temperature maintained in the combustion chamber is about 850 ºC. On the initial start of the plant, a liquid or gaseous fuel burner shall also be used to provide the required temperature. During the process, when the temperature in the combustion chamber starts decreasing, the burner is automatically turned on to maintain it. The bottom ashes generated from the incineration are removed from the combustion chamber, being pre-cooled with water. The device does not allow uncontrolled air entering into the process when removing the ash. The flue gases generated are supplied to a post-combustor where a burner maintains a temperature of 1100 ºC. The post-combustor is designed as a packed bed column, which makes it possible to maintain the temperature profile therein constant. The gas downtime in the post-combustor is more than 2 seconds. If necessary, a burner can keep the temperature in the post-combustor constant. After the post-combustor, the gases are separated into two streams. One stream goes to a recovery unit, where they are cooled down to 500 ºC. They then are sent to a recuperation unit, where they heat the air for the incineration process, and they are cooled down to 200 ºC, temperature of the wet thermometer is 79.1 °C. Next, they pass through a bag filter to separate the ash carried over with the gases. Thus, cooled and mechanically purified gases are delivered into a contact economizer [5] - direct water heat exchanger, where they indirectly heat the district heating water up to 75 ºC. Then they enter an absorber for their chemical treatment. The absorber uses sodium carbonate solution. In the process are formed: sodium fluoride, sodium chloride, sodium sulfite, sodium sulfate. When sodium carbonate is depleted, the solution is replaced. After the absorber, the gases enter a second economizer. There they heat the water, which in turn heats and humidifies the air for the incineration process. Flue gases leave the plant through a flue duct fully meeting the highest environmental requirements.

The second stream of gases is being mixed with the heated and humidified air and with a temperature of about 700 ºC is delivered to an entry of the rotary kiln.

The recovery unit is a Rankine cycle turbine [6], where electricity and heat are generated in the form of hot water for district heating purposes.

Advantages of the proposed installation

Small in size, operated almost automatically, no environmental pollution. The Rankine cycle turbine used to generate electricity operates at low temperatures with organic oils used in a closed cycle.

From an energy point of view: If we consider the installation as a black box, where the input is waste with high humidity and air with an external temperature necessary for combustion, and the output is flue gases with a temperature of 30-35 ^{o}C, with waste water that underwent heat treatment (the water that was part of the waste), slag from the combustion process, a solution of salts from gas cleaning. The rest is electrical energy and heat for heating purposes.

CONCLUSION

The construction of RDF separation and production plants is economically, technically and environmentally unfeasible. Renewable resources such as green and food waste are wasted instead of replacing fossil fuel energy.

The development of technologies should lead to the best use of the energy capacity of urban household waste.

By building several installations at different sites, it will not be necessary to build additional heat accumulator systems, since the heating network itself plays this role. The distances over which waste is transported will be reduced and the carbon footprint of its transport reduced.

Construction of local installations [3] for incineration of waste should be located next to the district heat and power stations. In Sofia, there are 4 large heat and power stations - Zemlyane HPS, Sofia HPS, Lyulin HPS and Sofia Iztok HPS; there is enough free space on their territory for the construction of the proposed installations.

REFERENCES

1. www.ec.europa.eu/eurostat
2. C. Stet, P. Ruiz, *RaboResearch - Economic Research* https://economics.rabobank.com/publications /2022/march/high-eu-carbon-prices-are-structural-inaction-no-option/ (2022)
3. D. Kolev, R. Lyutskanova, *Patent BG* 66232 B1 (2006)
4. I. Ganev, *Energy Forum,* 425 (2008)
5. D. Kolev, *Bulg. Chem. Commun.,* **35** (3), 153 (2003).
6. Turboden ORC units 2008 Turboden-wood Energy Information Day1 www.scribd.com/document/43070228/Turboden-woodEnergyInformationDay1
7. D. Kolev, 8th International Conference on Energy Efficiency and Agricultural Engineering, 2022, DOI: 10.1109/EEAE53789.2022.9831282
8. www.spto.bg
9. Public auction of Sofia Municipality (Bulgaria) 04-so-2022 from 26.05.2022.

Bulgarian Chemical Communications, Volume 55, Issue 4 (pp. 446-453) 2023 *DOI: 10.34049/bcc.55.4.5589*

Investigation of zinc sulfide phosphorescent materials obtained by a modified non-co-precipitative method

I. I. Kartev

High School of Mathematics – Plovdiv, Bulgaria

Received: June 20, 2023; Accepted: December 12, 2023

The purpose of this project is to investigate the qualities of ZnS-based phosphorescent materials, obtained by a simple wet chemical route, which does not involve co-precipitation of the base material and the modifier used to activate the ZnS. The method is adjusted, so halogenides are introduced as co-activators through the usage of the corresponding activator salt. Experiments, utilizing different activators (Mn, Cu and Ag) or investigating the presence of halogenides (Cl^-), trivalent cations (Al^{3+}) or co-activator, were conducted. The luminescent properties of all modified phosphors were measured in order to determine the optimal doping conditions for ZnS. Out of the determined conditions the peak activator concentrations and the halogenide additions were compared to the corresponding conditions reported in related research, where different synthesis routes have been used.

Keywords: ZnS, phosphors, non-co-precipitative, co-activation, activator halogenide

INTRODUCTION

There are several reported methods for synthesis of ZnS-based luminescent materials, which differ in the method of obtaining ZnS and the procedure of modification. The most common methods used often contain a co-precipitation route, whose main advantages are the homogenous activator distribution and the quality of the produced ZnS nanoparticles [1, 2]. From the large amount of research on this topic, different synthesis routes lead to different luminescent properties under the same doping conditions. The method used in this project involves separate precipitation of ZnS and activator addition. It is therefore expected that the procedure investigated in this project would give distinct results, because of its difference from the commonly used co-precipitation. This difference is related to ZnS purity, the possibility of adding halogenides as a counter-ion of the salt used to introduce the activator (using activator halogenide salts).

The hypothesis, which this project is trying to defend, expects an inhomogeneous glow surface of the prepared phosphors because of omitted co-precipitation. Furthermore, phosphors, being modified with activator halogenide salt, are expected to give better results, compared to other methods of halogenide addition.

A monovalent halogenide anion, when introduced to the ZnS before the firing process, can have its own effect on the efficiency of the incorporation, and therefore, on the quality of the phosphor. Its presence usually resolves the issue of imbalanced charge after an introduction of a foreign atom [3]. Another theory suggests that the halogenide ions begin to act as traps within the forbidden gap, when they become part of the ZnS crystal [4]. Alongside the electron traps formed from S^{2-} vacancies, this effect leads to an increase in the number of electrons in the trapped state, causing more electrons to be excited when the phosphor is exposed to UV light and therefore, increasing the intensity of the emitted light. In the co-precipitation method, both the base compound (ZnS) for the phosphor and its activator are obtained in a sulfide form, which requires additional introduction of the described halogenide anions, often in the form of alkali or ammonia chlorides [5]. The anions can also be included by adding the activator after the precipitation of ZnS and using the corresponding halogenide of the particular activator.

In the case, when a single activator is used, its concentration has a key influence on the phosphor properties. The concentration of the activator, which leads to a material with the best luminescent properties, regarding other variables, is often called peak concentration. A lower concentration implies formation of fewer recombination sites and causes fewer non-UV photons to be emitted, therefore, decreasing the intensity of the emitted light [2]. Using higher than the peak concentration can result in a wide variety of changes. For example, when a higher concentration of copper is used, it is expected to give rise to killer centers [6] leading to a stronger green fluorescence at lower

* To whom all correspondence should be sent:
E-mail: ivaylokartev@gmail.com

temperatures, and sustaining a blue fluorescent emission only at even lower temperatures. This changes the characteristic green-blue emission to yellow for measurements at room temperature.

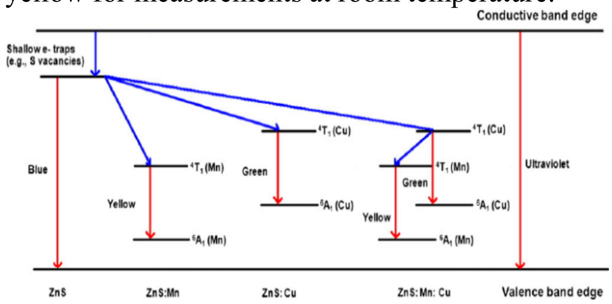

Scheme 1. Electron transitions in Mn:Cu co-activated phosphor.

A ZnS phosphor, activated with more than one modificator, is considered to be co-activated. The spectrum, emitted by a phosphor, co-activated with an ideal ratio of copper and manganese (peak ratio) consists of the individual wavelengths of the contributing activators, but also a shift towards higher wavelengths can be observed [7] (Scheme 1) The reason for occurrence of this shift can be similar to the effect of using higher than the peak concentration of one of the activators in the system of peak ratio. This shift can become even more evident, if one of the activators is used in excess to the other activator, compared to the peak ratio [3].

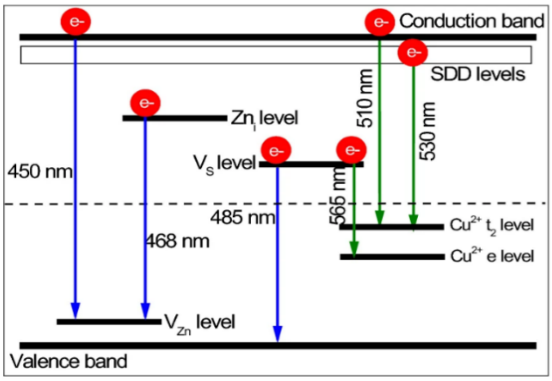

Scheme 2. Cu co-doping effect.

The graph (Scheme 2) helps visualizing the effect of Cu-co-doping on the suppression of blue photoluminescence [8] by comparison of the effect of copper recombination sites (denoted as $Cu^{2+}t_2$ (triplet state) and $Cu^{2+}e$ (singlet state)).

EXPERIMENTAL

Materials

The materials used for this project can be divided into chemicals, glassware, and other equipment. Purity grades are marked in brackets. If not otherwise stated, all used solutions are aqueous and all given fractions of solutions are mass fractions.

Chemicals used

$ZnSO_4.7H_2O$ (pure), powdered Zn, activated charcoal, powdered S, powdered Fe, dilute HCl, distilled H_2O (for the ZnS synthesis). $CuSO_4.5H_2O$ (high pure), $MnCl_2.4H_2O$ (high pure), $AgNO_3$ (high pure), $AlCl_3.6H_2O$ (high pure), conc. HCl (high pure), 25 % NH_3 (p.a.), $NaHCO_3$. (for the modification process)

Other equipment

For the synthesis: propane furnace, blowtorch, hot plate. For measuring the properties of each sample: camera – Sony DSC-HX400V, UV-vis spectrophotometer Thermo Scientific Evolution, Cary Eclipse fluorescence spectrophotometer, UV 365 nm and 256 nm lamps.

Procedure

The experimental procedure can be divided into three parts: synthesis of pure ZnS, modification process and measuring the properties of the final product.

1. *Synthesis of ZnS*

Commercially available ZnS is often contaminated with metal impurities, such as Fe, Co, Ni, Pb which can significantly decrease the luminescent properties of a phosphor derived from ZnS [6, 9]. This created the necessity of purifying the starting material – $ZnSO_4$.

1a. 500 mL of a 37.5 % solution of $ZnSO_4.7H_2O$ was prepared using distilled water.

1b. To the solution were added 30 g of powdered Zn, and the mixture was boiled for 30 min. This step involves a reduction of the metal contaminants, which are worse reducing agents than zinc (which make up the most impurities) back to their metallic forms.

1c. The solution was gravity-filtered, and the filtrate was collected.

1d. To the solution were added 30 g of activated charcoal, and the mixture was boiled for 1 h. This step removes impurities, introduced from the Zn powder in the previous step, as well as other contaminants [9].

1e. The solution was gravity-filtered, and the filtrate was collected.

1f. Using the gas generator, H_2S gas was bubbled through the purified solution. The gas was obtained from the reaction of 120 g of FeS and dilute HCl. ZnS is insoluble in water, which causes its precipitation.

1g. The mixture was filtered and the ZnS was collected.

2. *Modification process*

2a. A certain amount of a salt of the particular activator was dissolved in 100 mL of distlled water and 5 mL of the solution were taken. This step was taken to minimise any errors caused by measuring the weight of the activator salt which was added to a comparatively small amount to ZnS.

2b. A dilute NH_4Cl solution was made by mixing 25 % NH_3 solution and HCl. The amount of NH_4Cl taken, was in 7-fold excess, compared to the molar amount of the activator. (Such solution was not made for $MnCl_2.4H_2O$, because the source of chloride anions is the counterion of the activator in this case)

2c. The solution of co-activator was prepared as described in 2a with a concentration comparable to that of the other used activator.

2d. 2 g of ZnS were measured, and to them were added: the activator solution, the chloride solution (does not apply to Mn-activated samples and samples, showing the effect of absence of halogenides in the phosphor) and the co-activator solution (if such was being used for the particular probe) and distilled water.

Extra step: if Ag is being used as an activator, the previous step would generate a precipitate from AgCl, which will prevent the even distribution of the activator. To solve this issue, a few drops of NH_3 solution were added to dissolve the precipiate, forming a complex.

2e. All of H_2O in the mixture was boiled upon heating using a hot plate. The result of this step consists in an even distribution of the activator on the surface of ZnS.

2f. ZnS was collected and put into a quartz tube. The tube was filled with CO_2 gas produced from the reaction of $NaHCO_3$ and HCl. The gas acts as an inert atmosphere for the firing process.

2g. The firing process – the quartz tube was put into the preheated propane furnace and was heated for 10 min. After that, the produced phosphor was taken out.

The steps from 2a to 2g were repeated twice for the same concentration in order to yield reproducible results. The average result from the first and the second trial of the probe, was considered to be the most accurate one, and is therefore the type of result, presented in the section “Results”.

3. Measuring the characteristics of the phosphor

3a. Measuring the duration of glow. The phosphor was excited for 5 s using the 365 nm and the 256 nm UV lamps. After turning the UV source off, a RAW video (where each pixel represents an exact value of the light registered in the sensor of the device) of the phosphorescing probe was recorded [10]. The video was used as an input for a computer program, which takes the values, registered by the sensor in each pixel of the area of the phosphor, and takes its average value for each frame. The output of the program is a .csv file which can be used to calculate the duration of glow of a particular sample. The values (ranging from 0 to 255) in the results represent the excitement of the phosphor with the more suitable of the two wavelengths. The duration of phosphorescence was measured as the time, for which the pixel values became equal or smaller than the measured background value.

3b. The spectrum of phosphorescence and the UV-vis absorption spectrum were taken using a dedicated apparatus.

3c. Using the phosphorescence spectrophotometer and the already determined highest intensity wavelength emitted by the measured probe, the most suitable UV wavelength for the excitation of the used activator was determined.

RESULTS

The results, obtained from each conducted experiment, represent the values of the independent variables. The experiments can be devided into three types, depending on the activators and co-activators used:

1. Single activators - the purpose of the experiment is to deterimine the peak concentrations of each activator used in this project (Mn, Cu, Ag)
2. Co-activation – the purpose of this experiment is to investigate the effect of co-activation of ZnS using both Mn and Cu in different ratios.
3. Influence of halogenides and aluminium – this experiment aims to prove the important role of halogenides and aluminium on the overall properties of the phosphor.

Single activator – Manganese

The properties of six probes with different molar concentrations of Mn (0.14 mol%, 0.7 mol%, 2.1 mol%, 3.5 mol%, 4.9 mol% and 9.8 mol%) were measured.

- Glow duration – the duration of phosphorescence is measured according to the method, described in 3a.

Diagram 1 clearly shows the effect of the activator concentration on the duration of the phosphorescence – the peak concentration (in this case, 4.9 mol%) exhibits the longest glow and the duration gradually declines, as the concentration gets lower or higher than that peak concentration.

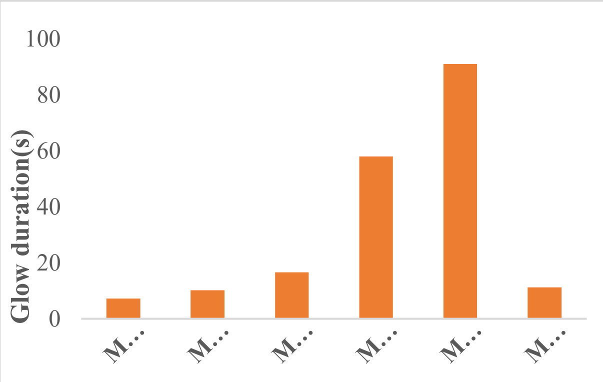

Diagram 1. Comparison of glow duration.

- Color – the color of a particular phosphor is represented by its phosphorescence spectrum as described in 3b.

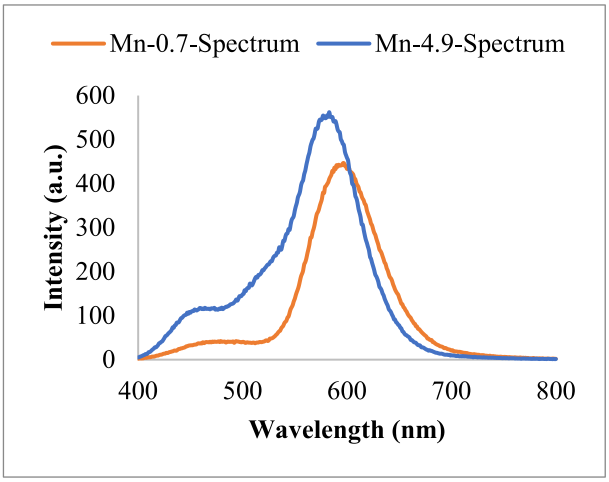

Graph 1. Phosphorescence spectrum of two Mn-doped phosphors

A characteristic change [11] of the color of glow is observed at different activator concentrations – a gradual shift from red (at 0.7 mol %) to green-yellow (at higher and lower than 0.7 mol %) is evident. This effect is also shown on Graph 1, where the wavelength of the light with highest intensity shifts from 582 nm (at 4.9 mol %) to 599 nm (at 0.7 mol %). The change of color can also be explained by the absence of light with wavelength below 550 nm in 0.7 mol %, since its presence contributes to the color of glow to look yellow-green.

Single activator – Copper

The properties of six probes with different molar concentrations of Cu (0.75 mol%, 1.5 mol%, 2.33 mol %, 3 mol %, 5 mol % and 7.5 mol %) were measured.

- Glow duration

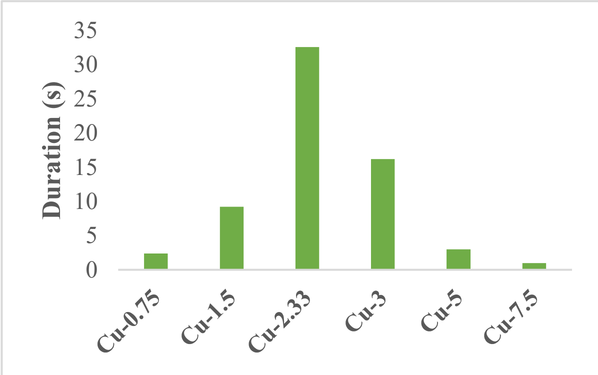

Diagram 2. Comparison of duration of glow.

Diagram 2 shows again the effect of the concentration of the activator on the duration of glow. Modification with copper has peak concentration of 2.33 mol % and using higher or lower concentration results in decreasing duration of phosphorescence.

- Color

Contrary to manganese-doped, copper-doped ZnS phosphors do not show any color shift, when different concentrations of activator were used. This is also shown in Graph 4 which shows very small deviation between the samples measured, which is smaller than the usually reported in other procedures [12].

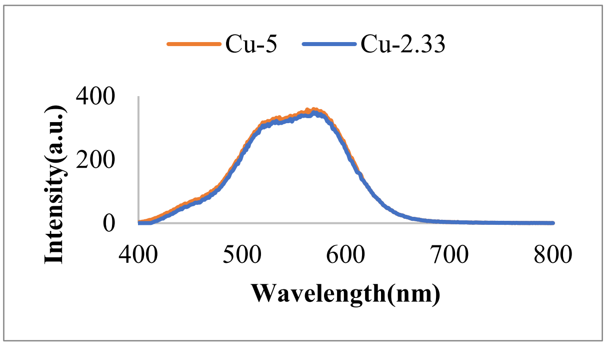

Graph 4. Spectrum of Cu-doped phosphor

Single activator – Silver

The properties of five probes with different molar concentrations of Ag (0.33 mol %, 0.75 mol %, 1.33 mol %, 2.66 mol %) were measured.

- Glow duration

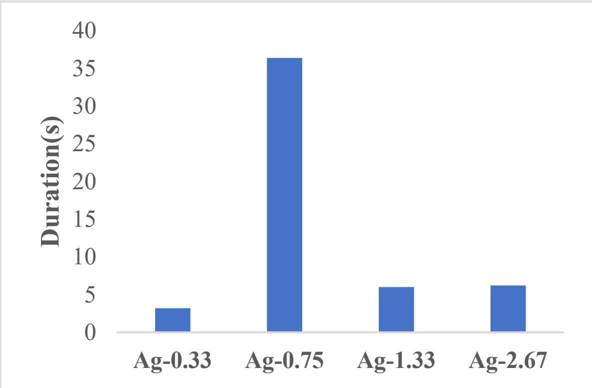

Diagram 3. Comparison of duration of glow

The graph shows that the peak concentration for ZnS modification with silver is 0.75 mol %. Probes with silver concentration, different than the peak one, tend to have significantly shorter duration of phosphorescence.

- Color

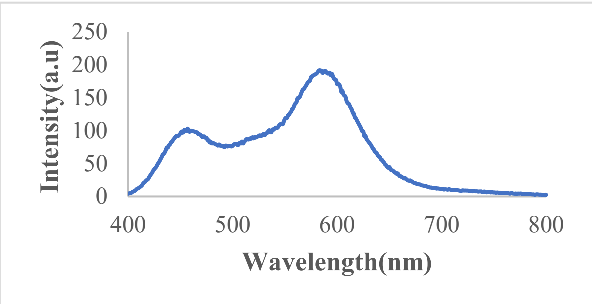

Graph 6. Phosphorescence spectrum of Ag-doped ZnS phosphors.

Silver-doped ZnS phosphors fluoresce and phosphoresce with a strong cyan color. Graph 6, which shows a phosphorescence spectrum of a sample with silver concentration of 0.75 mol%., reveals three wavelength peaks of emitted light – at 457 nm, at 518 and at 587 nm, which contribute to the overall color.

Manganese-Copper co-activation

The properties of five samples with different molar ratios of Mn and Cu (1.5 mol%:1.5 mol % (1:1), 3 mol %: 1.5 mol % (2:1), 4.5 mol %: 1.5 mol % (3:1), 1.5 mol %: 3 mol % (1:2) and 1.5 mol %: 4.5 mol % (1:3)) were measured.

- Glow duration

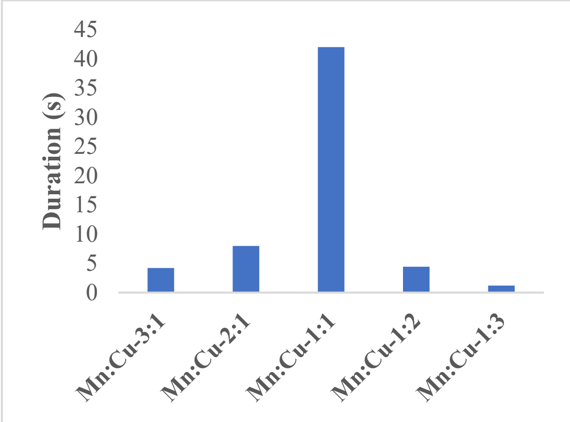

Diagram 4. Comparison of duration of glow

Manganese-Copper co-activated samples are generally short-lasting but give strong fluorescence. It is noticeable that in Diagram 4 the ratio Mn:Cu=1:1 acts as a “peak ratio” for the particular activators, as a ZnS phosphor doped with it, exhibits much longer phosphorescence than the other ratios.

- Color

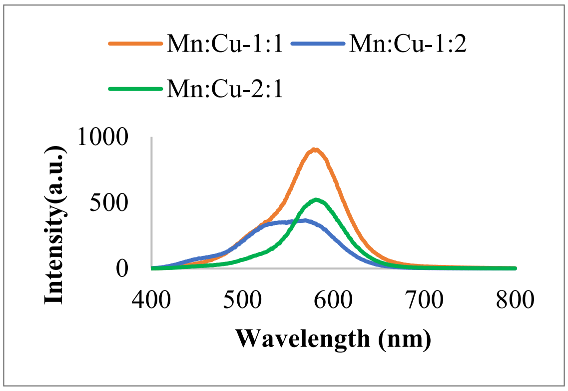

Graph 8. Phosphorescence spectra of three Mn-Cu co-activated phosphors

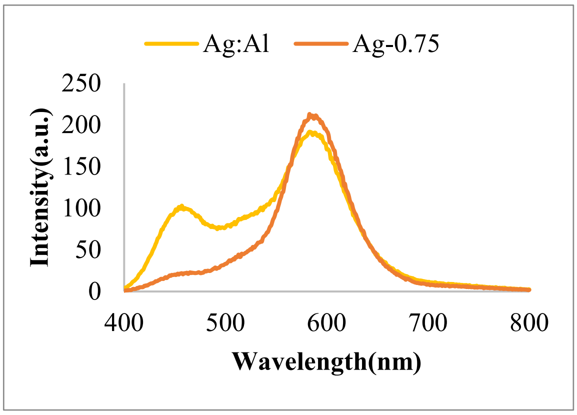

Graph 11. Comparison of Ag:Al co-activation and activation by Ag

The phosphorescing color of the sample is related to the ratio of the co-activators. A ZnS phosphor, doped with Mn:Cu-2:1, emits yellow light, with only one peak at 585 nm, which corresponds to the light emitted by a probe doped with Mn only. The sample, doped with Mn:Cu-1:2 emits green light, with two peaks at 525 nm and at 575 nm, which correspond to the two peaks, characteristic for ZnS with only Cu used as an activator. The phosphor with Mn-Cu ratio of 1:1, emits the 585 nm peak, characteristic for manganese, as well the two peaks, characteristic for copper-doped ZnS.

Co-activation Ag-Al

The properties of one probe with Ag concentration of 0.75 mol % (the found peak concentration of silver) and Al concentration of 0.11 mol % were measured.

- Duration of glow - the probe exhibits phosphorescence for a period of 40.6 sec, measured by the method, described in the procedure.
- Color and intensity

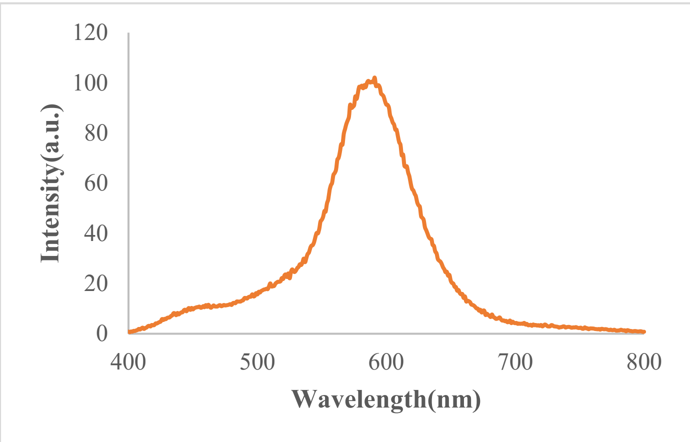

Graph 10. Spectrum of a Ag:Al co-activated phosphor

As Graph 10 and Graph 11 show, Ag:Al co-activated emits light with one peak at 598 nm which corresponds to one of the peaks of ZnS doped with only silver. The other two characteristic peaks of silver are absent in the light emitted from the Al co-activated probe.

Homogeneity of the phosphors

The degree of homogeneity can be determined qualitatively, using Photo 1. There are clearly noticeable spots with different intensity of glow and even different color. This is a sign of low degree of homogeneity, caused by local difference of activator concentration.

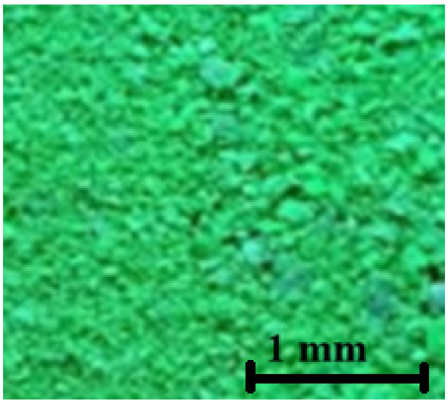

Photo 1. Inhomogeneous phosphor

DATA ANALYSIS

From the results presented in the previous section, several conclusive statements can be made. First, ZnS phosphors, doped with silver, show *the worst luminescent* properties, compared to the other phosphors modified with a single activator. This is also a common occurrence in other research, concerning this topic [13], and a number of possible explanations has been reported. The most evident one is caused by the different oxidation state of Ag^{+}, compared to that of other activators (Cu^{2+} and Mn^{2+}) and even to the cation of the base material – Zn^{2+}. This difference causes imbalance of charge, when silver is incorporated into the crystal lattice of ZnS, and a possible solution for solving the issue is the use of halogenides and trivalent cations [14]. For example, a chloride and a sulfide anion are able to balance the combined charge of a zinc and a silver cation. The situation is similar with the use of trivalent cations like Al^{3+} [15]. However, Ag:Al co-doped phosphors *show better phosphorescent properties than Ag-doped phosphors with added chloride*, both intensity-wise and duration-wise, which is also reported in other procedures, some including co-precipitation [16-19]. This leads to the assumption that the procedure of the addition of halogenides alongside single-activated phosphors *is less effective* than the addition of alumin

um and also to the direct conclusion of the big importance of balancing the charge of an activator with an oxidation state different from that of the ions of the base material. There are also other reasons for the less effective activation with silver. For example, silver can be easier reduced to its metallic form during the firing process than the other activators. This can lower the degree of retaining the original concentration, and lead to a poor-quality phosphorescent material. Furthermore, the reduction can be enhanced by the presence of organic contamination in the ZnS, which is harder to control than the heavy metal contaminants [9].

Another clearly noticeable phenomenon is the better luminescent properties of the Mn-doped phosphors over the Cu-doped ones. The use of activator chloride (in particular $MnCl_2$) has shown to yield phosphors with excellent luminescent properties (around 90 s phosphorescence for the peak concentration Mn-doped probe). Moreover, the decrease in properties of the phosphor when the concentration of the activator is different from the peak concentration, seems to be less steep with manganese than with copper. These effects are contrary to most of the results reported in papers, doing similar research – in the usual case copper-activated ZnS phosphors are reported to give a longer lasting, as well as brighter phosphorescence [7, 8, 20, 21]. This deviation from the commonly obtained results can be explained by the *less effective* addition of halogenides via the ammonium salts, compared to *using an activator halogenide* and it also proves the previously made assumption for the overall ineffectiveness of additional addition of halogenides. This also *partially proves the hypothesis,* because one of the main opportunities which this method provides, in contrast to other methods, namely the usage of activator halogenide, *actually shows to give better results*.

The phosphors, co-doped with Mn and Cu, phosphoresce for shorter periods of time, but all of the investigated ratios and concentrations emit light with high intensity (except the ratio Mn:Cu=1:1, where the phosphorescence also lasts longer). It is noticeable that the excess use of one activator over the other, *causes suppression of the light with wavelengths* characteristic for the activator with lower concentration [22]. This way, the spectrum shows that at 1:1 ratio between the activators, the peaks corresponding to each activator are clearly present; in the Mn:Cu-1:2 co-doped phosphor, the light with wavelengths, emitted from copper (527, 550 and 571 nm) suppress the light, emitted from manganese (which has a peak at 585-590 nm). This effect can be explained by the effect of using *one activator in excess to the other* in a co-activation system, already discussed in the theoretical background [5].

DISCUSSION

The main purposes of investigating this method of obtaining ZnS modified phosphors in this project were to determine the ideal doping conditions for the phosphors, and the benefits and disadvantages of the method. One of the main disadvantages, associated with this method is the general inhomogeneity of the produced phosphorescent materials. Although the followed procedure gave results proving that disadvantage, there are a few actions that can be done, in order to reduce its effects. One way of dealing with the issue is mixing the pure ZnS powder and the activator, used to modify it, using an ultrasonic stirrer. This is a much more efficient way of mixing the base material and the solution containing the activator, since ZnS is insoluble in water and the fine dispersion of its particles is crucial to dealing with the resulting inhomogeneity after removing the solvent from the mixture.

The most common sources of error, occurring in this project, are related to measuring different variables and constants.

- Weight - ± 1mg;
- Glassware volume measurement - ±1mL;
- UV-Vis and phosphorescence spectrophotometers – negligible source of error;
- Camera sensor – negligible source of error.

The method of using pixel values, taken from a RAW video, to determine the duration of phosphorescence, can be regarded as affordable, but objective and accurate for the purpose of the investigation. The idea of using pixel values has already been investigated and used [1], but the program used for taking and processing the data from the pixel values, was specifically written for the purposes of the project by the author himself.

Another source of error important to mention is the effect of the inhomogeneity of the phosphors, which leads to local differences in the concentration of the activator applied. The method of dealing with this issue when measuring the results is by taking average values of the two probes, made for each altered dependent variable, but still, there is a certain amount of error affecting the final results.

It is important to note that the phosphors, obtained in the followed procedure, are not in the form of nanoparticles. A possible step to be added to the procedure, could also be the addition of a capping agent, which can stabilize the formed ZnS nanoparticles [23-25]. The ZnS nanoparticles are the most widely produced form of the material in recent research, often being associated with co-precipitation being a part of the procedure followed, however, they can also be obtained by slight modification of the method used in this project.

CONCLUSION

The project has fulfilled its main aims. Doping conditions, approximate to the ideal conditions, were determined as the peak concentrations and the peak ratios for single activators and co-activators were found and shown in the table below.

Activator/ Co-activator	Peak concentration/ ratio	Duration of glow(s)
Mn, Cl	4.9 mol %	91
Cu	2.33 mol %	32.6
Ag	0.75 mol %	36.4
Mn:Cu	1.5 mol %: 1.5 mol %	42

The statement of the hypothesis was proven - using a chloride activator as a source of both activator and halogenide anion is more efficient than the external addition of halogenides. The opportunity for such addition can be regarded as the most notable advantage of this method, compared to other procedures. The other assumption, concerning the lack of homogeneity of the obtained phosphor, was also proven to be right. Attempts to resolve the lack of homogeneity, being the main source of error and simultaneously the main disadvantage of the method, were proposed and described in the discussion (mixing with ultrasonic stirrer, stabilizing the formation of nanoparticles).

Acknowledgement: *The author extends his sincere appreciation to the Inorganic Chemistry Department of the Chemical Faculty, Sofia University "St. Kliment Ohridski." Their generous provision of access to specialized equipment was instrumental in the successful execution of this research.*

REFERENCES

1. J. H. Park, S. H. Lee, J. S. Kim, T. W. Kim, H. L. Park, *Solid State Phenomena*, **128**, 53 (2007). https://doi.org/10.4028/www.scientific.net/SSP.128.53
2. Q. Lai, B. I. Lee, J. M. Kim, J. E. Jang, J. C. Choe, *Journal of Luminescence,* **104** (04), 261 (2003).
3. F. A. Kröger, *British Journal of Applied Physics*, **6** (S4), S58 (1955).
4. W. Hoogenstraaten, *Journal of the Electrochemical Society*, **100** (8), 356 (1953).
5. Y. Kotera, N. Kiyotaka, *BCSJ*, **33**, 721 (1960).
6. P. M. Jaffe, E. Banks, *J. Electrochemical Society*, **111**, 52 (1964).
7. M. H. A. Selma, M. I. Mukhlis, *Journal of Optical Technology*, **84** (7), 495 (2017).
8. H. Yun, et al. *Journal of Materials Science: Materials in Electronics*, **31** (3), 2617 (2020).
9. M. Saleh, K. G. Lynn, L. Jacobsohn, J. S. McCloy, *Journal of Applied Physics,* **125** (7), 757 (2019).
10. D. M. Sousa, et al., *Nature*, **8**, 15992 (2018), doi:10.1038/s41598-018-34268-z.
11. M. Yousefi, A. Khosravi, K. Rahimi, A. Nazesh, *European Physical Journal-Applied Physics, **45** (1), 10602* (2009).
12. Y. Chen, J. Duh, B. Chiou, C. C. Peng, *Thin Solid Films,* **7**, 9 (2001).
13. T. Hoshina, H. Kawai, *Japanese Journal of Applied Physics*, **19 (**2), 267 (1980).
14. F. A. Khoeger, J. A. M. Dikhoff, *Journal of the Electrochemical Society*, **99** (4), 144 (1952).
15. R. D. Amaranatha, et al. *Journal of Alloys and Compounds*, **582** (1), 257 (2014).
16. Y. Wu, Y. Shao, L. Jacobsohn, *Optical Materials,* **107**, 110015, (2020).
17. Q. Hua, C. Li-xin, S. Ge, et al. *J. Spectroscopy and Spectral Analysis*, **29**(02), 305 (2009).
18. M. Sharma, S. Şen, J. Gupta, M. Ghosh, S. Pitale, S. C. Gadkari, *Journal of Materials Research,* **33**, 3963 (2018).
19. A. M. Abdalla, A. Khan, S. Almalki, N. Kawaguchi, T. Yanagida, S. A. Alsareii, J. S. Algethami, *Radiation Physics and Chemistry,* **210**, 110999 (2023).
20. V. K. Chandra, B. P. Chandra, P. Jha, *Applied Physics Letters* , **103** (16), 161113 (2013).
21. V. Nguyen, T. M. C. Pham, D. X. Loc, K. A. Tran. *Journal of Physics: Conference Series,* **187**, 12016 (2009).
22. S. Ummartyotin, N. Bunnak, J. Juntaro, M. Sain, H. Manuspiya, *Solid State Sciences*, **14** (3), 299 (2012).
23. C. Corrado, et al. *Science of Advanced Materials*, **4** (2), 254 (2012). *Crossref*, doi:10.1166/sam.2012.1281.
24. D. Ch. Deka, A. Kalita, S. Bardaloi, M. P.C. Kalita, *Journal of Luminescence,* **210**, 269 (2019).
25. A. Rahdar, *Journal of Nanostructure in Chemistry,* **3**, 10 (2013).

AUTHOR INDEX

SUBJECT INDEX

Instructions about Preparation of Manuscripts

General remarks: Manuscripts are submitted in English by e-mail The text must be typed on A4 format paper using Times New Roman font size 11, normal character spacing. The manuscript should not exceed 15 pages (about 3500 words), including photographs, tables, drawings, formulae, etc. Authors are requested to use margins of 2 cm on all sides

Manuscripts should be subdivided into labelled sections, e.g. **Introduction, Experimental, Results and Discussion**, *etc*. **The title page** comprises headline, author's names and affiliations, abstract and key words. Attention is drawn to the following:

a) **The title** of the manuscript should reflect concisely the purpose and findings of the work. Abbreviations, symbols, chemical formulas, references and footnotes should be avoided. If indispensable, abbreviations and formulas should be givenin parentheses immediately after the respective full form.

b) **The author**'s first and middle name initials and family name in full should be given, followedby the address (or addresses) of the contributing laboratory (laboratories). **The affiliation** of the author(s) should be listed in detail by numers (no abbreviations!). The author to whom correspondence and/or inquiries should be sent should be indicated by asterisk (*) with e-mail address.

The abstract should be self-explanatory and intelligible without any references to the text andcontaining not more than 250 words. It should be followed by key words (not more than six).

References should be numbered sequentially in the order, in which they are cited in the text. The numbers in the text should be enclosed in brackets [2], [5, 6], [9–12], etc., set on the text line. References are to be listed in numerical order on a separate sheet. All references are to be given in Latin letters. The names of the authors are given without inversion. Titles of journals must be abbreviated according to Chemical Abstracts and given in italics, the volume is typed in bold, the initial page is given and the year in parentheses. Attention is drawn to the following conventions:a) The names of all authors of a certainpublications should be given. The use of "*et al*." inthe list of references is not acceptable.b) Only the initials of the first and middle names should be given. In the manuscripts, the reference to author(s) of cited works should be made without giving initials, e.g. "Bush and Smith [7] pioneered...". If the reference carries the names of three or more authors it should be quoted as "Bush *et al*. [7]", if Bush is the first author, or as "Bush and co-workers [7]", if Bush is the senior author.

Footnotes should be reduced to a minimum. Each footnote should be typed double-spaced at thebottom of the page, on which its subject is first mentioned.**Tables** are numbered with Arabic numerals on the left-hand top. Each table should be referred to inthe text. Column headings should be as short as possible but they must define units unambiguously.The units are to be separated from the preceding symbols by a comma or brackets. Note: The following format should be used when figures, equations, *etc*. are referred to the text (followed by the respective numbers): Fig., Eqns., Table, Scheme.

Schemes and figures. Each manuscript should contain or be accompanied by the respective illustrative material as well as by the respective figure captions in a separate file (sheet).As far as presentation of units is concerned, SI units are to be used. However, some non-SI units are also acceptable, such as °C, ml, l, etc.The author(s) name(s), the title of the manuscript, the number of drawings, photographs, diagrams, etc., should be written in black pencil on the back of the illustrative material (hard copies) inaccordance with the list enclosed. Avoid using more than 6 (12 for reviews, respectively) figures in the manuscript. Since most of the illustrative materials are to be presented as 8-cm wide pictures, attention should be paid that all axis titles, numerals, legend(s) and texts are legible.

The authors are required to submit the text with a list of three individuals and their e-mail addresses that can be considered by the Editors as potential reviewers. Please, note that the reviewers should be outside the authors' own institution or organization. The Editorial Board of the journal is not obliged to accept these proposals.

The authors are asked to submit **the final text** (after the manuscript has been accepted for publication) in electronic form by e-mail. The main text, list of references, tables and figure captions should be saved in separate files (as *.rtf or *.doc) with clearly identifiable file names. It is essential that the name and version of the word-processing program and the format of the text files is clearly indicated. It is recommended that the pictures are presented in *.tif, *.jpg, *.cdr or *.bmp format.

The equations are written using “Equation Editor” and chemical reaction schemes are written using ISIS Draw or ChemDraw programme.

EXAMPLES FOR PRESENTATION OF REFERENCES

REFERENCES

1. D. S. Newsome, *Catal. Rev.–Sci. Eng.*, **21**, 275 (1980).
2. C.-H. Lin, C.-Y. Hsu, *J. Chem. Soc. Chem. Commun.*, 1479 (1992).
3. R. G. Parr, W. Yang, Density Functional Theory of Atoms and Molecules, Oxford Univ. Press, New York, 1989.
4. V. Ponec, G. C. Bond, Catalysis by Metals and Alloys (Stud. Surf. Sci. Catal., vol. 95), Elsevier, Amsterdam, 1995.
5. G. Kadinov, S. Todorova, A. Palazov, in: New Frontiers in Catalysis (Proc. 10th Int. Congr. Catal., Budapest,(1992), L. Guczi, F. Solymosi, P. Tetenyi (eds.), Akademiai Kiado, Budapest, 1993, Part C, p. 2817.
6. G. L. C. Maire, F. Garin, in: Catalysis. Science and Technology, J. R. Anderson, M. Boudart (eds), vol. 6, SpringerVerlag, Berlin, 1984, p. 161.
7. D. Pocknell, *GB Patent* 2 207 355 (1949).
8. G. Angelov, PhD Thesis, UCTM, Sofia, 2001, pp. 121-126.
9 JCPDS International Center for Diffraction Data, Power Diffraction File, Swarthmore, PA, 1991.
10. CA **127**, 184 762q (1998).
11. P. Hou, H. Wise, *J. Catal.*, in press.
12. M. Sinev, private communication.
13. http://www.chemweb.com/alchem/articles/1051611477211.html.

Texts with references which do not match these requirements will not be considered for publication!!!

CONTENTS